UNIVERSITÀ
DEGLI STUDI
DI PADOVA

UNIVERSITA' DEGLI STUDI DI PADOVA
DIPARTIMENTO DI INGEGNERIA INDUSTRIALE

SCUOLA DI DOTTORATO DI RICERCA IN INGEGNERIA INDUSTRIALE
INDIRIZZO INGEGNERIA CHIMICA, DEI MATERIALI E DELLA PRODUZIONE
CICLO XXVII

DEVELOPMENT OF A "LAB ON A CHIP" PLATFORM FOR STUDYING THE CONTROL OF THE CIRCADIAN CLOCK BY METABOLIC CYCLES

Direttore della Scuola: Ch.mo Prof. Paolo Colombo
Coordinatore d'Indirizzo: Ch.mo Prof. Enrico Savio
Supervisor: Ch.mo Prof. Nicola Elvassore
Co-Supervisor: Ch.mo Prof. Joseph S. Takahashi

Dottoranda: Onelia Gagliano

Foreword

The work of this PhD program was performed at “Dipartimento di Ingegneria Industriale sede M via marzolo” of “Universitàˋ degli Studi di Padova” and at “Venetian Institute of Molecular Medicine” of “Fondazione per la ricerca biomedica avanzata onlus”. Part of the development a experimental setup for circadian clcok study was carried out at the Medical Center of University of Texas in Dallas, under the supervision of Prof. Joseph S. Takahashi.

I would like to thank Prof Nicola Elvassore for have supervising my work in these years and Prof Joseph S. Takahashi for the great opportunity of working with his group.

All the material reported in this dissertation is original unless explicit references to studies carried out by other people are indicated.
During this PhD program the following publications have been produced and:

1. Zambon A. Zoso A., Gagliano O., Magrofuoco E., Fadini G.P., Avogaro A., Foletto M., Quake S., Elvassore N., High temporal resolution detection of patient-specific glucose uptake from human ex-vivo adipose tissue on chip, Analitical Chemistry, submitted on December 2014.
2. Luni, S. Giulitti, E. Serena, L. Ferrari, A. Zambon, O. Gagliano, G. G. Giobbe, S. Knöbel, A. Bosio, F. Michielin, N. Elvassore, High throughput reprogramming and differentiation on chip, submitted 2015.

Part of this work have been presented at the following national and international conference:

1. O. Gagliano, A. Zambon, Y. Shan, J.S. Takahashi, N. Elvassore
   Investigation of circadian rhythms perturbation by metabolic stimulation in peripheral tissues through microfluidic technology. BMES 2014, San Antonio, Texas, USA, October 22th – 25th 2014.

2. C. Luni, S. Giulitti, E. Serena, A. Zambon, O. Gagliano, L. Ferrari, F.

Michielin, N. Elvassore. One-step high-throughput reprogramming and differentiation on a chip. International Society for Stem Cell Research 12th Annual Meeting ISSCR, Vancouver, Canada June 18th – 21st 2014.

3. C. Luni, S. Giulitti, E. Serena, A. Zambon, O. Gagliano, F. Michielin, N. Elvassore. One-step high-throughput reprogramming and differentiation on a chip. Keystone Symposia Conference. Stem Cells and Reprogramming, Olympic Valley, California, USA, April 6th-11th, 2014.

4. A. Zambon, A. Zoso, O. Gagliano, C. Luni, N. Elvassore. Dissection of organ cross-talk through human body on-a-chip. SAB visit. Venetian Institute of Molecular Medicine, Padova, Italy. November 22nd – 23rd, 2013.

5. C. Luni, S. Giulitti, E. Serena, A. Zambon, O. Gagliano, F. Michielin, N. Elvassore. One-step high-throughput reprogramming and differentiation on a chip. SAB visit Venetian Institute of Molecular Medicine, Padova, Italy. November 22nd – 23rd 2013.

6. O. Gagliano, A. Zoso, A. Zambon, N. Elvassore. Extrinsic clock-factors oscillatory dynamic on the circadian rhythm of peripheral tissues through microfluidic technology. Chronobiology Gordon Conference. Newport (Rhode Island, USA) July 14th-19th 2013.

7. Alice Zoso, Alessandro Zambon, O. Gagliano, Karim Bouzakri, Nicola Elvassore. Patient-specific insulin resistance investigation through in vitro microfluidic glucose uptake assay. 11th Annual VIMM meeting Marostica (VI), Italy October 19th – 20th 2012.

8. O. Gagliano, A. Zoso, A. Zambon, E. Grasso, N. Elvassore. Automazione e integrazione di piattaforme microfluidiche. GRICU 2012, Pescara, Italy, September 16th – 19th 2012.

Summary

Mammalian behavior and physiology are coordinated by an intrinsic molecular clock into rhythms that are synchronized with the 24 h solar day.
The circadian rhythms are an adaptation to the evolutionarily conserved environment, because they allow to coordinate temporally external environmental cycles (eg. light/ dark) with internal biological and physiological processes (eg. sleep/ wake). Forced misalignment of behavioral and circadian cycles in human subjects, have been associated with increased prevalence of obesity, diabetes and cardiovascular disease, in addition to certain cancers and inflammatory disorders.

Since dysfunction of circadian rhythms has strong effects on human health, there are many clinical studies dedicated to this aspect. However study the properties of the circadian cycle directly on man and his tissue is difficult and expensive due to technical and ethical reasons. On the other hand, the study on animal model provides information about the entire organism and does not permit a dissection of mechanisms and accurate evaluation at specific tissue level. Moreover, animal model could not fairly represent the human physiology. Alternatively, in vitro model, based on cell culture could be suitable to study circadian clock, however, conventional cell culture technology is poorly mimicking the oscillatory nature of *in vivo* signaling systems. A technology able of cyclically delivering periodic biochemical stimulations is required to characterize oscillatory behavior of circadian cell signaling.

The aim of the thesis is developing an *in vitro* model that resembles the cyclic dynamic fluctuations that can be correlated to the pertinent biological networks for dissecting the effects the metabolism on circadian clock;

First of all conventional methodologies were tested measuring a cyclic dynamic oscillation of circadian rhythms on cell culture derived from peripheral tissues in conventional Petri dish.

This approach allowed to rational understand the correlation between metabolite and hormone fluctuations and the circadian oscillators on cell culture, and to design *ad hoc* experiments that are unfeasible with conventional biological methods.

Different experimental setups were developed and fabricated, according to the complexity level of study, the type of the readout and the requirement of multiple independent biological experiments. All these microfluidic platforms were validated for long-term culture, fundamental requirement for circadian rhythm study. Quantitative analysis of circadian oscillators was performed through quantitative molecular biology analysis or bioluminescence assay, which provides evaluation of the circadian clock dynamics.

The results shows that the microfluidic technology could be suitable for hosting synchronized cell culture while allowing high-resolution temporal stimulations. The potential of this micro-scale approach will allow dynamic study on circadian behavior of peripheral tissues, opening a new perspective in circadian field.

Sommario

Comportamento mammiferi e fisiologia sono coordinate da un orologio molecolare intrinseca di ritmi che sono sincronizzati con giorno solare (24 h).
I ritmi circadiani sono un adattamento all'ambiente evolutivamente conservato, in quanto consentono di coordinare cicli ambientali temporalmente esterni (ad es. luce / buio) con i processi biologici e fisiologici interni (ad es. il sonno / veglia). Il disallineamento forzato dei cicli circadiani comportamentali e in soggetti umani, sono stati associati a una maggiore prevalenza di obesità, diabete e malattie cardiovascolari, oltre ad alcuni tipi di cancro e patologie infiammatorie.

Poiché la disfunzione dei ritmi circadiani ha forti effetti sulla salute umana, ci sono molti studi clinici dedicati a questo aspetto. Tuttavia studiare le proprietà del ciclo circadiano direttamente sull'uomo e su suoi tessuti è difficile e costoso a causa di motivi tecnici ed etici. D'altra parte, lo studio sul modello animale fornisce informazioni sull'intero organismo e non consente una dissezione di meccanismi e valutazione accurata a livello tessuto specifico. Inoltre, il modello animale non potrebbe rappresentare fedelmente la fisiologia umana. In alternativa, modelli in vitro, basati su colture cellulari potrebbe essere adatto per studiare l'orologio circadiano, tuttavia, la tecnologia di coltura cellulare convenzionale riesce ad imitare la natura oscillatoria dei sistemi di segnalamento in vivo con scarsi risultati. Una tecnologia in grado di fornire ciclicamente stimoli biochimici periodici è necessaria per caratterizzare il comportamento oscillatorio di segnalazione cellulare circadiano.

Lo scopo della tesi è di sviluppare un modello in vitro in grado di mimare fluttuazioni dinamiche e cicliche che possono essere correlate a reti biologiche pertinenti per sezionare gli effetti che il metabolismo ha sull'orologio circadiano;

Prima di tutto, sono state testate metodologie convenzionali, misurando un'oscillazione dinamica ciclica dei ritmi circadiani in coltura cellulare derivate da tessuti periferici in tradizionali Petri dish.

Questo approccio ha permesso di capire razionalmente la correlazione che esiste tra fluttazioni metaboliche ad ormonali e gli oscillatori circadiani sulle colture cellulari, e di progettare esperimenti *ad-hoc* che sono irrealizzabile con metodi biologici convenzionali.
Differenti configurazioni sperimentali sono stati sviluppati e realizzati, a seconda del livello di complessità di studio, del tipo di readout e della molteplicità di esperimenti indipendenti realizzabili. Tutte queste piattaforme microfluidica sono stati convalidati per la cultura a lungo termine, requisito fondamentale per lo studio del ritmo circadiano. L'analisi quantitativa degli oscillatori circadiani è stata effettuata attraverso l'analisi quantitativa di biologia molecolare o test bioluminescenza, che fornisce la valutazione delle dinamiche dell'orologio circadiano.

I risultati mostrano che la tecnologia microfluidica potrebbe essere adatto ad ospitare colture cellulari sincronizzate, consentendo stimolazioni temporali ad alta risoluzione. Le potenzialità di questo approccio micro-scala consentirà studio dinamico sul comportamento circadiano dei tessuti periferici e l'apertura di una nuova prospettiva nel campo circadiano.

CONTENTS

CHAPTER 1

Introduction: The circadian clock

This chapter will discuss the issue and importance of circadian clock in the human physiology and the research activity in this field. Moreover, it will highlight the limitations of the current approaches thus introducing the technology perspective that guided the thesis and the technological needs to make a step forward in the investigation of the biological processes behind the circadian clock.

1.1 The circadian clock

Mammalian behavior and physiology are coordinated by an intrinsic molecular clock into rhythms that are synchronized with the 24 h solar day (from Latin *circa diem*, meaning "about a day") (Partch C.L. et al., 2014).

The circadian rhythms are an adaptation to the evolutionarily conserved environment, because they allow to coordinate temporally external environmental cycles (eg. light/ dark) with internal biological and physiological processes (eg. sleep/ wake). The coordination of the internal time with the external time allows to prepare the organism to daily-based environmental changes. Among different physiological processes the circadian clock ensures the maintenance of energy homeostasis. (Bell-Pedersen D. et al, 2005; Mohawk et al, 2012).

For instance it maintains synchrony with the environmental cycles of light and nutrients. It has been known for many years that numerous aspects of metabolism exhibit daily rhythmicity, including many types of circulating and intracellular metabolites, feeding-related hormones, and ingestive behaviors (Green C. B. et al, 2008).

For keeping this coordination, that determines the rhythmicity of biological activities and behavior, is fundamental the internal oscillator that controls the circadian rhythms of gene expression. The oscillator consists of a network of genes called clock genes, which are characterized by having an oscillating gene expression profile that is repeated with a period of approximately 24 hours. The clock genes create a self-regulating circuit with a negative feedback loop able to support its own expression

The oscillator is located inside every cell in the body, where it receives signals that carry information on external environmental rhythms. These synchronizing signals, called also cues of entrainment[1], can change the period, the phase and amplitude of the expression of clock genes. The oscillator regulates the expression of genes in the cell and arranges temporally physiology so that opposite reactions (eg. glycolysis / gluconeogenesis) does not occur at the same time (Albrecht U., 2012; Mohawk J.A. et al, 2012).

1.1.1 Cellular and molecular architecture of circadian system

The cell-autonomous molecular clock in mammals is generated by two interlocking transcription/translation feedback loops (TTFL) that function together to produce robust 24 h rhythms of gene expression. The core TTFL is driven by four integral clock proteins: two activators, CLOCK and BMAL1, and two repressors, PER and CRY (Figure1.1).

CLOCK and BMAL1 are subunits of the heterodimeric basic helix-loop-helix-PAS (PER-ARNT-SIM) transcription factor CLOCK:BMAL1, which activates transcription of the repressor Per and Cry genes, as well as other clock-controlled

[1] Synchronization of an internal circadina oscillator to an environmental stimulus that occurs at regular internals (usually with ~24 h periodicity).

output genes. PER and CRY proteins heterodimerize in the cytoplasm and translocate to the nucleus to interact with CLOCK:BMAL1, inhibiting further transcriptional activation.

As PER and CRY proteins are degraded through ubiquitin (Ub)-dependent pathways, repression on CLOCK:BMAL1 is relieved and the cycle begins again with □~24 h periodicity.

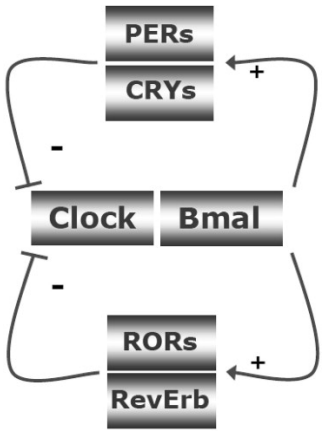

Figure 1.1: Simplified version of the molecular core clock mechanism. The core loop is formed by Clock:Bmal1 and Per and Cry 1. The Clock:Bmal1 heterodimer stimulates the transcription of Per and Cry. Subsequently, Per's and Cry's heterodimerize, translocate to the nucleus, and inhibit Clock:Bmal1 activity. As a consequence, Clock:Bmal1 transcriptional activity drops, which reduces the transcription of Per and Cry genes, thereby activating Clock:Bmal1 again. Additional loops formed by RevErbs and RORs enhance the robustness of the core loop (Source Kalsbeek A. et al, 2014).

A second TTFL is generated through transcriptional activation by the retinoid-related orphan receptors (RORa) and repression by REV-ERBα. TTFL drives rhythmic changes in Bmal1 transcription and introduces a delay in Cry1 mRNA expression that offsets it from genes regulated strictly by CLOCK:BMAL1. Although rhythmic changes in BMAL1 abundance are not required to drive the

core TTFL loop, the ROR/REV TTFL-induced delay in Cry1 expression is crucial for proper circadian timing. The presence of cooperative, interlocking feedback loops provides robustness against noise and environmental perturbations to help maintain accurate circadian timing, and also helps to generate phase delays in circadian transcriptional output that optimally time gene expression for local physiology (Partch C.L. et al, 2014).

A more detailed representation of the TTFL is reported in Figure 1.2.

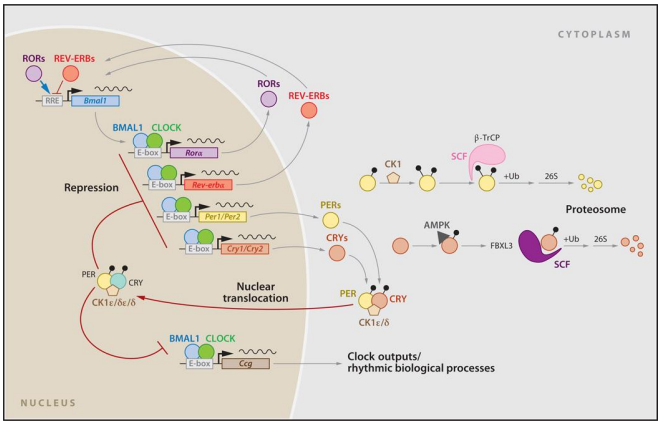

Figure 1.2: Detailed autoregulatory transcriptional feedback loop of the circadian clock in mammals. (Source Mohawk J.A. et al, 2012).

1.1.2 The circadian clock in the body: a hierarchical timing system

The ability of living systems to sustain approximately 24-hour rhythms in the absence of environmental cues shows that most daily oscillations are not responses to the diurnal cycle, but rather are generated by an internal clock (Herzog E.D., 2007).

The mammalian circadian system is composed of a central clock in the suprachiasmatic nucleus (SCN) and a network of peripheral oscillators located in all of the major organ systems (Figure 1.3).

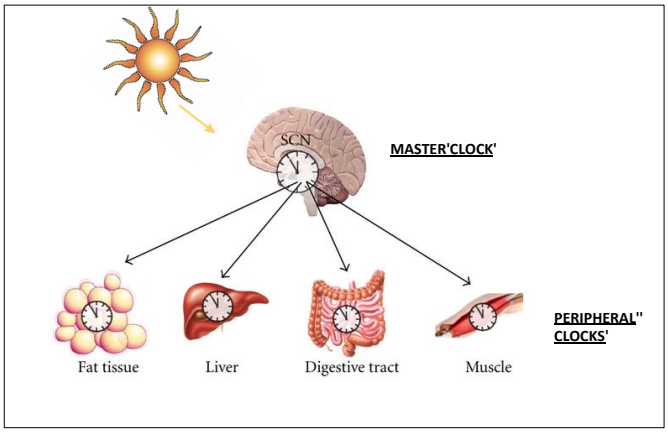

Figure 1.3: Schematic organization of circadian clock: the SCN derives "time of day" information from environmental light signal providing timing cues to peripheral tissues via the autonomic nervous system and hormones (modified from Froy O., 2012).

The 'master' internal clock in mammals is located in the hypothalamic suprachiasmatic nucleus (SCN), that is composed of bilateral nuclei containing approximately 10.000 neurons each, capable of independently generating self-sustained circadian rhythms (Takahashi J. S. et al, 2008). The SCN functions as a network in which the population of SCN cells are coupled together and oscillate in a coherent manner (Herzog E.D., 2007).

This oscillator is synchronized to daily light-dark cycles by direct photic inputs (Figure 1.4) received from the retina through the retinohypothalamic tract (RHT), being the light the most dominant Zeitgeber[2]; the retina, together with the RHT, represent the sole light input pathway in mammals and, through retinal photoreceptors, allow the entrainment of the circadian system by light (Lowrey P.L. et al, 2004).

[2] German word meaning "time giver". A synchronizing agent capable of resetting a pacemaker or synchronizing a self-sustaining oscillation. The zeitgeber "gives" the local time, not the ability to keep time, which the organism already possesses.

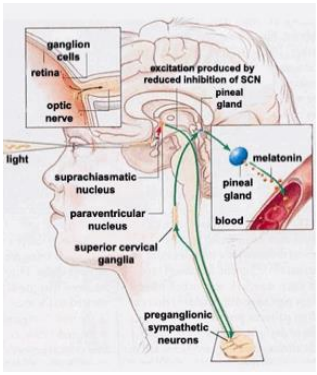

Figure 1.4: Suprachiasmatic nucleus (SCN), and other neurological structures, that are involved in human circadian rhythm control (Source http://thebrain.mcgill.ca).

The dynamics of the spatial and temporal coordination of rhythms in the SCN have been studied recently with the advent of single-cell circadian reporter technology, which has revealed unexpected complexity in the temporal architecture of the nucleus (Evans J.A.et al, 2011; Foley L.E. et al, 2011; Yamaguchi S. et al, 2003).

Thanks to the high sensibility of this technology it is possibile to isolate the circadian rhythms at single unit level, allowing to investigate the single cell behavior that may be different from that of the entire population.

At the single-cell level, SCN neurons exhibit a wide range in cell autonomous circadian periods that vary from 22 to 30 hours (Ko C.H. et al, 2010; Liu A.C. et al, 1997; Welsh D.K. et al, 1995). Intercellular coupling among SCN neurons acts to mutually couple the entire population to a much narrower range that corresponds to the circadian period of the locomotor activity rhythm which is extremely precise (Herzog E.D. et al, 2004). The heterogeneity in intrinsic period of the SCN cells confers at least two important functions: phase lability and phase plasticity.

Intrinsically shorter period cells have earlier phases and intrinsically longer period cells have later phases within the SCN, this is a reflection of phase lability (Yamaguchi S. et al, 2003).

Under different photoperiods (e.g., long vs. short photoperiod light cycles), the waveform of the SCN population rhythm is modulated such that in short photoperiods, the SCN waveform is narrow and high amplitude; whereas, in long photoperiods, the SCN waveform broad and low amplitude, this is a reflection of phase plasticity (Inagaki N. et al 2007; VanderLeest H.T. et al 2007).

The SCN, as master clock, is able to set the phase of cell-autonomous, self-sustained cellular oscillators in peripheral tissues through both neuronal and humoral signaling pathways, which control diverse physiological functions (Figure 1.5) (Asher G. et al, 2011).

Examples of SCN-directed circadian rhythms include feeding, the sleep-wake cycle, glucose metabolism, insulin secretion, and even learning and memory (Eckel-Mahan K. et al, 2013).

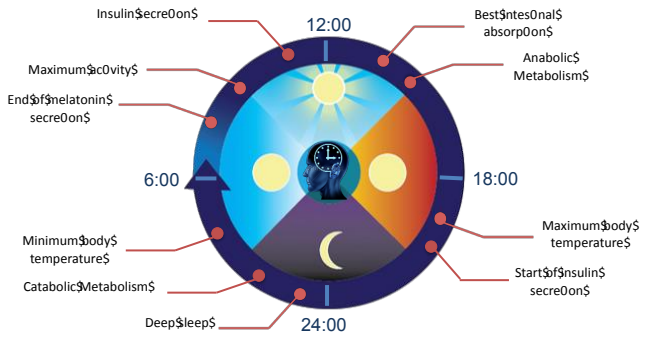

Figure 1.5: The SCN coordinates appropriate metabolic responses within peripheral tissues with the light-dark cycle.

Although the SCN drives behavioral rhythms and coordinates, the many peripheral clocks so that they maintain proper phase relationships with each other, it is now known that peripheral clocks can themselves also be entrained by various stimul, such as food, and temperature (Green C.B. et al, 2008).

Therefore, the organization of the circadian system, shown in Figure 1.6, requires a combination of:

1) autonomic innervation of peripheral tissues:

the SCN controls peripheral oscillators through both sympathetic and parasympathetic pathways (Mohakw J.A. et al, 2012). For example, sympathetic innervation from the SCN to the paraventricular nucleus of hypotalamus (PVN) to the liver results in daily rhythms of plasma glucose, presumably by directly influencing the rhythm of hepatic gluconeogenesis (Cailotto C. et al, 2005; Kalsbeek A. et al, 2004);

2) endocrine signaling:

it was demonstrated that the glucorticoid hormones have a role of entrainment signals for peripheral oscillators, in particolar the rhythmic release of the glucocorticoids could shift the phase of peripheral tissues in vivo (Balsalobre A. et al, 2000);

3) temperature:

in most organisms, temperature is a powerful entraining agent for circadian rhythms; however, in mammals external temperature cycles are very weak entraining agents and this has been attributed to the fact that homeotherms regulate their body temperature and can defend their body temperature against environmental fluctuations;

4) local signals:

in addition to controlling hormone secretion and body temperature directly, the SCN coordinates rhythms in behavioral processes, such as locomotor activity and feeding, which can influence endocrine function and body temperature. These behaviors, feeding in particular, can regulate peripheral clocks at the local level, modulating local signaling pathways and metabolic processes (Mohakw J. A. et al, 2012).

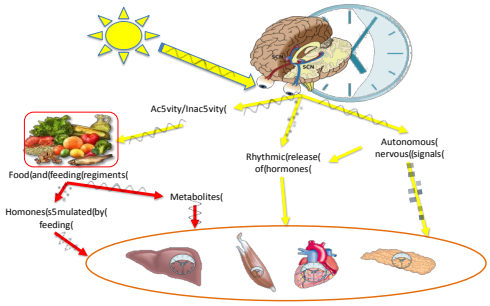

Figure 1.6: Resetting signals for central and peripheral clocks. The SCN dictates rhythms in peripheral tissues and physiological activities, such as locomotor activity, sleep-wake cycle, blood pressure, and heart rate. Light, food, and feeding regimens affect either the central clock in the SCN or the peripheral clocks.

1.1.3 Peripheral oscillators and properties

For many years, neurons of the suprachiasmatic nucleus (SCN) in the hypothalamus were thought to contain the unique mammalian clock controlling circadian rhythmicity of peripheral tissues via neural and humoral signals. Surprisingly, the cloning and characterization of mammalian clock genes have revealed that they are expressed in a circadian manner throughout the body. It is generally accepted now that peripheral cells contain a circadian clock which is similar to the one present in SCN neurons (Figure 1.7).

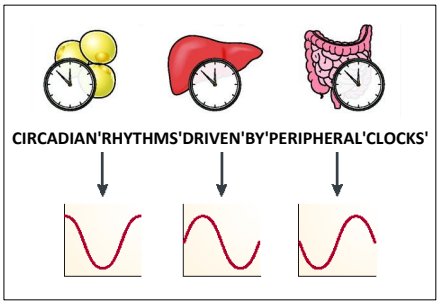

Figure 1.7: Schematic representation of self-sustained circadian rhythms in peripheral tissues.

Indeed, analysis of clock gene expressions in mammals revealed that most of their corresponding mRNA products accumulated in a circadian manner not only in the SCN but also in a variety of peripheral tissues including liver, muscle, kidney and lung (Balsalobre A. et al. 1998; Zylka M.J. et al, 1998).

Surprisingly, it was demonstrated that even mammalian fibroblasts cultured in vitro for about 30 years were still capable of circadian gene expression when treated with a serum shock (Balsalobre A. et al., 1998).

A following study showed that the glucocorticoid hormone analog dexamethasone induces circadian gene expression in cultured rat-1 fibroblasts and transiently changes the phase of circadian gene expression in liver, kidney, and heart (Balsalobre A. et al., 2000).

By exploring glucocorticoid signaling, which does not affect the central circadian pacemaker in the SCN, it has determined that peripheral oscillators can be phase delayed or phase advanced during the entire 24-hour day; in particolar, the SCN clocks can be defined as pacemakers which are able to independently generate and maintain their circadian oscillations whereas peripheral clocks are oscillators which require external signals (serum/glucorticoid shock, temperature cycle (Buhr E.D. et al, 2010)) to sustain and/or to synchronise their circadian rhythms.

With the discovery of peripheral oscillators (Balsalobre A. et al 1998; Yamazaki S. et al 2000; Yoo S.H. et al 2004) and the apparent ubiquity of clock mechanisms (Yagita K. et al 2001), a critical question concerns the similarity and differences in the SCN pacemaker as compared to peripheral oscillators.

This result has led to a critical question concerning the similarity and differences in the SCN pacemaker as compared to peripheral oscillators.

In particolar it was demonstrated that a wide range of peripheral tissues shows to have the capacity to generate circadian oscillator (Plautz J.D. et al, 1997); however, in all such cases, there appears to be a dichotomy between the SCN and peripheral oscillators. The SCN can express persistent, self-sustained oscillations (>30 cycles in isolation), whereas peripheral rhythms damp out after two to seven cycles (Yamazaki S. et al, 2000). This finding has led to a widely accepted hierarchical model of the mammalian circadian system in which the SCN acts as a pacemaker, independently able to both generate and sustain its own circadian oscillations, and necessary to drive circadian oscillations in peripheral cells of neural and non-neural origin (Schibler U. et al, 2003). Consistent with this model

is the observation that peak expression of core circadian genes in peripheral tissues is phase-delayed by 3–9 hours relative to their maximal expression in the SCN, suggesting that the SCN phase leads and drives the peripheral circadian rhythms (Zylka M.J. et al, 1998).

Afterward, Yoo S.H. et al. have observed a long-term persistent and robust circadian oscillations, for more than 20 days, in explanted tissues (liver and lung), as well as those found in the SCN. This finding, also confirmed in a following study on peripheral tissues explanted from SNC-lesioned mice, suggesting that peripheral circadian rhythms contain the molecular component required for SCN-indipendent, persistent circadian oscillation (Yoo S.H. et al, 2004).

To define further the role of the SCN in relation to peripheral clocks, they were developed methods to study the circadian properties of peripheral tissues at the level of single cells, using the mPer2Luc reporter animals. Closely spaced cells in the same culture did not have similar phases, implying a lack of functional coupling among cells; individual fibroblasts result to be independent, non-damping circadian oscillators, however, lack of oscillator coupling in dissociated cell cultures leads to a loss of synchrony among individual cells and damping of the ensemble rhythm at the population level.

These results suggest to consider the SCN as a phase coordinator, preventing internal desynchronization among persistently rhythmic peripheral clocks with tissue-specific periods, rather than as a pacemaker driving peripheral oscillations (Nagoshi E. et al, 2004; Welsh D.K. et al, 2004; Leise T.L et al, 2012).

1.2 Circadian rhythms and metabolism: reciprocal control

Interesting findings show that regulation of metabolism by the circadian clock and its components is reciprocal (Figure 1.8), suggesting that metabolism and circadian clocks are tightly interlocked: clocks drive metabolic processes, and various metabolic parameters affect clocks, producing complex feedback relationships (Green C.B. et al., 2008).
In the next paragraphs it will be described in more detail the intimate connection between these two systems, whose function is influenced reciprocally.

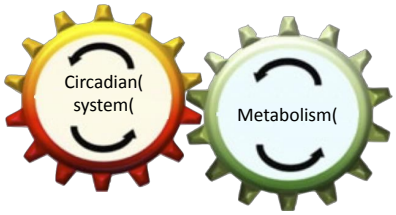

Figure 1.8: Schematic representation of the reciprocal interplay between circadian rhythms and metabolism.

1.2.1 Circadian regulation of the energy metabolism

The most important function of the circadian system is to maintain energy homeostasis by anticipating changes in the external environment and preparing the internal molecular environment to respond to these changes; this requires a close cooperation between signaling systems and gene regulation.
There are three main ways through which the circadian clock influences the expression of metabolic genes in peripheral organs:
a) direct regulation at the level of the promoters of metabolic genes;
b) rhythmic expression of transcription factors that regulate metabolic genes;
c) modulation of sensors metabolic state.

Direct regulation at the level of the promoters of metabolic genes

Many promoters of genes that control metabolism are recognized directly by the transcriptional machinery of the clock. Two prominent examples of direct regulation will have on key genes of cholesterol synthesis and glucose.

In rats, the enzyme that catalyzes the reaction HMGCR limiting of cholesterol synthesis has circadian activity with a maximum peak during the night, the active phase of the rats. The gene transcription of *Hmgcr* is rhythmic and is determined by the binding of rhythmic BMAL1 and REV-ERBα to his promoter.

The transcriptional activators BMAL1 / CLOCK regulate so circadian genes of gluconeogenesis. In mice BMAL1 and CLOCK bind E-box sequences in the promoters of genes Fbp1, PCK1, G6PC, Pcx with a peak during the day, when mice are inactive and do not feed (Koike N. et al, 2012).

Rhythmic expression of transcription factors that regulate metabolic genes

The clock controlled genes are expressed with different phases. This is because not all genes are transcribed directly from BMAL1 / CLOCK: the transcription of some CCGs is mediated by other transcription factors.

For example, in mouse liver dimer BMAL1 / CLOCK binds E-box sequences in the promoters of transcription factors such PARbZIP DBP, TEF and HLF and drive their rhythmic transcription with a peak during the day, that is, during the inactive phase of the rat. These factors recognize the D-box sequences of many genes involved in detoxification and drive the circadian transcription (Yang X. et al, 2006).

Modulation of sensors metabolic state

The sensors of the metabolic state act as an interface between the cellular environment and gene expression. The clock propagates the circadian information to the metabolic pathways interacting with the sensors of the metabolic state and modulating their effect on gene expression.

They are of two categories: (i) nuclear receptors and (ii) enzymes involved in cellular signaling, sensitive to the levels of NAD^+ and AMP.

(i) Nuclear receptors are able to sense the metabolic state binding endocrine substances and metabolic signals related to diet. The ligand activates the receptor, which translocates to the nucleus and acts as a transcription factor. PER2 and

CRY interact with nuclear receptors and modify the activity, thus that indirectly modulate the expression of their target genes, many of which are involved in metabolism.

The glucocorticoid receptor (GR) is a nuclear receptor activated by steroid hormones such as cortisol and the synthetic hormone dexamethasone. When activated, it translocates to the nucleus and can act either as an activator that as a transcriptional repressor. CRY1 and CRY2 interact with GR active and promote its repressive action. Since CRY1/2 are expressed rhythmically, also their interaction with the GR is circadian (Lamia K.A. et al, 2011).

PER2 interacts with several nuclear resceptors in a tissue-specific.

In the liver, PER2 interacts with the nuclear receptor HNF4α and together bind the gene promoter Hnf1α. HNF1α and HNF4α are transcription factors involved in glucose homeostasis (Schmutz I. et al, 2010).

In white adipose tissue, circadian PER2 interacts with nuclear receptor PPARγ and inhibits its transcriptional activity preventing the binding to promoters of genes involved in lipid metabolism. The deletion of Per2 alters both the phase and amplitude of the transcription of target genes of PPARγ in white adipose tissue and KO mice have an altered lipid metabolism (Grimaldi B. et al., 2010).

(ii) enzymes involved in cellular signaling that use as cofactors NAD^+ and AMP, act as molecular sensors metabolic state, in fact the ratios $NAD(P)^+$/ NAD(P)H and AMP/ATP reflect the state energy and reductive power oof the cell. Thus the activity of these enzymes depends on the presence of NAD^+ and AMP, and when, since actived, trigger a signal cascade that ends with the regulation of metabolic pathways and gene expression.

The circadian clock can act on this two-levels system: regulating the activity of the sensors, or by modulating the levels of NAD^+ present.

A sensor metabolic state regulated circadian clock is AMPK, a heterotrimeric kinase activated by AMP. In the early stages of fasting, the cellular levels of AMP rise and trigger different signaling directed to raise the energy levels of the cell. In this context also AMPK is activated and acts promoting catabolic processes and inhibiting anabolic processes, such as the synthesis of lipids, carbohydrates and proteins. The activity of AMPK is circadian, as well as the expression of its subunits β2 that promotes nuclear localization of the enzyme, with a peak during the day in mice. The day coincides with the inactive phase of the rat, then with his

fasting period. Therefore, in line with the anticipatory function of the circadian clock, the activity of AMPK is maximum in correspondence with the period in which the rat is fasted and also AMP levels are higher, favoring thus the expression of catabolic pathways during the rest phase. (Lamia K.A. et al., 2009).
The levels of NAD^+ depend on the nutritional status of the organism, but they are also indirectly regulated by the circadian clock. Indeed, the enzyme NAMPT, responsible of the NAD^+ pathway, is regulated directly by BMAL1/CLOCK. The circadian oscillation of NAD^+ has effect on many enzymes sensitive to the concentration of this cofactor. Of particular importance are the deacetylase sirtuins that modify histones and transcription factors; they are indirectly involved in the regulation of mitochondrial function, in lipid metabolism and glucose and oxidative stress. Among these it should be mentioned SIRT1, that has circadian activity in mice and plays a key role in the regulation of PER2, BMAL1 and CLOCK, implementing thus an important feedback between energy metabolism and the circadian system (Nakahata Y. et al, 2008).

1.2.2 Metabolic feedback on circadian clock

Not only the circadian clock regulates energy metabolism, but also the metabolic signals send feedback to the circadian system peripheral, modulating the phase, amplitude, period. The existence of this feedback is made evident by experiments in which mice with intact SCN are fed during their resting phase. In this case, it is noted that the phase of gene expression is altered in peripheral organs but not in the SCN. In mouse liver, two days of treatment is sufficient to translate the circadian phase of the expression of 10 hours (Stokkan K.A. et al, 2001).
Moreover, recent studies have shown that a high-fat diet in mice leads to changes in the period of the locomotor activity rhythm and alterations in the expression and cycling of canonical circadian clock genes, nuclear receptors that regulate clock transcription factors, and clock-controlled genes involved in fuel utilization in the hypothalamus, liver, and adipose tissue (Kohsaka A. et al, 2007).
Some of the molecular mediators involved in the feedback are those sensors involved in the metabolic state already seen in the previous section: the nuclear receptors and enzymes sensitive to levels of NAD^+ and AMP. They have a dual

role: to propagate the circadian information to the metabolic pathways and transduce information metabolic clock.

The kinase AMPK, regulates the repressive axis of the circadian clock at both CRY1 both of PER2 level (Figure 1.9). AMPK phosphorylates CRY1 and promotes its recognition by the ubiquitin-proteasome system and then the degradation (Lamia K.A. et al, 2009). AMPK acts indirectly on PER2, activating the kinase CKIε, responsible of phosphorylation that makes PER2 recognizable for degradation. Consistent with these observations, the over-activation of AMPK metformin-mediated, a drug for type II diabetes, shortens the period of the circadian cycle (Um J.H. et al, 2007).

SIRT1 is a deacetylase activated by NAD^+. SIRT1 deacetylates PER2, promoting its degradation, and BMAL1, counteracting the activity of CLOCK. Experiments on fibroblasts and rat liver have shown that SIRT1 is required to obtain a high oscillation amplitude of the circadian genes. Indeed knockdown of SIRT1 causes a reduction of the oscillation of the mRNAs of Per2 and Bmal1, probably because the absence of SIRT1 determines an increase of PER2 acetylation and even its accumulation. Higher levels of PER2 imply greater repression of the expression of Bmal1 and consequently a reduced activation of the Per2 expression. Since SIRT1 is sensitive to the levels of NAD^+, its activity varies with the metabolic state of the cell and varies accordingly its modulation amplitude circadian oscillation (Asher G. et al, 2008).

Another class of enzymes sensitive to the levels of NAD^+ are the poly-ADP-ribose polymerases (PARPs), which synthesize ADP polymers using NAD^+. One of these enzymes, PARP1, the dimer interacts with BMAL1/CLOCK and poly-ADP-ribosila CLOCK, changing its affinity for DNA. PARP1 has circadian activity with a peak during the day, the inactive phase of the rat. If the mouse is fed only during the day, the activity of PARP1 is translated of 12 hours, while in the knockout PARP1 mice more time is needed to shift the circadian expression in peripheral organs than is seen in WT . These observations suggest that PARP1 transmits nutritional signals to the circadian clock causing a synchronization of the peripheral clocks caused by nutrition (Asher G. et al, 2010).

The metabolism of glucose, lipids, proteins and nucleotides, influence cellular levels of UDP-GlcNAc, the substrate of the enzyme O-GclNac-transferase (OGT). This enzyme is responsible for the post-translational modification of many

proteins, including those of the circadian clock. In mice, the overexpression of OGT promotes the transcription of Per2 mediated by BMAL1/CLOCK. Indeed OGT adds an O-GclNac in BMAL1 on a site of ubiquitination, increasing stability. The inhibition of the synthesis of UDP-GlcNAc, leads to a lengthening of the circadian period and a reduction in the amplitude of oscillation of Bmal1 (Li M. et al, 2013).

Some transcription factors act as mediators between the metabolic signals and the regulation of the clock gene transcription of the clock.

The nuclear receptor PPARα is induced during fasting and regulates the expression of Bmal1 binding directly his promoter. In mice, the KO of PPARα causes a reduction in amplitude of the oscillation of Bmal1 mRNA (Canaple L. et al, 2006). PGC1α is a transcriptional coactivator, induced by fasting, that, activating RORα, activates the transcription of Bmal1. In this way it contributes to integrate energy metabolism with the circadian rhythm. (Liu A.C. et al., 2007)

The FOXO transcription factors are activated by signaling pathway triggered by insulin. Insulin acts on hepatocytes as synchronizer of circadian rhythm (Yamajuku D. et al, 2012). In mouse liver FOXO3 activates transcription of Clock; In the knockdown of FOXO3 rhythmicity of the liver is strongly reduced, but the phenotype is recovered by the overexpression of Clock (Chaves I. et al., 2014).

The glucose induces the expression of several transcription factors, one of these is TIEG1 (or KLF10); TIEG1 acts as a transcriptional repressor of Bmal1 directly by binding to its promoter. In rat fibroblasts, both the treatment with glucose and the over-expression of Tieg1 induce repression of Bmal1, and the knockdown of Tieg1 presents a circadian period shorter (Hirota T. et al, 2010).

Here we show that a high-fat diet in mice leads to changes in the period of the locomotor activity rhythm and alterations in the expression and cycling of canonical circadian clock genes, nuclear receptors that regulate clock transcription factors, and clock-controlled genes involved in fuel utilization in the hypothalamus, liver, and adipose tissue. These results indicate that consumption of a high-calorie diet alters the function of the mammalian circadian clock (Kohsaka A. et al, 2007).

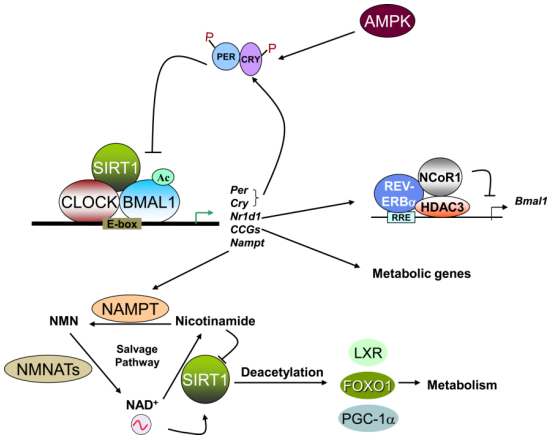

Figure 1.9: Interpalay between regulators of circadina clock and metabolism (Source Sahar S. et al, 2012).

1.3 Circadian disruption and metabolic pathology

Although it has been known for several decades that many metabolic processes, such as glucose and cholesterol metabolism, or renal function are regulated by the circadian clock, it is only in the past few years that the severe metabolic consequences of circadian disruption have emerged (Figure 1.8) (Eckel-Mahan K. et al, 2009).

Metabolic syndrome and obesity have been observed in mice harboring mutations in the clock genes, which encode for transcription factors that affect both the persistence and period of circadian rhythms (Turek F.W. et al, 2005). The ablation of the pancreatic clock is sufficient to render the islet refractory to glucose and insulin secretagogues, resulting in hyperglycemia, obesity and certain features of metabolic syndrome including steatosis, adipose hypertrophy, and hyperlipidemia (Marcheva B. et al., 2010).

Moreover, activities not considered by the circadian system as night shifts, repeated trips with changes of time zone and sleep deprivation, forcing metabolism to respond to unexpected stimuli. The presence of feedback from the

metabolic signals to oscillators, result in a change in the rhythm of peripheral clocks. Therefore the pacemaker is desynchronized respect to the other oscillators and the regulation of homeostasis is not optimal.

Indeed, epidemiological studies have identified a correlation between metabolic syndrome and shift work; obesity, high triglycerides, and low concentrations of high density lipoprotein (HDL) cholesterol seem to cluster together more often in shift workers than in day workers, which might indicate an association between shift work and the metabolic syndrome (Karlsson B. et al, 2001; De Bacquer D. et al, 2009).

It has been suggested that increased activity during what was 'rest' time in the pre-modern world, together with sleep disruption, have been associated with increased prevalence of obesity, diabetes and cardiovascular disease, in addition to certain cancers and inflammatory disorders (Bass J. et al, 2010).

Forced misalignment of behavioral and circadian cycles in human subjects, caused by being active and eating at biological night time, was recently shown to cause a decrease in leptin and an increase in glucose and insulin levels (Scheer F.A. et al, 2009). Moreover, food intake during rest phase (Arble D.M. et al, 2009) and exposure to light at night (Fonken L.K. et al, 2010) have been shown to cause weight gain in mice. With particular regard to feeding, intriguing behavioral studies in humans suggest that nocturnal feeding patterns ("night-eating syndrome") may represent an risk for metabolic disease (Allison K.C. et al, 2007).

At the clinical and epidemiologic level, several lines of evidence suggest that circadian disruption is associated with cardiovascular and metabolic complications across large segments of the human population (Laposky A.D. et al., 2008).

These observations raise the possibility that chronic misalignment between the cycles of rest and activity, and those of fasting and feeding, may contribute to the initiation and progression of obesity and metabolic syndrome.

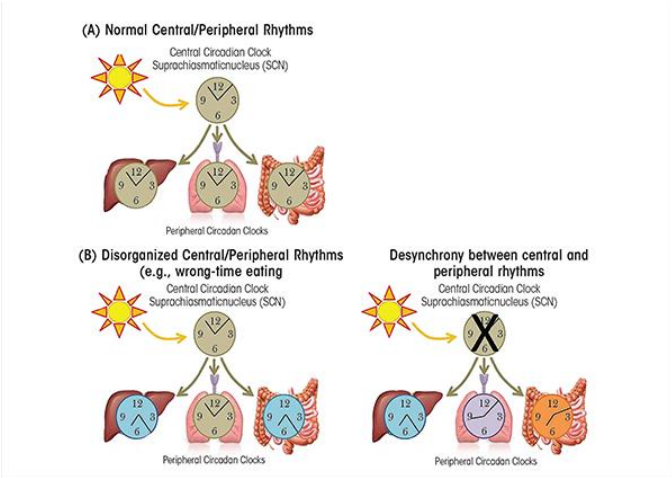

Figure 1.10: Central and peripheral circadian rhythms. (A) Under healthy, (B) wrong-time eating and (C) desynchrony conditions (Source Voigt R.M. et al,).

1.4 Motivation and aim of the thesis

The study of circadian rhythms is a complex problem at high social impact, that is studied by different experimental models and techniques complementary to understand their characteristics and properties.

Since dysfunction of circadian rhythms has strong effects on human health, there are many clinical studies dedicated to this aspect. However study the properties of the circadian cycle directly on man and his tissue is difficult and expensive due to technical and ethical reasons.

In particular how the environmental condition or human behavior affects the clock is of fundamental importance for maintain healthy life-style.

A major impediment in the study of human circadian rhythms is the difficulty and expense of assessing circadian rhythms in people. Because circadian clocks must be studied in temporal isolation, human circadian studies have demanded strict requirements of isolating subjects from environmental cues under constant conditions for a prolonged period of time. Unlike a mouse, it is difficult to convince a person to spend weeks living in temporal isolation. Thus, only a few investigators have had the resources and facilities necessary for such experiments (Takahashi J.S. et al, 2008). Therefore, surrogate measurements for assessing human circadian rhythms are essential. These have taken two forms. The first approach has been to assess 'diurnal preference' or 'chronotype' of subjects using questionnaires, hormonal markers and actigraphy to measure phase of entrainment of circadian rhythms while living in the real world (Roenneberg, T. et al, 2003; Ancoli-Israel S., 2003). A second approach has been to develop cell-based and molecular methods to assess circadian rhythms in humans by biopsy or blood sample (Brown S.A. et al, 2005).

However the study on humans require huge effort to develop methods that are effective and robust in defining inter-individual phenotypic differences, but also that would be sufficiently cost-effective to screen large number of subjects (Takahashi J.S. et al, 2008).

For these reasons, the model organism for the in vivo study of role of circadian rhythms is the mouse. This is widely used to investigate what the relationship between the signals coming from the suprachiasmatic nucleus circadian and metabolism and viceversa.

This approach is based on the analysis of circadian and psychological behavioral and responses of mice carrying a functional knockout of a particular circadian gene of interest in different conditions of light: dark (L : D) cycles (Pereira D.S. et al, 2014), or healthy mice exposed to external cues, such as high fat diet (Kohsaka A. et al, 2007).

However, the study on mouse provides informations about the entire organism without dissecting the single contribution of the different organs (SCN, liver, lung, skeletal muscle) in relation to the circadian rhythms.

To investigate the organization of peripheral circadian clocks, cultures of peripheral organs explanted and cell lines are maintained in long-term culture, that allow to know some signaling pathway of interest using classical methods in cell biology, such as qPCR and western blot (Lee C. et al, 2001).

With the introduction of the transgenic animals and cell lines with a DNA construct in which the promoter of a circadian gene is fused to the luciferease reporter gene, the study of the peripheral clocks is totally changed.

Using this non invasive assay, it is able to measure real-time expression of circadian and circadian output genes, as well as the protein dynamic of the circadian genes. Serial measurement of rhythms from individual tissue samples greatly reduces the intersample variability seen using conventional sampling methods and, importantly, reduces the number of tissue samples required. In animal experiments, this has the potential to drastically reduce the number of experimental animals (Yamazaki S. et al, 2005).

Although the in vitro approach allows to investigate the properties of the single oscillators, shows even some limitations: in a classical culture in a petri dish it is possible to study the biology in static conditions, but it is not simple mimicking the in vivo physiology, where the concentrations of proteins, metabolites and hormones change during the day.

The aim of the thesis is developing a in vitro model that resembles the cyclic dynamic fluctuations of metabolites and hormones (i.e. glucose, insulin), and even circadian related pathological alteration, at which the peripheral tissues are exposed in vivo.

A valid tool to achieve this complex model is the microfluidic technology for its capacity of delivering periodic extracellular chemical stimuli that mimics the

pulsatile nature of in vivo signaling systems in order to better characterize cell signaling dynamics.

This approach was already used in some recent works for studying the circadian gene oscillations on algae and mold, demonstrating that it is a great strategy for investigating molecular responses under various conditions of culture with a good control of the micronviromental, permitting long duration measurements with high spatial and temporal resolution (Teng S.W. et al, 2013; Lee K.K. et al, 2013; Danino T. et al, 2010).

Therefore, the first specific aim of this thesis is the development a cell model able to apply systematic stimuli that can be correlate to the pertinent biological networks for dissecting the effects the metabolism on circadian clock; the second one is to couple the model thus made with a methods of quantitative and imaging analysis for detecting the circadian genes expression.

References

Allison K.C., Crow S.J., Reeves R.R., West D.S., Foreyt J.P., Dilillo V.G., Wadden T.A., Jeffery R.W., Van Dorsten B. and Stunkard A.J., Binge eating disorder and night eating syndrome in adults with type 2 diabetes, *Obesity (Silver Spring)*, 2007, **15**, 1287–1293.

Arble D.M.,Bass J., Laposky A.D., Vitaterna M.H. and Turek F.W., Circadian Timing of Food Intake Contributes to Weight Gain, *Obesity*, 2009, **17**, 2100–2102.

Asher G., Schibler U., Crosstalk between Components of Circadian and Metabolic Cycles in Mammals, *Cell Metabolism*, 2011, **13**, 125–137.

Asher G., Reinke H., Altmeyer M., Gutierrez-Arcelus M., Hottiger M.O. and Schibler U., Poly (ADP-ribose) polymerase 1 participates in the phase entrainment of circadian clocks to feeding, *Cell*, 2010, **142**, 943–953.

Asher G., Gatfield D., Stratmann M., Reinke H., Dibner C., Kreppel F., Mostoslavsky R., Alt F.W. and Schibler U., SIRT1 regulates circadian clock gene expression through PER2 deacetylation, *Cell*, 2008, **134**, 317–328.

Albrecht U., Timing to Perfection: The Biology of Central and Peripheral Circadian Clocks , *Neuron*, 2012, **74**, 246-260.

Ancoli-Israel S., The role of actigraphy in the study of sleep and circadian rhythms. *Sleep*, 2003, **26**, 342–392.

Balsalobre A, Brown SA, Marcacci L, Tronche F, Kellendonk C, Holger M. Reichardt H.M., Schutz G. and Schibler U., Resetting of circadian time in peripheral tissues by glucocorticoid signaling, *Science*, 2000, **289**, 2344–2347.

Balsalobre A., Damiola F. and Schibler U., A Serum Shock Induces Circadian Gene Expression in Mammalian Tissue Culture Cells, *Cell*, 1998, **93**, 929–937.

Bass J. and Takahashi J. S., Circadian integration of metabolism and energetics, *Science*, 2010, **330** , 1349-1354.

Bell-Pedersen D., Cassone V.M., Earnest D.J., Golden S.S., Hardin P.E., Thomas T.L. and Zoran M.J., Circadian rhythms from multiple oscillators: lessons from diverse organisms, *Nature Reviews Genetics,* 2005, **6**, 544-556.

Berson D.M., Strange vision: ganglion cells as circadian photoreceptors, *Trends of Neuroscience*, 2003, **26**, 314–320.

Brown S.A., Ripperger J., Kadener S., Fleury-Olela F., Vilbois F., Rosbash M. and Schibler U., The period length of fibroblast circadian gene expression varies widely among human individuals, *PLoS Biol.*, 2005, **3**, e338.

Buhr E.D., Yoo S.H. and Takahashi J.S., Temperature as a Universal Resetting Cue for Mammalian Circadian Oscillators, *Science*, 2010, **330**, 379-385.

Cailotto C., La Fleur S.E., Van Heijningen C., Wortel J. and Kalsbeek A., The suprachiasmatic nucleus controls the daily variation of plasma glucose via the autonomic output to the liver: are the clock genes involved?, *Eur. J. Neurosci*ence, 2005, **22**, 2531–2540.

Canaple L., Rambaud J., Dkhissi-Benyahya O., Rayet B., Tan N.S., Michalik L., Delaunay F., Wahli W. and Laudet V., Reciprocal regulation of brain and muscle Arnt-like protein 1 and peroxisome proliferator-activated receptor alpha defines a novel positive feedback loop in the rodent liver circadian clock, *Mol. Endocrinol*., 2006, **20**, 1715– 1727.

Cermakian N. and Sassone-Corsi P., Multilevel regulation of the circadian clock, *Nature Review*, 2000, **1**, 59-67.

Chaves I., van der Horst G. T. J., Schellevis R., Nijman R. M., Koerkamp M. G., Holstege F. C. P. and Hoekman M. F. M., Insulin-FOXO3 Signaling Modulates Circadian Rhythms via Regulation of Clock Transcription. *Current Biology*, 2014, **24**, 1248–1255.

Danino T., Mondragon-Palomino O., Tsimring L. and Hasty J., A synchronized quorum of genetic clocks, *Nature*, 2010, **463**, 326-330.

De Bacquer D., Van Risseghem M., Clays E., Kittel F., De Backer G. and Braeckman L., Rotating shift work and the metabolic syndrome: a prospective study, *Int. J. Epidemiol.*, 2009, **38**, 848-854.

Eckel-Mahan K. and Sassone-Corsi P., Metabolism and the circadian clock converge, *Physiology Review*, 2013, **93**, 107-135.

Evans J.A., Leise T.L., Castanon-Cervantes O. and Davidson A.J., Intrinsic regulation of spatiotemporal organization within the suprachiasmatic nucleus. *PLoS One*., 2011, **6**, e15869.

Foley L.E., Gegear R.J. and Reppert S.M., Human cryptochrome exhibits light-dependent magnetosensitivity, *Nature Communications* , 2011, **2**, Article number: 356.

Fonken L.K., Workman J.L., Walton J.C., Weil Z.M., Morris J.S., Haim A. and Nelson R.J., Light at night increases body mass by shifting the time of food intake, *PNAS*, 2010, **107**, 18664–18669.

Green C.B., Takahashi J.S. and Bass J., The meter of metabolism, *Cell*, 2008, **134**, 728-742.

Grimaldi B., Bellet M.M., Katada S., Astarita G., Hirayama J., Amin R.H., Granneman J.G., Piomelli D., Leff T. and Sassone-Corsi P., PER2 Controls Lipid Metabolism by Direct Regulation of PPARγ, *Science*, 2010, **12**, 509–520.

Herzog E.D., Neurons and networks in daily rhythms, *Nature Reviews Neuroscience*, 2007, **8**, 790-802.

Herzog E.D., Aton S.J., Numano R., Sakaki Y. and Tei H., Temporal precision in the mammalian circadian system: a reliable clock from less reliable neurons, *.J Biol. Rhythms*, 2004, **19**, 35-46.

Hirota T., Kon N., Itagaki T., HoshinaN., Okano T. and Fukada Y., Transcriptional repressor TIEG1 regulates Bmal1 gene through GC box and controls circadian clock work, *Genes to Cells*, 2010, **15**, 111–121.

Inagaki N., Honma S., Ono D., Tanahashi Y. and Honma K., Separate oscillating cell groups in mouse suprachiasmatic nucleus couple photoperiodically to the onset and end of daily activity, *Proc. Natl. Acad. Sci. USA*., 2007, **104**, 7664–7669.

Kalsbeek A., La Fleur S., Van Heijningen C. and Buijs R.M., Suprachiasmatic GABAergic inputs to the paraventricular nucleus control plasma glucose concentrations in the rat via sympathetic innervation of the liver, *J. Neuroscience*, 2004, **24**, 7604–7613.

Karlsson B., Knutsson A. and Lindahl B. Is there an association between shift work and having a metabolic syndrome? Results from a population based study of 27 485 people, *Occup Environ Med*, 2001, **58**, 747-752.

Ko C.H., Yamada Y.R., Welsh D.K., Buhr E.D., Liu A.C., Zhang E.E., Ralph M.R., Kay S.A, Forger D.B. and Takahashi J.S., Emergence of noise-induced oscillations in the central circadian pacemaker, *PLoS Biol*., 2010, **8**, e10.1371.

Kohsaka A., Laposky A.D., Ramsey K.M., Estrada C., Joshu C., Kobayashi Y., Turek F.W., and Bass J., High-Fat Diet Disrupts Behavioral and Molecular Circadian Rhythms in Mice, *Cell Metabolism*, 2007, **6**, 414–421.

Koike. N., Yoo S.H., Huang H.C, Kumar V., Lee C., Kim T.K. and Takahashi

J.S., Transcriptional Architecture and Chromatin Landscape of the Core Circadian Clock in Mammals, *Science*, 2012, **338**, 349-354.

Lamia K.A., Papp S.J., Yu R.T., Barish G.D., Uhlenhaut N.H., Jonker J.W., Downes M. and Evans R.M., Cryptochromes mediate rhythmic repression of the glucocorticoid receptor, *Nature*, 2011, **480**, 552–556.

Laposky A.D., Bass J., Kohsaka A. and Turek F.W., Sleep and circadian rhythms: Key components in the regulation of energy metabolism, *FEBS Letters*, 2008, **582**, 142–151.

Lee C., Etchegaray J.P., Cagampang F.R.A., Loudon A.S.I. and Reppert S.M., Posttranslational Mechanisms Regulate the Mammalian Circadian Clock, *Cell*, 2001, **107**, 855–867.

Lee K.K., Ahn C.H. and Hong C.I., Circadian rhythms in Neurospora crassa on a polydimethylsiloxane microfluidic device for real-time gas perturbations, *Biomicrofluidics*, 2013, **7**, 044129.

Leise T.L., Wang C.W., Gitis P.J. and Welsh D.K., Persistent Cell-Autonomous Circadian Oscillations in Fibroblasts Revealed by Six-Week Single-Cell Imaging of PER2::LUC Bioluminescence, *Plos ONE*, 2012, **7**, e33334.

Li M., Ruan H., Hughes M.E., Lee J., Singh J.P., Jones S.P. and Yang X., O-GlcNAc signaling entrains the circadian clock by inhibiting BMAL1/CLOCK ubiquitination. *Cell Metabolism*, 2013, **17**, 303–310.

Liu A.C., Welsh D.K., Ko C.H., Tran H.G. and Zhang E.E., Intercellular coupling confers robustness against mutations in the SCN circadian clock network, *Cell*, 2007, **129**, 605–616.

Liu C., Weaver D.R., Strogatz S.H. and Reppert SM, Cellular construction of a circadian clock: period determination in the suprachiasmatic nuclei, *Cell*, 1997, **91**, 855–860.

Lowrey P.L. and Takahashi J. S, Mammalian circadian biology: elucidating genome-wide levels of temporal organization, *Annu Rev Genomics Hum Genet*., 2004, **5**, 407–441.

Marcheva B., Ramsey K.M., Buhr E.D., Kobayashi Y., Su H., Ko C.H., Ivanova G., Omura C., Mo S., Vitaterna M.H., Lopez J.P., Philipson L.H., Bradfield C.A., Crosby S.D., JeBailey L., Wang X., Takahashi J.S. and Bass J., Disruption of the clock components CLOCK and BMAL1 leads to hypoinsulinaemia and diabetes, *Nature,* 2010, **466**, 627-631.

Mohawk J.A., Green C.B., and Takahashi J.S., Central and Peripheral Circadian Clocks in Mammals, *Annual Review Neuroscie*nce, 2012, **35**, 445–462.

Nagoshi E., Saini C., Bauer C., Laroche T., Naef F. and Schibler U., Circadian Gene expression in individual fibroblasts: cell-autonomous and self-sustained oscillators pass time to daughter cells, *Cell*, 2004, **119**, 693–705.

Nakahata Y., Kaluzova M., Grimaldi B., Sahar S., Hirayama J., Chen D., Guarente L.P, Sassone-Corsi P., The NAD+-dependent deacetylase SIRT1 modulates CLOCK-mediated chromatin remodeling and circadian control, *Cell*, 2008, **134**, 329–340.

Partch C.L., Green C.B., and Takahashi J.S., Molecular architecture of the mammalian circadian clock, *Trends in Cell Biology*, 2014, **24**, 90-99.

Pereira D.S., van der Veen D.R., Gonçalves B.S.B., Tufik S., von Schantz M., Archer S.N. and Pedrazzoli M,, The effect of different photoperiods in circadian rhythms of Per3 knockout mice, *BioMed Research International Volume*, 2014, Article number: 1707952014.

Plautz J.D., Kaneko M., Hall J.C. and Kay S.A., Independent photoreceptive circadian clocks throughout drosophila, *Science*, 1997, **278**, 1632-1635.

Roenneberg T., Wirz-Justice A. and Merrow M., Life between clocks: daily temporal patterns of human chronotypes, *J. Biol. Rhythms*, 2003, **18**, 80–90.

Rollag M.D., Berson D.M. and Provencio I., Melanopsin, ganglion-cell photoreceptors, and mammalian photoentrainment. *J Biol Rhythms*. 2003, **18**, 227–234.

Sahar S. and Sassone-Corsi P., Regulation of Metabolism: The Circadian Clock dictates the Time, *Trends Endocrinol Metab*, 2012, **23**, 1–8.

Scheer F.A., Hilton M.F., Mantzoros C.S. and Shea S.A., Adverse metabolic and cardiovascular consequences of circadian misalignment, *PNAS*, 2009, **106**, 4453–4458.

Schibler U., Ripperger J. and Brown S.A., Peripheral circadian oscillators in mammals: time and food, *J.Biol. Rhythms*, **18**, 250-260.

Schmutz I., Ripperger J.A., Baeriswyl-Aebischer S. and Albrecht U., The mammalian clock component PERIOD2 coordinates circadian output by interaction with nuclear receptors, *Genes & Dev*, 2010, **24**, 345–357.

Stokkan K.A., Yamazaki S., Tei H., Sakaki Y. and Menaker M., Entrainment of the circadian clock in the liver by feeding, *Science*, 2001, **291**, 490–493.

Takahashi J. S., Hong H.K., Ko C.H. and McDearmon E.L., The genetics of mammalian circadian order and disorder: implications for physiology and disease, *Nature Reviews Genetics*, **9**, 2008, 764-775.

Teng S.W., Mukherji S., Moffitt J.R., de Buyl S. and O'Shea E.K., Robust circadian oscillations in growing cyanobacteria require transcriptional feedback, *Science*, 2013, **340**, 737–740.

Turek F.W., Joshu C., Kohsaka A., Lin E., Ivanova G, McDearmon E., Laposky A., Losee-Olson S., Easton A., Jensen D.R., Eckel R.H., S. Takahashi J.S., and

Bass J., Obesity and metabolic syndrome in circadian Clock mutant mice, *Science*, 2005, **308**, 1043–1045.

Um J.H., Yang S., Yamazaki S., Kang H., Viollet B., Foretz M. and Chung J.H., Activation of 5′-AMP-activated Kinase with Diabetes Drug Metformin Induces Casein Kinase Iε (CKIε)-dependent Degradation of Clock Protein mPer2, *The Journal of Biological Chemistry*, 2007, **282**, 20794-20798.

VanderLeest H.T., Houben T., Michel S., Deboer T., Albus H., et al., Seasonal encoding by the circadian pacemaker of the SCN., *Current Biology*, 2007, **17**, 468–473.

Voigt R.M., Forsyth C.B. and Keshavarzian A. M.D, Circadian Disruption: Potential Implications in Inflammatory and Metabolic Diseases Associated With Alcohol, *Alcohol Research: Current Reviews*, 2013, **35**, 87-96.

Welsh D.K., Yoo S.H., Liu A.C., Takahashi J.S. and Kay S.A., Bioluminescence imaging of individual fibroblasts reveals persistent, independently phased circadian rhythms of clock gene expression, *Current Biology*, **14**, 2289–2295.

Welsh D.K., Logothetis D.E., Meister M. and Reppert S.M., Individual neurons dissociated from rat suprachiasmatic nucleus express independently phased circadian firing rhythms, Neuron, 1995, **14**, 697–706.

Yagita K., Tamanini F., van der Horst G.T.J. and Okamura H., Molecular mechanisms of the biological clock in cultured fibroblasts, *Science*, 2001, **292**, 278-281.

Yamaguchi S., Isejima H., Matsuo T., Okura R., Yagita K., Kobayashi M. and Okamura H., Synchronization of Cellular Clocks in the Suprachiasmatic Nucleus, *Science*, 2003, **302**, 1408-1412.

Yamajuku D., Inagaki T., Haruma T., Okubo S., Kataoka Y., Kobayashi S., Ikegami K., Laurent T., Kojima T., Noutomi K., Hashimoto S. and Oda H., Real-time monitoring in three-dimensional hepatocytes reveals that insulin acts as a synchronizer for liver clock, *Scientific Reports,* 2012*,* **2**, Article number: 439.

Yamazaki S. and Takahashi J.S., Real-Time luminescence reporting of circadian gene expression in mammals, *Methods Enzymol*, 2005, **393**, 288–301.

Yamazaki S., Numano R., Abe M., Hida A., Takahashi R. Ueda M., Gene D. Block G.D., Sakaki Y., Menaker M. and Tei H., Resetting central and peripheral circadian oscillators in transgenic rats, *Science*, 2000, **288**, 682-685.

Yang X., Downes M., Yu R.T., Bookout A.L., He W., Straume M., Mangelsdorf D.J., Evans R.M., Nuclear Receptor Expression Links the Circadian Clock to Metabolism, *Cell*, 2006, **126**, 801–810.

Yoo S.H., Shin Yamazaki S., Lowrey P.L., Shimomura K., Ko C.H., Buhr E.D., SiepkaS.M., Hong H.K., Oh W.J., Yoo O.J., Menaker M., and Takahashi J.S. PERIOD2::LUCIFERASE real-time reporting of circadian dynamics reveals persistent circadian oscillations in mouse peripheral tissues., *Proc. Natl Acad. Sci. USA*, 2004, **101**, 5339–5346.

Zylka M.J, Zylka M.J. Shearman L.P., Weaver D.R. and Reppert S.M., Three period homologs in mammals: differential light responses in the suprachiasmatic circadian Clock and oscillating transcripts outside of brain, *Neuron*, 1998, **20**, 1103-1110.

CHAPTER 2

Microfluidic technology for cell biology

This chapter will review the microfluidic technology for cell culture, highlighting the state of art and the perspectives; moreover they will be introduced the basis requirements for cell culture and improvements and advantages when microfluidic approach is used in biology.

2.1 State of art of microfluidic technology in cell culture and perspectives

Microfluidics has the potential to significantly change the way modern biology is performed. This technology uses elastomeric materials, tipically (polydimethylsiloxane) (PDMS), are relatively easy to fabricate, and are compatible with most biological assays (El-Ali J. et al, 2006). Moreover, it has the unique ability to integrate biosensor technology with microscopy-based read-outs. In combination with automated imaging systems possessing high-throughput capabilities and new data processing and storage strategies, microfluidics provides new tools for highly parallel, multiplexed assays with a higher information quality (van Midwoud P.M., et al, 2010).

Microfluidic devices offer the ability to work with smaller reagent volumes, shorter reaction times, and the possibility of parallel operation. They also hold the promise of integrating an entire laboratory onto a single chip (i.e., lab-on- a-chip). In addition to the traditional advantages conferred by miniaturization, the greatest potential lies in the physics of the microscale. By understanding and leveraging microscale phenomena, microfluidics can be used to perform techniques and experiments not possible on the macroscale, allowing new functionality and experimental paradigms to emerge (Beebe D.J. et al, 2002).

Microfluidic cell culture platforms combine the advantages of miniaturization and real-time microscopic observation with the ability to pattern cell culture substrates controlling parameters of the cell microenvironment at relevant length and time scales (Rhee S.W. et al., 2005).They can also vary the composition of culture medium over space using gradient generators (Chung B. G. et al, 2005; Kim S. et al, 2010; Lee P. J et al, 2006, Zambon A. et al, 2014), creating cell culture conditions that are more physiological than those found in other in vitro systems, in terms of nutrients exchange rates and tunable mechanical stimulation (Leclerc E. et al, 2006; Zhou J. et al 2012).

Microfluidic cell systems are applied to many different situations, from 2D and 3D cell culture systems (Kuo C.T. et al, 2012). These systems differ on how cells are seeded: as monolayer on a substrate surface (2D systems), or on 3D scaffolds (3D systems). 3D cell-culture models have recently garnered great attention because they often promote levels of cell differentiation and tissue organization not possible in conventional 2D culture, because more closely resemble cell behaviour in vivo (Pampaloni F. et al, 2007). Several studies, for example, have shown that there are different mechanisms of drug resistance in three-dimensional cultured cancer cells compared to two-dimensional cultured cells (Chen A.A. et al 2010; Tung Y.C. et al, 2011).

A number of 3D microfluidic perfusion culture systems have been developed recently for application in complex biological processes such as *in vitro* organ development (Huh D. et al, 2011). For tissue types that are highly perfused *in vivo*, such as the liver and kidney, microfluidic perfusion culture may more accurately mimic the in vivo microenvironment, where cells are in close proximity with the microvascular network (Domansky Z. et al, 2010). Considerable progress has been made in the design and use of novel microfluidic

devices for culturing cells and for subsequent treatment and analysis (Young E.W.K et al, 2010; Pasirayi G et al, 2011). Automated cell culture screening systems based on a microfluidic chip are recently built including valves, mixers and pumps, capable of controlling fluid (Gómez-Sjöberg R. et al, 2007).

Microfluidic systems are in development that not only model biological environments but also physically mimic biological tissues and organs; such 'organs on a chip' could have an important role in expediting early stages of drug discovery and help reduce reliance on animal testing (Neuzil P. et al, 2012).

Co-culture or multitissue-based microfluidic devices integrate two or more cell types in two-dimensional or three-dimensional cell cultures to simulate various human organs on a single chip (Baker M., 2011; van Midwoud P. M. et al, 2010; van Midwoud P. M. et al, 2011). These systems aim to mimic the tissue–tissue interfaces in the body or at least some of the physiologically relevant processes that are part of the so-called ADME (absorption, distribution, metabolism and elimi- nation) processes in the body (Esch M. B. et al, 2010). This approach delivers results of drug efficacy and toxicity on an organ level, may provide valuable information for early-phase decisions in future drug development. Moreover, patient-derived cells could even lay the groundwork for personalized medicine, providing the ability to optimize drug concentrations and compositions for different patient groups or even individual patients (Neuzil P. et al, 2012).

2.2 Principles of the cell culture microfluidic technology

The techniques to maintain and grow cells in vitro are considerably changed over time from their introduction (Carrel A., 1912) and new methods have been developed for culturing, expanding, differentiating and de-differentiating cells. The basic tools and requirements for cell culture have not changed significantly since then, but substantial improvements have been obtained with the introduction of technology in biology (Mehling M. et al, 2014).

The field of microfluidic is significantly impacting cell biology research and application and emerging as powerful tool for tissue engineering (Figure 2.1) (Khademhosseini A. et al., 2006).

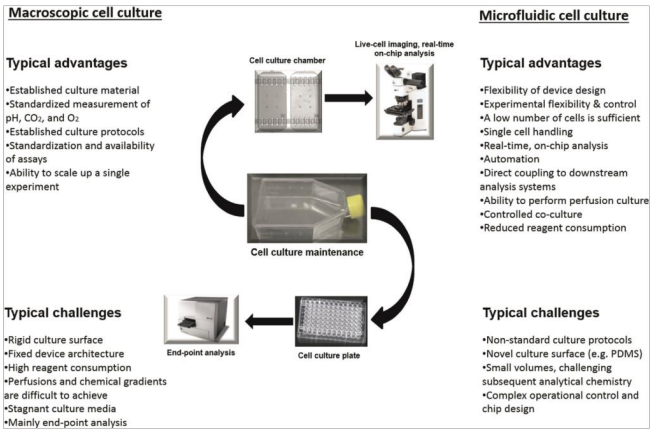

Figure 2.1: Overview of advantages and challenges of both macroscopic and microfluidic cell culture (Source Halldorsson S. et al., 2015).

Microfluidic cell culture allows controlling fluid flow in the micro- and nano-liter scale in precisely defined geometries and facilitates simultaneous manipulation and study cells effectively on both a single- and multi-cellular level with high-resolution and localized application of experimental environment with biomimetic physiological conditions (Breslauer D.N., et al, 2006), demonstrating to be a valid tool to satisfy the principal requirements for a cell culture (Table 2.1).

REQUIREMENTS FOR CELL CULTURE	MICROFLUIDIC STRATEGY
Control of temperature (T=37 °C) and gases (pCO_2=5%)	PDMS permeability to gases and incubator
Medium change and delivery of nutrients	Precise, continuous or transient, medium change by syringe or integrated on-chip pumps
Mimick normal and pathological physiology in vivo	Fast and cyclic stimuli, coherent with in vivo signaling system (high A/V)
Imaging Analysis	PDMS trasparency
Experimental data statistically significant	High capacity of parallelization (high-throughput experiments)

Table 2.1: Requirements for cell culture and microfluidic strategy for developing an in vitro model for biological applications.

In particular the intrinsic property of gases permeability and biocompatibility of PDMS, with which microfluidic devices are manufactured, allows to support cells culture and keep it at temperature of 37 °C and CO_2 partial pressure of 5%, placing the platform in a standard incubator, as it happens for the traditional cultures in dish.

Although static culture systems are simple to operate and economical to manufacture, in terms of long-term cell culture, they may not be appropriate due to the risk of contamination caused by repeated manual intervention. Most importantly, the culture environment in such a system may fluctuate due to the intermittent medium replacement processes.

Microfluidics provides high degree of control over cell culture conditions with high spatial and temporal resolution in various aspects (Figure 2.2). The ability of exactly timing fluid flow using liquid-handling systems, external (syringe pumps) or in-chip integrated (pneumatic valves), allows precise chemical and physical control of the microenvironment; the nutrients delivery to the cells with flow rates of microliters and nanoliters range, by continuous or transient media exchange, represents a significant improvement in precision compared to the traditional hand-held pipette (Wu M.H., 2009).

This advantage allows to mimic a cell's natural microenvironment, for example by continuous perfusion culture or by fast or low medium exchanges; two works in our lab showed the possibility to control the glucose and oxygen concentrations with high temporal and spatial accurance (Zambon A. et al, 2014; Martewicz S. et al, 2012).

Microfluidic cell culture devices bring the cell population down to a few hundred cells, or even a single cell, making it possible to capture perturbations to individual cells, increasing the spatial and temporal resolution for a given experimental setup.

The fact to have a high surface-to-volume ratio allows to provide fast and cyclic stimuli, a controlled supply of nutrients and removal of metabolites and accumulation factors, and dynamic analysis of output in response to a specific input (Young E.W.K. et al, 2010).

Moreover this technology offers the possibility to deliver not only chemical but also mechanical signals, providing an extra degree of control over cultured cells (Morgan J.T., et al, 2012).

PDMS based microfluidics provides excellent live cell imaging conditions as PDMS offers transparency and stable optical features, and the optical aberrations and auto-fluorescence induced by small volumes of cell culture medium in such devices are generally negligible.

In combination with microscopes, biosensor integrated or other analytical and quantitative methods commonly used in cell biology and diagnostics, such as high-throughput qPCR, microfluidic cell culture devices therefore allow powerful characterization of a multitude of cellular responses on a single cell as well as population level (Mehling M. et al, 2014).

The small dimensions of spatially separated microfluidic compartments allow assembly of a multitude of individually controllable cell culture chambers on a single device. This facilitates high parallelization of experiments, high throughput of samples and reactions and thus improvement of reproducibility, as well as a reduction in reagent costs.

High potential for parallelization allows the recording of millions of data points of given biological processes during a single experiment: experimental replicates can be performed to achieve statistically significant results in a reasonable amount of time, that is impossible with the standard biological approach (Vyawahare S., 2010).

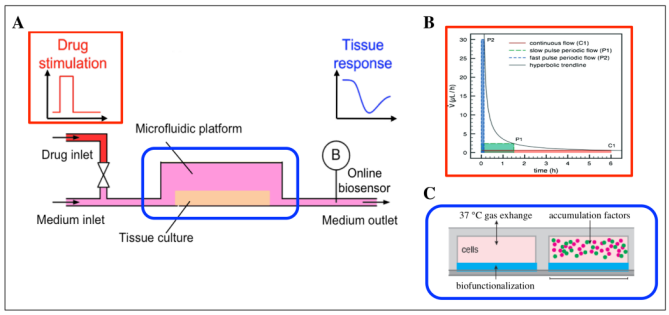

Figure 2.2: (A) Schematic rapresentation of microfluidic platform; (B) examples of stimulation protocols; (C) schematic rapresentation of the cellular micronviromental.

2.3 Conclusions

Microfluidic technology is emerged as a powerful tools for addressing some of the challenges in cell biology. In biological research many advantages are possible with the introduction of microfluidic technology. In particular the capacity to implement cyclic stimulation with an accurate control of microenvironment is one of the crucial aspects that can be achieved.

Orchestration of cellular operations requires precise conversion of chemical signals from the environment into intracellular messages that cells must interpret with their internal signaling pathways. Some cues from the environment and chemical messengers are regularly frequency-encoded, as happens for all those metabolic signals that regulate our circadian clocks.

Despite the wealth of models (in vivo, in vitro and mathematical) available for studying, predicting and interpreting the mechanisms mediating the conversion of extracellular signals into cell responses, there is a lack of experimental setups that enable manipulation and further elucidation of this process.

The approach of cell culture microfluidic technology allows to deliver periodic extracellular chemical stimuli that mimics the pulsatile nature of in vivo signaling systems in order to better characterize cell signaling dynamics real-time, even circadian clock dependent.

In the next chapter they will be described the microfluidic devices designed during this PhD thesis, the strategic choises and prerequisites for developing a strong model of in vitro cell culture.

References

Baker, M. Tissue models: a living system on a chip. *Nature,* 2001, **471**, 661–665.

Beebe D.J., Mensing G.A. and Walker G. M., Phisics and applications of microfluidics in biology, *Annual Revie Biomed.Eng.*, 2002, **4**, 261-286.

Breslauer D.N., Lee P.J. and Lee L.P., Microfluidics-based systems biology, *Mol Biosyst.*, 2006, **2**, 97-112.

Carrel A., Pure cultures of cells, *Journ. Exp. Med.*, 1912, **16**, 165-168.

Chen A. A., Underhill G. H. and Bhatia S. N. Multiplexed, high-throughput analysis of 3D microtissue suspensions, *Integr. Biol.,* 2010, **2**, 517–527.

Chung, B. G., Flanagan L.A., Rhee S.W., Schwartz P.H., Lee A.P., Monuki E.S. and Jeon N.J., Human neural stem cell growth and differentiation in a gradient-generating microfluidic device, *Lab on a Chip*, 2005, **5**, 401-406.

Domanski Z., Ciesielski M., Baran B., Network flow model for microfiltration, *Civil and Environmental Engineering Reports*, 2010, **5**, 53-62.

El-Ali J., PK Sorger P.K., KF Jensen K.F., Cell on chips, *Nature*, 2006, **442**, 403-411.

Esch M.B., King T.L. and Shuler M.L., The role of body-on-a-chip devices in drug and toxicity studies. *Annu. Rev. Biomed. Eng.,* 2011, **13**, 55–72.

Gómez-Sjöberg R., Leyrat A.A., Pirone D.M., Chen C.S. and Quake S.R., Versatile, fully automated, microfluidic cell culture system, *Analytical Chemistry*, 2007, **79**, 8557-8563.

Halldorsson S., Lucumi E., Gomez-Sjoberg R., and Fleming R.M.T., Advantages and challenges of microfluidic cell culture in polydimethylsiloxane devices, *Biosensors and Bioelectronics*, 2015, **63**, 218–231.

Huh D., Hamilton G.A., Ingber D.E, From 3D cell culture to organs-on-chips, *Trends in Cell Biology*, 2011, **21**, 745-754.

Khademhosseini A., Langer R. and Borenstein J. and Vacanti J.S., Microscale technologies for tissue engineering and biology, *PNAS*, 2006, **8**, 2480- 2487.

Kim S., Kim H.J. and Jeon N.L., Biological applications of microfluidic gradient devices, *Integr Biol (Camb)*, 2010, **2**, 584-603.

Kim L., Vahey M.D., Lee H.Y. and Voldman J., Microfluidic arrays for logarithmically perfused embryonic stem cell culture, *Lab on a Chip*, 2006, **6**, 394-406.

Kuo C.T., Chiang C.L., Huang R.Y.J., Lee H. and Wo A.W., Configurable 2D and 3D spheroid tissue cultures on bioengineered surfaces with acquisition of epithelial–mesenchymal transition characteristics, *NPG Asia Materials*, 2012, **4**, e27.

Leclerc E., David B., Griscom L., Lepioufle B., Fujii T., Layrolle P. and Legallaisa C., Study of osteoblastic cells in a microfluidic environment, *Biomaterial*, 2006, **27**, 586–595.

Lee P. J., Hung P.J., Rao V.M. and Lee L.P. Nanoliter scale microbioreactor array for quantitative cell biology, *Biotechnology and Bioengineering*, 2006, **94**, 5–14

Martewicz S., Michielin F., Serena E., Zambon A., Mongillo M., Elvassore N., Reversible alteration of calcium dynamics in cardiomyocytes during acute hypoxia transient in a microfluidic platform, *Integrative Biology* , 2012, **4**, 153-164.

Mehling M. and Tay Savas, Microfluidic cell culturem, *Current Opinion in Biotechnology*, 2014, **25**, 95-102.

Morgan J.T.., Wood J.A., Shah N.M., Hughbanks M.L., Russell P., Barakat A.I. and Murphy C.J., Integration of basal topographic cues and apical shear stress in vascular endothelial cells, *Biomaterials*, 2012, **33**, 4126-4135.

Pampaloni F., Reynaud E.G. and Stelzer E.H.K. , The third dimension bridges the gap between cell culture and live tissue, *Nat. Rev. Mol. Cell Biol*., 2007, **8**, 839-845.

Pasirayi G., Auger V., Scott S.M., Rahman K.S.M.P., Islam M., O'Hare L. and Ali Z., Microfluidic bioreactors for cell culturing: A review, *Micro and Nanosystems*, 2011, **3**,137-160.

Rhee S.W., Taylor A.M., Tu C.H., Cribbs D.H., Cotman C.W. and Jeon N.L., Patterned cell culture inside microfluidic devices, *Lab on Chip*, 2005, **5**, 102-107.

Tung Y.C., Hsiao A.Y., Allen S.G., Torisawa Y.S., Ho M. and Takayama S., High-throughput 3D spheroid culture and drug testing using a 384 hanging drop array. *Analyst,* 2011, **136**, 473–478.

van Midwoud P.M., Merema, M.T. Verpoorte E. and Groothuis G.M.M., A microfluidic approach for *in vitro* assessment of interorgan interactions in drug metabolism using intestinal and liver slices. *Lab Chip,* 2010, **10**, 2778–2786.

van Midwoud P.M., Verpoorte E. and Groothuis G.M.M., Microfluidic devices for in vitro studies on liver drug metabolism and toxicity, *Integr. Biol.,* 2011, **3**, 509–521.

Vyawahare S., Griffiths A.D., Merten C.A., Miniaturization and parallelization of biological and chemical assays in microfluidic devices, *Chem Biol.*, 2010, **17**, 1052-1065.

Wu M.H., Simple poly(dimethylsiloxane) surface modification to control cell adhesion, *Surface and Interface Analysis*, 2009, **41**, 1-16.

Young E.W.K. and Beebe D.J., Fundamentals of microfluidic cell culture in controlled microenvironments, *Chem. Soc Rev.*, 2010, **39**, 1036-1048.

Zambon A., Zoso A., Luni C., Frommer W.B., Elvassore N., Determination of glucose flux in live myoblasts by microfluidic nanosensing and mathematical modeling, *Integr Biol*, 2014, **6**, 277-88.

Zhou J. and Niklason L.E, Microfluidic artificial "vessels" for dynamic mechanical stimulation of mesenchymal stem cells, *Integr Biol (Camb)*, 2012, **4**, 1487-97.

CHAPTER 3

Development of microfluidic technology for circadian study on a chip

This chapter relates to design a development of microfluidic cell culture technology for circadian rhythms *in vitro* study. After an analysis of requirements and constrains necessary for the circadian study, the rationale for the design of microfluidic platform will be described. The microfluidic prototypes developed in this thesis, will be validated from biological point of view.
Feasibility of long-term cell culture within microfluidic platform will be provided.

3.1 Rationale of microfluidic platform design for the circadian study

Major components of energy homeostasis, feeding, glucose and lipid metabolism, are subjected to circadian regulation that synchronizes energy intake and expenditure with changes in the external environment.
For example it would be interesting mimicking the daily oscillation of hormones and metabolites during the prandial and postprandial cycle, for understanding the crosstalk between circadian clock and glucose metabolism.

Microfluidic technology looks to be a valid experimental strategy to achieve this complex model, for its capacity of delivering periodic extracellular chemical stimuli that mimics the metabolic and hormonal oscillations; moreover it allows to investigate the circadian molecular behavior by coupling analysis of circadian gene expression by quantitative techniques (qPCR) and optical microscopy (luminescence acquisition through luciferase gene-reporter assay), highlighting the mechanisms that ensure the synchrony between peripheral clocks and entrainment signals and the even those that lead to desynchrony.

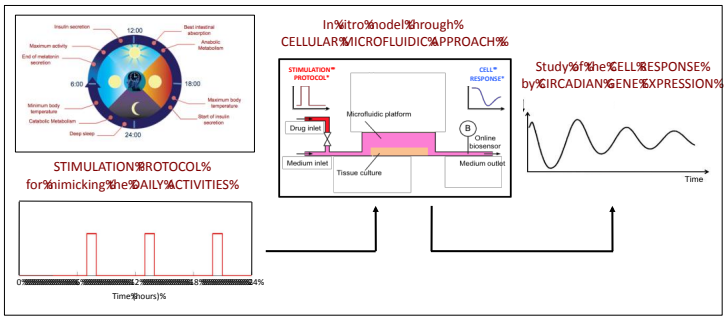

Figure 3.1. Schematic representation of principal units and operation necessary for developing circadian study on a chip.

3.2 Design of the microfluidic device: project strategies

The aim of this paragraph is to describe experimental requirements and consequently design solutions to effective develop a microfluidic technology for *in vitro* circadian study.

The design constrains related to specific circadian could be clustered in different classes:

1. experimental set-up (cell culture system, medium delivery and stimulation approach, portability);
2. experimental measurement of circadian target (type of read-out, integration with analysis equipments);
3. target of study (population or single cell behavior).

Figure 3.2 shows the different approaches of microfluidic technology in biological field.

Increase the automation degree, if on the one hand, ensures high sample throughput and flexibility on the other increases the complexity of the systems; opposite considerations can be made if the ease to use is examined.

It is obvious that low complexity-based devices are suitable during the preliminary and initial phases of study, for optimization of cell culture conditions, coating, seeding density and numbers of daily medium exchanges, in order to develop a robust *in vitro* cell culture model. Once these parameters are optimized, more complex platforms can be implemented in terms of miniaturization degree, integration with liquid handling systems and software, and parallelization for increasing the highthroughput of the biological experimentation.

The requirement to perform fast and cyclic perturbations, that mimic the in vivo physiological conditions, needs an accurate control of metabolites and, in general, entrainment factors, delivery with high temporal resolution; the advantage of being able to integrate the microfluidic device with liquid handling systems, off- and on-chip integrated, makes possible the implementation of different stimulation protocols in the same chip and a dynamically study the cell response.

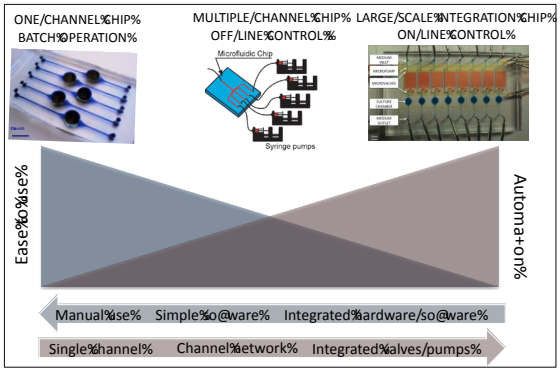

Figure 3.2: Schematic representation of different approaches of microfluidic technology in biology.

During this work three different experimental set-up, depending on the level of complexity, were used for specific phase of the thesis:

i) Platform A (one-channel chip) for fast biological validation;

ii) Platform B (multiple channel chip off-line liquid handling) for biological validation of cyclic perturbations;

iii) Platform C (large scale integration chip on line liquid handing) for multiple parallel independent biological experiments exposes to cyclic perturbations.

Platform A (one-channel chip)

The first prototype developed for the study of circadian clock on a chip (Figure 3.3) consists of ten indipendent parallel channels (18 x 1.5 x 0.2 mm) with well-shaped reservoirs for fresh medium upstream and tubing connection downstream.

In this case the procedures of coating, cell seeding, medium change and sample collection are made by hand held pipette.

This approach does not allow performing study of the system dynamics, but it is suitable to optimize all conditions necessary for a more complex analysis. It has been used for testing if the microfluidic technology is a valid tool for in vitro circadian rhythms study. It was used to optimize the mRNA extraction from the microfluidic cell culture for performing analysis of gene expression. The surface area of culture chamber, of 27 mm^2, is sufficient to perform downstream quantification of genetic material by qPCR technique, obtaining informations about the expression of circadian genes of interest at different time points.

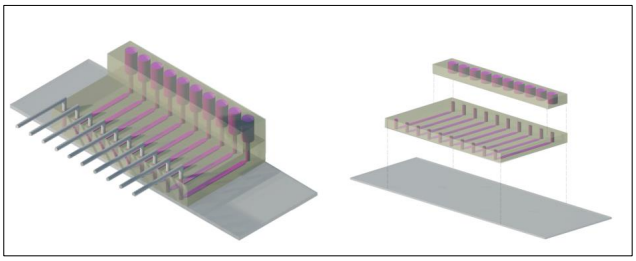

Figure 3.3: Schematic representation of Platform A. The exploded view show the single parts that composed the chip: a bottom glass slide serves as a sealing surface for cell culture adhesion and proliferation, the microfluidic channels serve to make better the cellular microenvironment and the upstream wells serve as a fresh medium reservoir.

Although, this approach was very easy to use, was shown to be very limited in term of readout; it is not able to generate data in efficient manner, especially in cases of elevate number of time points, given that the mRNA extraction involves a manual action by operator.
This issue reduces considerably the parallelization and the high throughput tipical of the microfluidic approach.

Platform B (multiple channel chip off-line liquid handling)
This device was developed in order to increase the efficiency in term of readout and at the same time to perform dynamic studies of circadian behavior by integration a liquid handling system off-chip.
Figure 3.4 shows the different component of this experimental set-up. This experimental setup is integrated within a luminescence microscopy thanks to the collaboration with the J.S. Takahashi lab (University of Texas - Dallas), one of the top laboratories that works in circadian field.

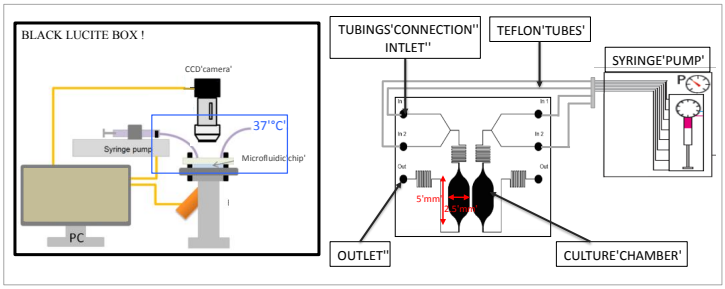

Figure 3.4: Schematic representation of the different part of Platform A. The chip connected to the syringe pump is placed on the stae of microscope for real-time bioluminescence imaging.

The chip consists of two parallel culture chambers (5.0 x 2.5 x 1.0 mm), whose surface is imposed by dimension of observation field of a 10x objective (5 x 5 mm), in order to monitor the circadian behavior in both chambers at the same time; every culture chamber exhibits two independent inlets, connected to the pump by teflon tubes, in order to perfuse the cells with different composition media.

The serpentine was design as gas-equilibration unit: the permeable PDMS will allow fast gas transport leading to equillibration of media in term of carbon dioxide concentration and oxygen concentration in the medium. This particolar function is not required when a buffer with costant pH was used.

This approach is a fair balance between the two approaches, single-channel and highly integrated chip. All procedures for cell culture integration (coating, cell seeding) are manually made, on the other hand after the connection to the pump, every procedure, such as medium delivery, is automatically managed.

The remote control of the liquid handling system syringe pump allows to implement any medium delivery and stimulation protocol with accurate temporal resolution.

Furthermore, the integration with a luciferase reporter assay ensures on-chip analysis of circadian gene expression by time-lapse microscopy. The microfluidic chip together to liquid-handling system was placed on the stage of an inverted microscope integrated with a CCD camera, allowing the real-time detection of the photons emission from the luciferase-reporter cell lines, whose intensity depends on level of gene expression of interest. Luminescence reporters have been used successfully in studies of circadian rhythms, allowing real-time measurements of circadian variations in gene expression (Yamazaki S., et al, 2005).

Using transgenic luciferase-reporter cell lines it is possible to monitor the genic expression the expression of a gene of interest in continuous. More details about luciferase reporter assay are reported in § 4.2.

This approach opens new perspectives in the chronobiology research and in particular in the study of crosstalk between circadian and metabolic systems.

The possibility to interact with the cellular microenvironment during the acquisition of circadian behavior by imaging permits to explore mechanisms still unknown.

Platform C (large scale integration chip on line liquid handing)

The last protype that we design for circadian study was an improvement of Platform A in term of high throughput.

A typical circadian experiment requires continuous monitoring of biological readouts over a period of time ranging between days and weeks. In order to provide a technology able to simultaneously investigate a number of different experimental conditions, we specifically design a multi-chamber microfluidic systems capable of performing indipendent experiments.

The possibility of fabricating miniature devices with complex fluidic architectures together with the flexibility of parallelization and automation ensures to develop a high throughput microfluidic platform for studying the circadian clock in peripheral tissues by metabolic cycles.

In particolar, we focus our design in a mLSI (microfluidic Large Scale Integration) that allows to investigate the effects of different physiological perturbations on the peripheral circadian clocks, over long-term culture, with high temporal resolution.

Moreover this device has to satisfy the requirements of high throughput in terms of readout both in sampling collection downstream culture chamber and real-time imaging analysis.

The device (Figure 3.5) developed and fabricated in PDMS by multilayer soft lithography techniques, consists of 32 individually addressable culture chambers (18 x 1.5 x 0.2 mm), with a volume of 5.4 ul each. In the chip there are also 16 bypass channels that allow flow channels wash out and changing media concentration without perturbation of the cell culture environment.

Individual liquid handling offers access to multiple and customized experimental conditions in terms of cell culture environments from chamber to chamber as well as a function of time.

Every procedure (coating of cell surface, cell loading, delivery and change of reagents for cell manipulation experiments) occurs sequentially in the 32 chambers, through a network of flow distribution, by 3 independent inlets, while the discard removal by 2 independent wastes.

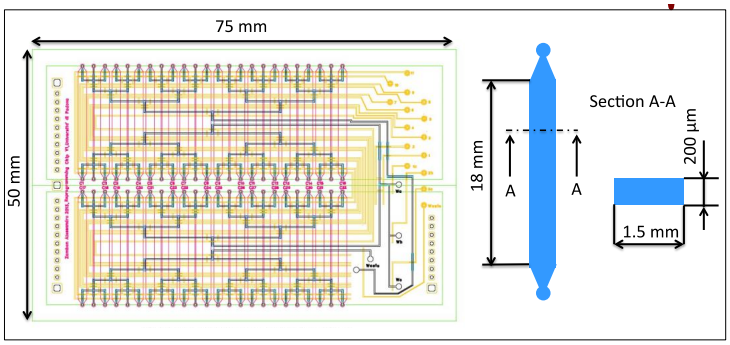

Figure 3.5: Schematization of the microfluidic chip, platform C. In yellow the control line; in green the distribution line; in purple di cell culture chamber.

Multilayer soft lithography have been used to fabricate the microfluidic chip (Gómez-Sjöberg R., et al, 2007; Unger M.A. et al, 2000) in order to obtain 3 PDMS layers; each one is separately cast from a different mold (Figure 3.6).
The three layers differ each other for its own specific functionality:

- the control layer (CL) provides the pneumatic control of the valves network;
- the flow layer (FL) allows the delivery of medium to the cell cultures;
- the chamber layer (CHL) allocates the cellspermitting the cell culture.

More details about the design and fabrication the microfluidic device are reported in Appendi A1.

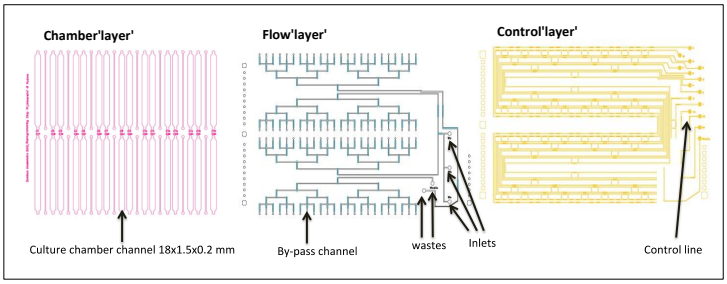

Figure 3.6. Schematization of the microfluidic chip, platform C. Detailed view of the three separated layers.

Before use microfluidic chip has been technically validated. First of all all the valves on the chip must close automatically together when the relative control line is pressurized. Secondly any delaminations have to be absent when an high pressure is applied (30 psi to the CL, 10 ps other layes) If the chip is robust enough for at least 24 hours it will become a valid candidate for a further experiment. Fluido dynamic has alse been tested in order to dertermine the correct residential time, volume, time delay for the sequence of operations necessary during the automatic liquid handling. The chip has been tested with food dyes.

3.3 Cell culture integration within microfluidic platform

The common elements of microfluidic devices developed in this thesis is the culture chamber and the procedures for providing robust long-term cell culture.
Biological issues have to be considered in order to define the main constrain for platform design.
The phase of cell integration is made manually by hand-held pipette or by automatized system in the large scale integration chip. This phase includes preliminary coating for enhancing adhesion of the cells to the glass. The tuning operation parameters are:

(i) *extracellular matrix chamber coating*

choosing the correct coating is critical in order to achieve an uniformcell seeding. In microfluidic devices, glass is often used as cell culture substrate because it can be permanently bonded to the PDMS chipby plasma activation. While glass is an attractive cell substrate material for PDMS microfluidic devices and microscope imaging, it can present many issues to cell adhesion. The cell substrate material allows cell attachment via adhesive proteins or peptides adsorbed from the cell culture media, or pre-immobilized cell attachment protein, such as gelatin and collagen (El-Ali J. et al, 2006).

(ii) *density of cell seeding*

this parameter had important effects on the process of cell expansion and cell-cell crosss talk in the microfluidic chamber; different cell densities lead to changes in cell-to-cell paracrine signaling that influences the proliferation of the culture; therefore the optimization of variable is crucial for the future of the experiment (Gómez-Sjöberg R. et al, 2007).

After cell culture integration, the chip was placed in a standard incubator, for temperature and gases control, providing a water bath to limit medium evaporation.

System automation makes the platform completely free to any manual operation and enables to perform dynamic perturbations of the cellular microenviromental.
In this stage, tubings, filled with sterile culture medium or stimulation buffers, are connected to the inlets or outlets of each channel, depending on the pump works in aspiration or expiration mode. The managment of medium exchanges and every protocol of stimulation for inducing cell proliferation and perturbation of cellular microenvironment occurs by *ad-hoc* software implementation for the specific experimental aim.

3.4 Biological Validation of microfluidic platforms

Both microfluidic devices were tested and validated for long-term cell culture (2-15 days)
The quality of proliferation is due to the system capability of cell integration and feeding turnover, that allowed to obtain an healthy confluent cell layer, as shown in Figure 3.7. Every protocol of culture medium change for nutrients delivery is reported in Appendix 1.
We have biological validated the microfluidic device by culturing human fibroblasts, as reported in Figure 3.7, obtaining proliferating long-term cell culture up to 15 days.
All microfluidic platforms were biologically validated by long term cell culture (Figure 3.7 and 3.8).

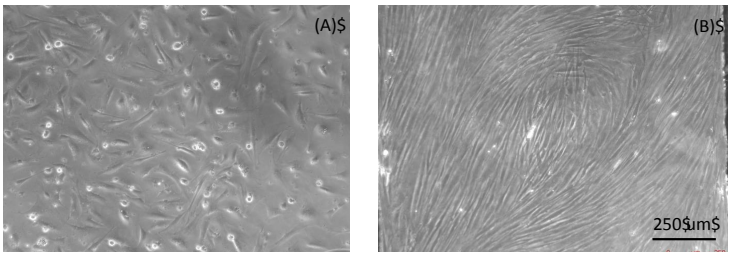

Figure 3.6: Phase image of human fibroblasts inside microfluidic culture chamber of Platform A, at different stage of confluence, respectively at 3 (A) and 10 days (B) from seeding.

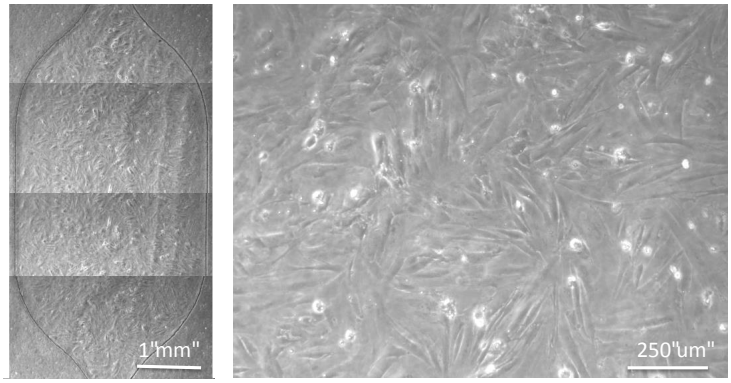

Figure 3.7: Human fibroblast culture integrated in microfluidic chamber of Platform B. On the a detail captureed with 20x objective.

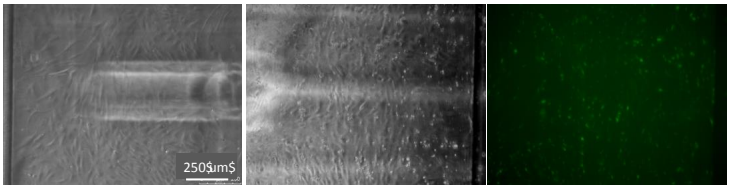

Figure 3.8: Human fibroblasts integrated in microfluidic chamber of Platform C.

3.4 Conclusions

In this chapter, the development of the following three types of microfluidic device derives from the bio-tecnological state of art of our lab and the improvements performed step by step in order to obtained a robust *in vitro* model for study of circadian rhythms: i) platform A for fast biological validation; ii) platform B for biological validation of cyclic perturbations; iii) platform C for multiple parallel independent biological experiments exposes to cyclic perturbations.

Moreover we design and development different liquid-handling system that could be classified into two different approaches:

- Off-chip liquid control, by syringe pumps
- On-chip liquid control, by pneumatic valves on-chip integrated.

Both approaches ensure a precise chemical and physical control of the microenvironment with temporal resolution.

Moreover, the microfluidic platforms used during this PhD thesis, have been developed in order to obtain devices as simple and easy-to-use as possible, while maintaining the following capability:

- long-term cell culture integration;
- accurate dynamic perturbation by chemical stimulus;
- quantitative analysis of circadian targets:
  - sample collection downstream culture chamber;
  - real-time analysis by optical microscopy.

References

El-Ali J., Sorger P.K. and Klavs F. Jensen K.F., Cell on chips, *Nature*, 2006, *442*, 403-411-

Gómez-Sjöberg R., Leyrat A.A., Pirone D.M., Chen C.S. and Quake S.R., Versatile, fully automated, microfluidic cell culture system, *Analytical Chemistry*, 2007, **79**, 8557-8563.

Unger M.A., Chou H.P., Thorsen T., Scherer A. and Stephen R. Quake–S.R., *Science*, 2000, vol 288, 113-116

Yamazaki S. and Takahashi J.S., Real-Time Luminescence Reporting of Circadian Gene Expression in Mammals*, Methods Enzymol*, 2005, **393**, 288–301

CHAPTER 4

Metabolic perturbations of circadian clock using conventional approach

In this chapter, we first described the conventional approach used for investigating the circadian behavior on *in vitro* cell culture in a Petri dish. These conventional methods were used for confirming the relevance of the entrainment signals, in particular both metabolic and hormonal signals, in the synchronization of a cell culture. Finally, the limitations of conventional methods as well the potential of microfluidic technological for the in vitro study of circadian clock of pheripheral tissus will be discuessed.

4.1 Molecular analysis of the circadian behavior in cell culture

Conventional approach for the analysis of circadian gene expression in cell populations is mainly based on two different analytical techniques:

- Realtime RT-PCR or quantitative RT-PCR (qRT-PCR);
- luminescence gene-reporter assay.

In the next paragraph, concise description of the methods will be provided.

4.1.1 Realtime RT-PCR

Real time RT-PCR (Reverse Transcription Polymerase Chain Reaction) or quantitative PCR (qPCR) is a molecular biology assay aimed at the precise quantification of the levels a target mRNA sequence relatively to a reference sequence. The reference sequence is usually chosen among "house-keeping" genes, which expression is assumed to be constant among the same cell type. RT-PCR is currently the most sensitive method of RNA detection available.

The assay is based on a two step process:

i) retrotrascription (RT) of the mRNA extract from a cell population to DNA molecules;

ii) amplification by Polymerase Chain Reaction (PCR) of the cDNA with quantification of cDNA amount at each amplification cycle (in "real-time").

The first step process it allows the conversion of the mRNA template extracted from the cell into a complementary DNA (cDNA) using a reverse transcriptase, which is an enzyme able to generate complementary DNA from an RNA molecules in a process termed reverse transcription. The cDNA could be sucessively used as a template for exponential amplification using PCR.

The step of cDNA amplification are based on standard PCR: after a first step of Taq polymerase activation by 95°C heating, cycles of denaturation (95°C) in which every double stranded DNA molecul is broken apart, primer annealing (the termperature of this step is primer specific) in which the primer sequences specific for the target gene anneal to the complementary sequences and elongation (60°C), allows the polymerase to synthetize the complementary strand of DNA beginning with the primer sequence. At every cycle fluorescence emission from the sample is acquired after the annealing step.

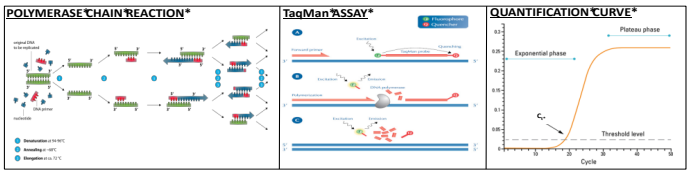

Figure 4.1: schematic description of the TaqMan assay used in this thesis

The cDNA quantification is performed mainly by fluorescence probes activated when interacting with the DNA double strand. At each amplification cycle, the amount of double stranded amplicons grows exponentially doubling at every cycle, and the fluorescence intensity of the sample grows proportionally until the plateau of the reaction is reached.

In this thesis, among different quantification methods we use the TaqMan assay. It is based on a pair of fluorophore-quencher covalently bound to a short sequence of DNA, so the fluoorescence of the probe is effectively quenched by the proximity of the two molecule. The DNA short sequence is designed specifically to bind to a strand of the target cDNA between the recognized primer sequence. During the amplification step, the Taq polymerase will digest the probe while synthetising the new DNA strand, separating the fluorophore from the quencher, allowing the fluorescence to be emitted. The fluorescence intensity will increase linearly with the amount of new DNA strands synthetized. The specificity of this assay is due to the direct dependence of the probe digestion on the amplification of the specific target cDNAsequence.

The intensity of the fluorescence emitted during Real-Time PCR is correlated to the amount of DNA product formed. Figure 4.1 show a model of amplification plot used for the quantification.

It is important to underline, that the TaqMan assay used in this thesis ensures high sensitivity and high specificity excluding the probability of aspecific mRNA sequance detection and other possible technical artefact.

The quantification is based on the cycle number (Ct) in which the specific fluorescence produced by the genuine amplification of the target gene surpasses in intensity the non-specific background fluorescence.

Because specific errors can be introduced (due to difference in the starting amount of RNA, quality of RNA or difference in efficiency of cDNA synthesis and PCR amplification), a cellular RNA is simultaneously amplified with the target gene, wich serves as an internal reference against which other RNA values can be normalized.

The most common gene used for the normlization, termed housekeeping genes, are ß-actin, a cytoscheletal protein and glyceraldehyde 3-phosphate

dehydrogenase (GAPDH), a glycolitic enzyme. In this thesis the housekeeping gene used is GAPDH.

The amount of the target gene in the sample, normalized to an endogenous heousekeeping gene and relative to the normalized calibrator, is given by $2^{-\Delta\Delta Ct}$, where

$$\Delta\Delta Ct=\Delta Ct \text{ (sample)}-Ct(\text{calibrator})$$

and ΔCt is the Ct of the target gene subtracted from the Ct of the housekeeping gene.

In this work, it was used the ABIPrism 7000 Sequence-Detection-System (Applied Biosystems) and TaqMan probes (Applied Byosystem) for performing Real-Time PCR**.**

In conclusion, qRT-PCR allows accurate and quantitative analysis of multiple genes in the same time. On the other hand, it require to prepare large number of samples (at least two for each time point) given that the mRNA extraction from the cell culture entails cell destruction. For these reasons, the study of dynamic response of gene expression to biochemical perturbations by Real Time PCR is associated to a huge experimental effort.

4.1.2 Luminescence genetic-reporter assay

Genetic reporter systems have contributed greatly to the study of gene expression and regulation and they are most frequently used as indicators of transcriptional activity in cells. Typically, a reporter gene is joined to a promoter sequence of the gene of interest. The cells are assayed for the presence of the reporter by directly measuring the reporter protein itself or the enzymatic activity of the reporter protein. In an ideal case, the meaurable quantitative activity of the reporter protein is strivtly correlated to the level of expresion of the gene of interest.

Thus, in contrast to qPCR, the luminescence genetic-reporters assay allows temporally-resolved quantification of a gene expression. For this reasons, this approach hasbeen used successfully in studies of circadian rhythms allowing real-

time measurements of circadian variations in gene expression. This continuous noninvasive measurement of reported gene from cell and tissue cultures could result in drastic reduction in the number of parallel experiments required with qPCR (Yamazaki S., et al, 2005).

On the other hand, becasuse the complexity of genetic manipulation and the limied possibility of simultaneously measuring more than one reporter protein, only single gene expression can be evaluated (respect to multiple gene expression obtained from qPCR).

Using luciferase as reporter protein in transgenic luciferase-reporter cell lines, derived by genetic engineering technology (luciferase *knockin* mice or stable plasmid transfection), it is possible to monitor the genic expression of a gene of interest in continuous manner by acquiring the luminescence signal from cell culture.

Luciferase reporter gene

A gene consists of multiple functional parts, including the coding region that specifies the protein to be made and regulatory elements that control the transcription of the coding region.

The luciferase reported gene are obtained fusing the putative regulatory elements to a reporter gene and monitoring the amount of the reporter protein expressed. Because reporter expression is under the control of the fused genetic elements, reporter expression is directly correlated with the activity of the regulatory elements (Figure 4.2).

Transfering the luciferase reporter construct in a cell culture is relatively simple, because occurs by normal transfection procedures.

Details about the a virus production are reported in Appendix A3.

Two agents are essential for the bioluminescent reaction to occur:

- luciferase, the enzyme that catalyzes the reaction,
- the luciferase substrate.

Chemical energy from ATP is converted to light by an enzyme-catalyzed reaction whose reactants are luciferin, adenosine triphosphate (ATP), and oxygen (O2); the enzyme luciferase catalyzes the reaction. The final products of this reaction are

oxidized luciferin ("oxyluciferin"), adenosine monophosphate (AMP), inorganic pyrophosphate (PPi), carbon dioxide (CO2), and light (Figure 4.2).

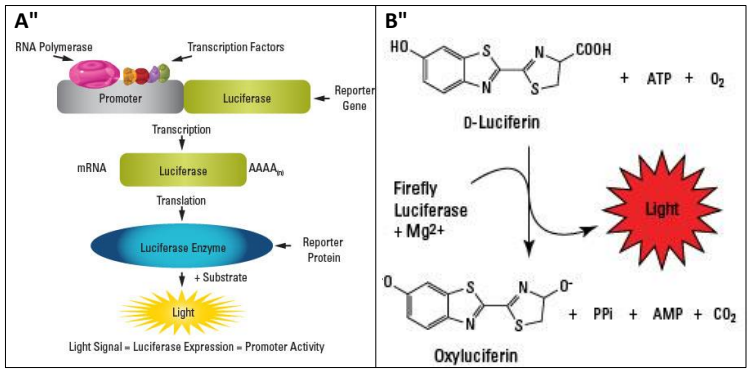

Figure 4.2: (A) The schematic representation of the the luciferase reported gene; (B) The bioluminescence reaction.

Photons emitted from bioluminescent reactions are typically measured using a photomultiplier tubes (PMTs) or luminescence imaging systems. In both cases, high sensitive detectors are necessary.

During the thesis, we made a number of tentatives for adapting existing detector or imaging systems to the luminescence acquisition from luciferase-reporter cell lines. All these tentative has been carried out at the Venetian Institute of Molecular Medicine (Padova). Bioluminescence systems, such as conventional plate reader equipped with photomultiplier tubes, did not have the proper sensitivity to acquire robust luminescence signals from microfluidic cell culture. On the other hand, microscope imaging systems equipped with high performance cameras for high sensitive imaging and image analysis (Second generation CMOS camera with sCMOS sensor) showed strong limitations in the long-term acquisition necessary for circadian study.

To properly carachterize the possibility of using microfludic cell culture in combination with luciferase-reporter cell lines for circadian study, we start a

collaboration with Prof. Joseph S. Takahashi (University of Texas Southwestern Medical Center, investigator at the Howard Hughes Medical Institute). Takahashi's research group discovered the genetic basis for the mammalian circadian clock in 1994 and identified the Clock gene in 1997 and developed for the first time circadian clock gene luciferase-reporter.

Because the huge experience and the facilities available in the Takahashi'lab, I spent six months as visitng scientist at University of Texas Southwestern under the supervision of Prof. Joseph S. Takahashi for properly testing the potential of microfludic approach in circadian study using luciferase-reporter cell lines.

For the work of the thesis, two main equipments were used: an automatized Petri dish luminescence reader and a luminescence microscope.

The LumiCycle (Actimetrics Inc., Evanston, IL) is a luminescence reader composed of 32channel carousel unit holding one 35mm diameter petri dishand it was used for the fast screening circadian experiments. In this device, light output is measured by photon-counting methods, integrating, or measuring the area under the chemical reaction's light emission curve for a set period of time. This unit has no thermo-controller and needs to be placed in an incubator at 37°. One of the unique features of this unit is that it is designed for multiusers; loading new samples, taking out old samples, and/or pharmacological stimulations can be done without disrupting the recordings on other channels.

Spatial resolution luminescence imaging, which is particular adapted to properly carachterized microfludic luminescence signals from microfludic cell culture, were performed using luminescence inverted microscope. Although luminescence from luciferase reporter is extremely weak, using high-sensitive cooled CCD cameras it was possible to detect both population and single-cell signal. In particular, series 600s camera made by Spectral Instruments, containing a black-thinned CCD thermoelectrically cooled to -90 °C with a rated quantum efficiency of ~92% at 560 nm was used. The microscope was equipped with thermo controller and dark cabinet for avoiding any light contaminations.

4.2 Synchronization of circadian rhythms

Single cell studies showed that closely spaced cells in the same culture did not have similar phases, implying a lack of functional coupling among cells (Welsh D.K. et al, 2004).

Many different stimuli are capable of initiating rhythmicity in cultured cells. These include serum (Balsalobre A. et al, 1998), dexamethasone (Balsalobre A. et al, 2000), forskolin (Yagita K. et al, 2000), fibroblast growth factor (FGF), and epidermal growth factor (EGF) (Akashi M. et al, 2000; Balsalobre A., Marcacci L. et al, 2000) and glucose (Hirota T. et al 2002); Thus, they show to be phase coordinators (Figure 4.3), as SCN for the entire organism, preventing internal desynchronization among persistently rhythmic peripheral clocks (Nagoshi E. et al, 2004; Leise T.L et al, 2012).

The damping of the oscilatory behavior of circadian gene expression is correlated to the uncoupling of single cell oscilators. Thus, we could be able to reinitiate rhythmicity in damped cultures by delivering specific entrainement signals or by simply changing the medium (Figure 4.3). In this latter case, this reinitiation could be due to removal of toxic substances in the old medium, replacement of depleted critical components, or simply to the shocks associated with the medium change (e.g., temperature, pH, and mechanical agitation). Any or all of these stimuli could act to restart oscillators that had stopped or to resynchronize multiple oscillators within the tissue (Yamazaki S. et al, 2000).

These are important aspects to be considered in synchronization of circadian rhythms within microfluidic cell culture, which requires high frequency of medium delivery.

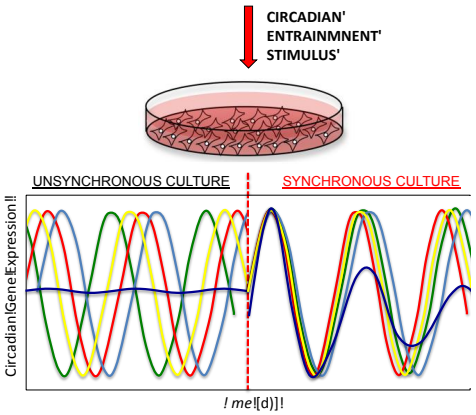

Figure 4.3: Schematic rapresentation of synchronization of circadian rhythms of a cell culture imposing a entrainment signal. Before the synchronization the self-sustained circadian rhythms of the single cells are not in phase each other, resulting in a low amplitude of the population rhythm (blue curve); after synchronization the cells are synchronized to the same frequence and the average signal (blue curve) displays oscillatory behavior.

We used some of the synchronization treatments citated earlier (dexamethasone, serum shock, glucose and insulin). More details are reported in Appendix A2.

As preliminary results we synchronized the circadian rhythm of a human fibroblasts cell culture in a Petri dish using dexamethasone (1nM) and serum shock (10% FBS contained in culture medium). Although both entrainment stimuli enable to induce a robust circadian cycle, in our hand, dexamethasone shock produces more robust 24 h rhythms of gene expression in the cell culture. Figure 4.4 shows the mRNA accumulation profiles of *BMAL1* a *PER2* analyzed by qPCR technique, during the 48 hours following the dexamethasone shock; 12 time points were analyzed, for each time point n=3 independent measurements were performed and each measurement is based on n=2 technical replicates (qPCR was performed in double).
The expression of *BMAL1* and *PER2* mRNA is rhythmic and in antiphase of 12 hrs, according the mechanism of transcription/translation feedback loop that regulates the molecular circadian clock.

These results are consistent with the in vitro models reported in literature (Basalobre A. et al, 2000).

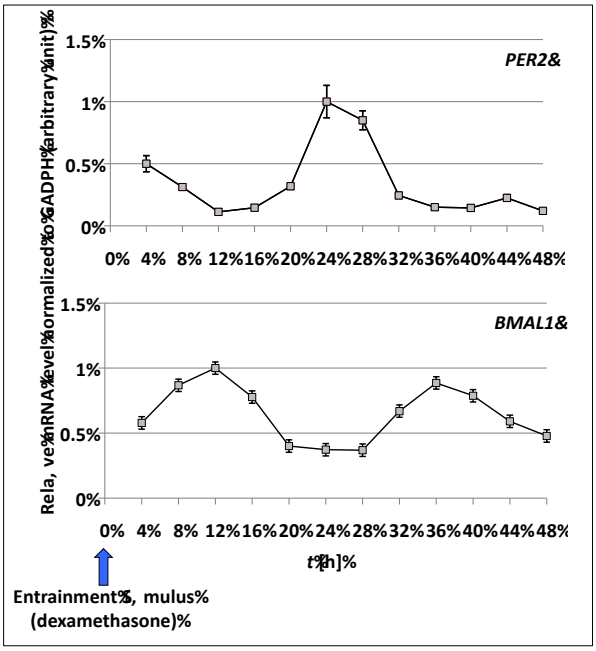

Figure 4.4: Temporal profiles of clock gene expression, *BMAL*1 and *PER*2, in human fibroblasts, after the synchronization (t=0) with dexamethasone. The mRNA level of clock genes was normalized to housekeeping gene (GADPH) expression. Values represent the mean ± SD (n = 3 per time point).

The qPCR analysis is very accurate and sensitive analysis with the advantage to be able to study the expression of any gene of interest; on the other hand, it implicates that the experiments should be stop to extract mRNA samples from the cell culture and it makes impossibile to have high temporal resolution of dinamics of circadian gene oscillation.

For these reasons, we used the luciferase reporter gene assay enables to monitor the rhythms of circadian genes in non invasive manner and to measure real-time its expression, allowing for evaluation of the persistence and dynamics of molecular rhythms.

Necessary condition for following this approach is to use a lucifersase reporter cell line.

In this regard we operated in two different way using:

- a primary *Per2*::Luc (*Per2* Luciferase Reporter) cell line derived from trangenic mice, that show with a DNA construct in which the promoter of the *Per2* gene is fused to the luciferase reporter gene were made for monitoring the circadian oscillation of the transcription;
- stable transfection of cell lines using lentivirus-mediated gene delivery. The lentiviral vector system is superior to traditional methods such as transient transfection and germline transmission because of its efficiency and versatility: it permits efficient delivery and stable integration into the host genome of both dividing and non-dividing cells. Once a reporter cell line is established, the dynamics of clock function can be examined through bioluminescence recording.

  In particolar we produced a lentivirus for the Bmal1::luciferase (Bmal1::Luc) gene reporter, that can be used for generate luciferase cell lines both in mouse and human cells.

  The procedures of the virus production and the generation of Bmal1::Luc reporter lines are described in Appendix A3.

Figure 4.5 shows a stable oscillation of *Per2*::Luc cell line after a circadina entrainment by serum shock, with a period of [22.99 ± 0.06] h (n=3).

The Per2::Luc cell culture is a clonal cell line (#128 clone of *p53* mutant immortalized ear fibroblasts) derived from *Per2*::Luc *knockin* mice.

The luminescente signals acquired by LumiCycle every 10 min.

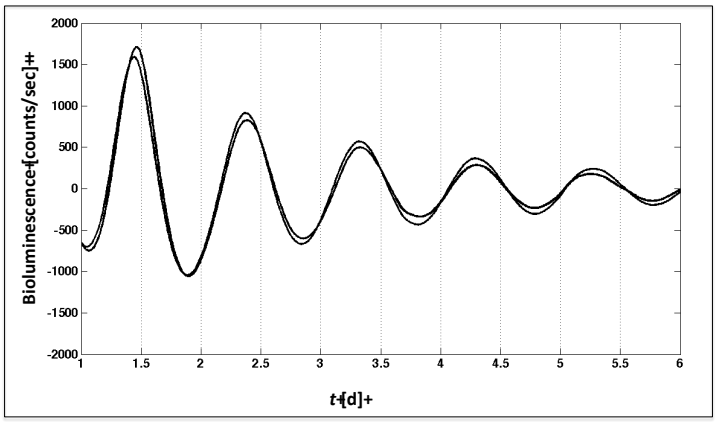

Figure 4.5: Long-term luminometer recording of luminescence in 3.5 mm from two culture dishes containting *Per2*::Luc mouse line, after serum shock (10% FBS).

The long-term acquisition of circadian gene expression allows to investigate many parameters of interest, such as period, amplitude and damping rate of the oscillation.

This analysis, performed by LumiCycle data analysis program (Actimetrics, Evanston, IL; courtesy of D. Ferster), is obtained after to subtracted the baseline to the raw data.

The baseline subtraction is made to avoid the frequent drastic changes in the baseline in the first few days in culture, that are also sample-dependent.

Period calculation is obtained from baseline-subtracted data by the 'sin fit' method.

This function identifies the largest sinusoidal component in the data by calculating a power spectrum by the following equation (1) as a function of a range of closely spaced frequencies:

$$P(f) = \sum_{i=1}^{N} Y(t_i)\sin(2\ ft_i) \div^2 + \sum_{i=1}^{N} Y(t_i)\cos(2\ ft_i) \div^2 \qquad (1)$$

The power, *P(f)*, is calculated by performing the summations at each frequency, *f*, over all *N* data points comprising the baseline-corrected data series, *Y(t)*, at each

of the corresponding time points, t_i. The period ($1/f_{peak}$) corresponding to the peak power is selected as the dominant period, after which the associated optimal phase is calculated.

The amplitude and the damping rate are determinated fitting the data to a sine wave multiplied by an exponential decay factor. The damping rate (d) is the time constant of the following exponential fit:

$$Y=A\{[\sin(2\pi f+\Phi)][\exp(-t/d)]\} \quad (2)$$

where d is the damping rate, Y is the luminescence (counts/min), A is the amplitude, f is the frequency of the sine wave, Φ is the phase of the oscillation and t is time. The data are fit to a low-order polynomial to get a baseline, which is thensubtracted from the raw data. A Fourier transform is performed to find the dominant frequency and phase. The time points for the peaks and troughs of the dominant sine wave are taken from the baseline-subtracted data, and the time points are then fitted to an exponential decay, which gives the amplitude (A) and the time constant of the damping (d). Damping rate (d) is the number of days required for the amplitude of the rhythm todecrease to 1/e (~=36.79%) of the starting value.

For instance, the values of amplitude and damping rate, relative to Figure 4.5 are of 2490 ± 180 counts/s and 2.2 ± 0.2 days, respectively.

4.3 Metabolic and cyclic perturbations of circadian clock

Motivation

The main biological hypothesis of this thesis is that the daily physiological fluctuations of hormones and metabolites can affect the circadian behavior can be affected from metabolic fluctuations.

Emerging evidences suggests that not only the circadin clock controls the metabolic homeostasis but also metabolic processes feed-back into the circadian clock can influence clock gene expression (Kovac J. et al, 2009). It was shown that rhythmic feeding is both necessary and sufficient to drive the

circadian expression of liver genes (Hara R. et al 2001; Kornmann B. et al 2007) and that by restricting food intake to the rest phase (i.e., the light period for nocturnal animals) it is possible to set the peripheral clocks and the central SCN clock to two different time zones, 12-h apart.

Blood glucose homeostasis can be seen as a paradigm of the circadian control of energy metabolism. Its concentrations in the blood are highly rhythmic because of changes in insulin sensitivity and insulin secretory capacity of endocrine pancreas.

Indeed, whereas during the activity/feeding period blood glucose is mainly of dietary origin, during the resting/starvation period glucose is progressively recruited from endogenous glucose production in the liver to maintain blood glucose levels within a relatively narrow range. In this process liver glycogen content undergoes large daily fluctuations to sustain blood glucose levels, as glycogen synthesis and degradation are specifically recruited during the activity/feeding and resting/starvation periods, respectively (Peret J. et al 1973; Armstrong, S., 1980).

Therefore, using conventional approach, we tested the possible effects of cyclic perturbations on circadian behavior, first, imposing different levels of glucose, and then modulating levels of glucose and insulin together.

Figure 4.6 shows the schematic protocol of the 4 cyclic glucose and insulin perturbation; that can be summarized in two phase:

- stimulation phase, by alternate cycles of high (20 mM) and low levels (2 mM) of glucose every 12 h, for three days;
- recording phase, in which the bioluminescence signal is acquired by lumicycle in two different constant concentration of glucose, high or low. No media changes are performed during recording phase.

The perturbations by glucose fluctuations (before the recording) studied are 4:

1. ciclyc of 12 h **H**igh glucose medium pulse - **12** h **L**ow glucose medium pulse (HL 12h);
2. ciclyc of 12 h **L**ow glucose medium pulse - **12** h **H**igh glucose medium pulse (LH 12 h);

3. ciclyc of 12 h **H**igh glucose medium pulse - **12** h **H**igh glucose medium pulse (HH 12h);
4. ciclyc of 12 h **L**ow glucose medium pulse - **12** h **L**ow glucose medium pulse (LL 12 h);

moreover, circadian response to each of these stimulations was studied both in low (-L) and high (-H) glucose level, during the recording phase.

During the stimulation phase we used chemical serum-based media, istead of animal serum (FBS- fetal bovine serum), whose nutrients concentration is random because is animal-dependent; this strategy allows to make sure of the medium composition, given that we want to manipulate its composition without background effects.

The chemical serum used is B27 (gibco-lifetechnologies).

The exact composition of the different media used for these experiments is reported in Appendix A2.

Afterwards we stimulated the cell culture by cyclic perturbations, modulating glucose and insulin together; in particular we decided to use high glucose concentration medium (20 mM) with 50 nM of insulin and low glucose medium (2 mM) without insulin.

The experiment aims to understand if 'oscillating' hystory before the recording, that mimics mebabolic and hormonal fluctuaction, can alterate the circadian clock.

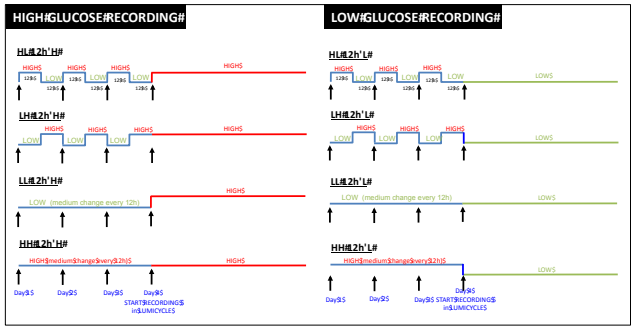

Figure 4.6: Schematic representation of the experimental strategy with two different conditions of recording, in high and low glucose level, respectively.

Oscillatory glucose perturbation in constant insulin level

As cellular model we used #128 *Per2*::Luc cell line. Brifely they were seeded in confluent layer the day before the stimulation protocol, in DMEM 10% FBS and with 25 mM of glucose. The bioluminescence signal was acquired by LymiCycle in continuous for 6 days.

Because the conventional glucose concentration used in the experiment is high (25 mM), we decided to considered the condition HH 12h-H as control for all the cases.

Figure 4.7 shows the circadian oscillation of *Per2* gene in the 4 conditions of perturbation, in high glucose recording for 6 days; the signals presents a stable period for all the acquisition and a robust amplitude for almost all 6 days.

There are not significant difference in term of period and amplitude among all conditions.

Consequently the shift phase, calculated as the absolute value of time different peak-to peak between each condition compared to the control (HH 12h-H), results trascurable, given that it is around 0.5 h in average for all protocols.

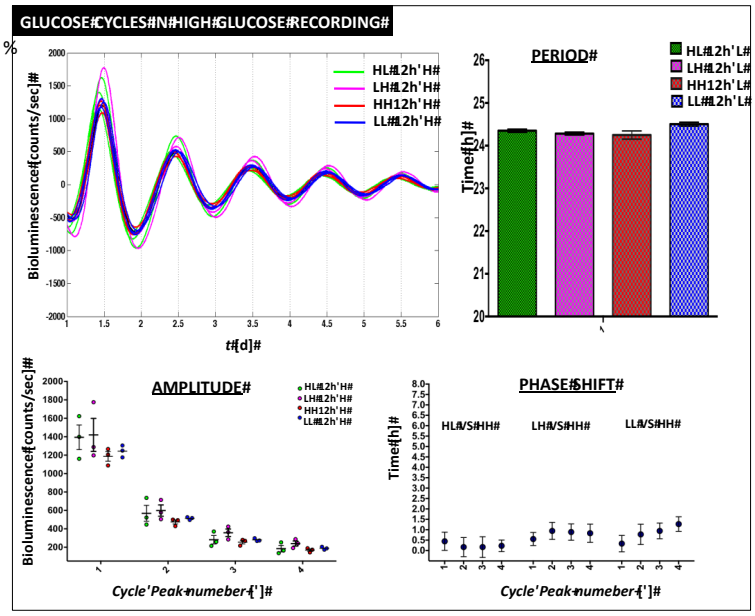

Figure 4.7: *Per2* luminescence rhythms after alternate cycles of two different glucose levels (20 mM and 2 mM); 6 day luminescence recording was performed in high glucose condition (20 mM). Period, amplitude and phase shift are reported in the 3 integrative panels. Each experiemental condition is based on n=3 independet biological replicates.

The experiment was replicated in the same way for the first part of cyclic perturbation but using a low glucose medium during the recording phase.

Figure 4.8 shows the *Per2* luminescence acquired for 6 days; there is not relevant difference among the perturbations in period and amplitude, and also the phase shift, calculated compared to the control condition (HH 12h-L) remains below 1.5 h.

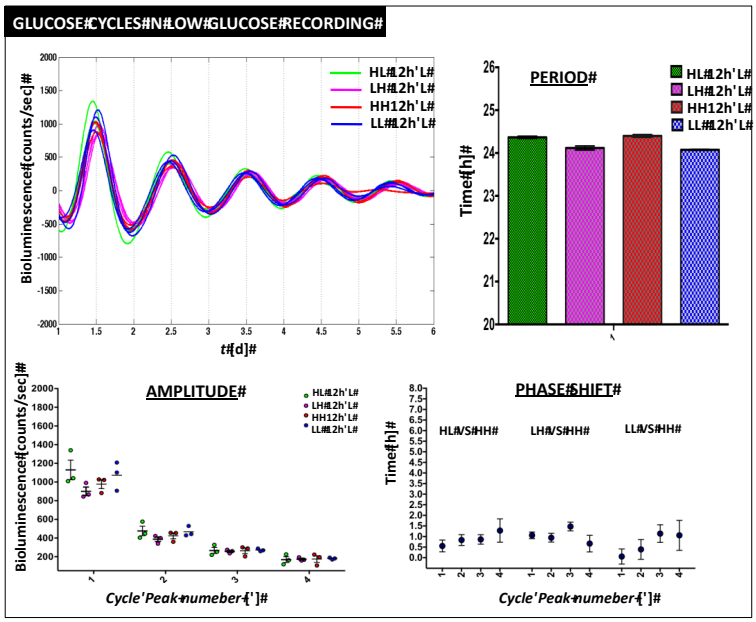

Figure 4.8: *Per2* luminescence rhythms after alternate cycles of two different glucose levels (20 mM and 2 mM); 6 day luminescence recording was performed in low glucose condition (2 mM). Period, amplitude and phase shift are reported in the 3 integrative panels. Each experiemental condition is based on n=3 independet biological replicates.

Oscillatory glucose and insulin perturbation

From previously experiments (Figure 4.7 and 4.8) it is clear that the different glucose pre-treatments have not strongly influenced the circadian behavior.

Considering that the glucose changes in the blood in postprandial state are closely related to insulin level, we decided to modulate both glucose and insulin. Specifically, we used a chemical serum without insulin, that was added (50 nM) just in the medium with high glucose (20 mM).

Because the insulin experiments require insulin-free media, we seeded the #128 *Per2*::Luc cell line in media without insulin three day before starting the stimulation.

The temporal expression patterns of *Per2* acquired after the 4 cyclic glucose-insulin perturbations (Figure 4.9), in high glucose-insulin recording, show to be sensitive to the different perturbations. In particular, while the quantitative analysis shows that the period was not affected by the cyclic metabolic and hormonal perturbations, the amplitude and the phase shift seem differentially perturbed in LH 12h-H conditions.

The amplitude of the first peak of *Per2* in LH 12h-H is relatively lower than the control amplitude (HH 12h-H), with $p<0.05$.

The effect of perturbations is more evident in the phase shift graph; particular the LH 12h-H stimulation provides an increasing phase advance a in the range of [4.5 ± 0.2 : 5.8 ± 0.5] h between peak 1 and 4, compare to the control (HH 12 h-H), with $p<0.0001$.

The LL 12h-H also produce smaller positive phase shift in the range of [2.389 ± 0.22 : 2.67 ± 0.32]h between peak 1 and 4, compared to the control ($p<0.01$).

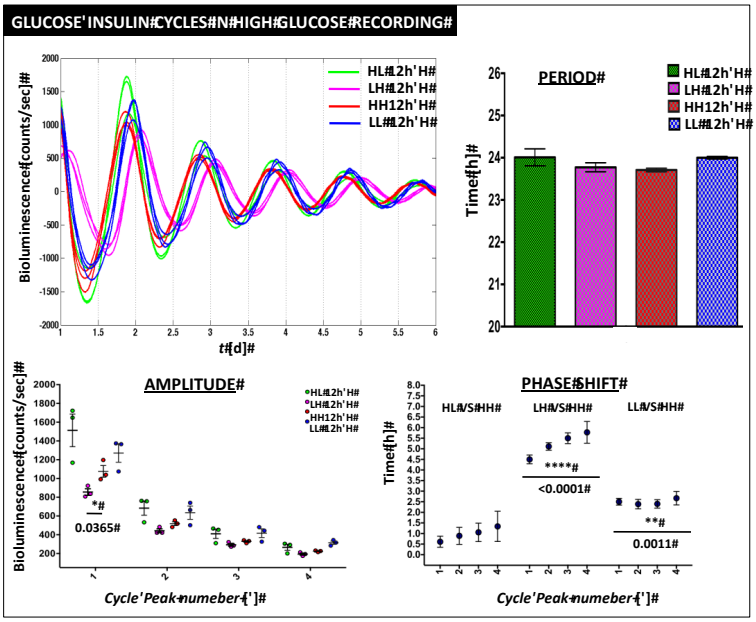

Figure 4.9: *Per2* luminescence rhythms resulting by alternate cycles of two different glucose and insulin levels (20 mM- 50nM and 2 mM- 0 nM glucose-insulin); 6 day luminescence recording was performed in high glucose condition (20 mM). Period, amplitude and phase shift are reported in the 3 integrative panels. Each experimental condition is based on n=3 independe biological replicates.

The experiment was replicated in low glucose medium, without insulin, during the recording phase and the *Per2*::Luc bioluminescence signals are shown in Figure 4.10. As for the previous case (Figure 4.9), the glucose and insulin perturbations induce some alteration in the circadian behavior.

In particular, the period of LH 12h-L is significantly longer (23.3 ± 0.3 h) compared to the control, HH 12 h-L, (25.0 ± 0.5 h), with $p<0.01$.

Moreover the quantification of amplitude showes relevant difference between the HL 12h-L and HH 12h-L ($p<0.05$).

The phase shift remains the parameter that feels more the effect of the cyclic perturbations imposed.

In particular LH 12h-L exibits a phase advance in a range of [3.55.33 ± 0.40 : 4.83 ± 0.58] h between peak 1 and 4, compared to the control.

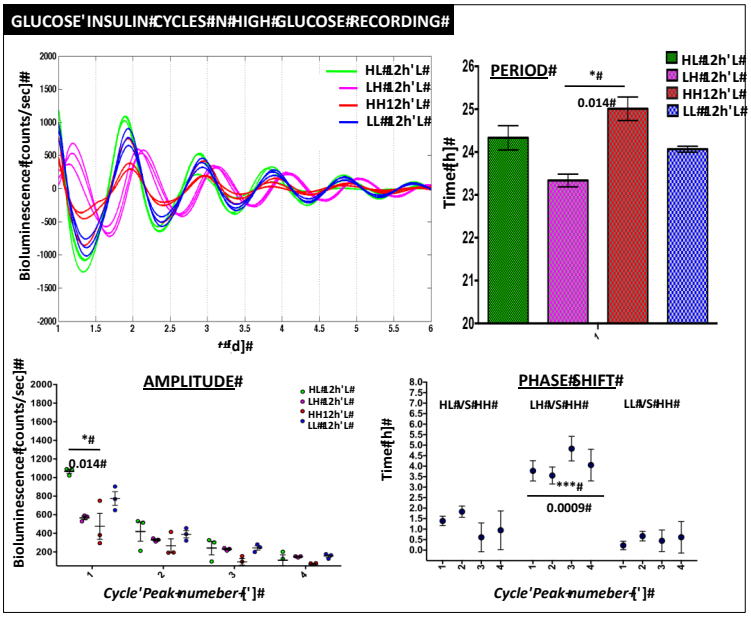

Figure 4.10: *Per2* luminescence rhythms resulting by alternate cycles of two different glucose and insulin levels (20 mM- 50 nM and 2 mM- 0 nM glucose-insulin); 6 day luminescence recording was performed in low glucose condition (2 mM). Period, amplitude and phase shift are reported in the 3 integrative panels. Each experimental condition is based on n=3 independent biological replicates.

In order to have a complete vision of the effect of each cycle perturbation on the circadian behavior, it was plotted the phase shift at the third cycle-peak, for all conditions.

Statistic analysis shows that the LH 12h-H and LH 12h-L stimulations produce a very high phase shift on the *Per2* expression, in condition of glucose and insulin fuctuation.

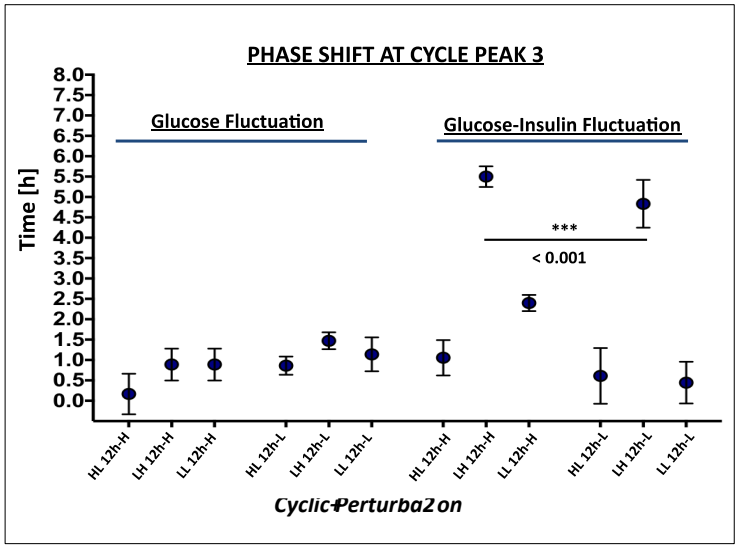

Figure 4.17: Phase shift produced from all conditions at the third cycle peak.

All together these results stronlgy suggest that the oscillatory glucose variations alone, it is not sufficient for elicting circadian resyncrhonization on cell culture derived from pheripheral tissues. The phase shift can only altered when glucose and insulin are oscilatory delivered together. However, the reason why only in the LH 12h condition we observed reproducible phase shift require more specific study.

4.4 Conclusions

In this chapter, first of all, we describe two different molecular methods, qPCR and luciferase reporter gene assay, selected for analysing the temporal oscilatory behavior of the circadian genes. We also discussed about the advantages of using qPCR for quantitative multiple circadian gene expressions

for a single time point or the efficacy of following the temporal dynamic of single circadian gene using luciferase reporter gene assay.

Both metodology were tested mesuaring a cyclic dynamic oscillation of circadian rhythms on cell culture derived from pheripheral tissues in conventional Petri dish.

In order to rational understand the correlation between metabolite and hormone fluctuations and the circadian oscilators on cell culture, we design a set of experiments in which we expose cell culture to 12 h cyclic perturbation.

The results cleary show how oscillatory perturbation of glucose and insulin togheter could affect the circadian bheavior with particular influence on the phase shift. These date are quite important in the context of this thesis because they are actually confirming that the hypothesis of metabolic perturbation on circadian rhythms could be relevant in peripheral tissue.

This data provide only some experimental evidence, but new more experiment and deeply study between cyclic perturbation a clock bheavior are needed.

However what is also emerged from the measure reported in this chapter is the militation of the conventional technology in performning new experimetal investigations.

For instance, it would be of paramount importance to perturb the system with specific daily metabolic fluctuactions and hormonal oscillations while simulatneously recording the circadian oscillatory behaviors.

Moreover, the conventional cell culture technology, which is based on batch experiment management by manual medium chenge, allow only couple of cyclic perturbations within the 24 daily cycle. In contrast, the oscillatory behavior of metabolic and hormonal stimuli in the body are based on multiple oscillations during the day time, which are possible to reproduced without the integration of automatized approach within cell culture technology.

In conclusion, from this chapter, it is clear that the lacking of simultaneos perturbation recording systems and the low level of automatization in the conventional cell culture methods represent a strong limitation to further progress in circadian field. In particular, these main limitations strongly reduce the capacity of investigation, compromizing the rational understanding of the mechanistic correlation between metabolic perturbation and genetic oscillation in pheripheral tissues.

The microfludic tehcnology could overcome all these limitation and open a completely new perspective in circardian study. The proof of concept that the microfluidic technolgy could be sucesefully used in the circadian experiments are described in the next chapter.

References

Armstrong, S., A chronometric approach to the study of feeding behavior, *Neuroscience and Biobehavioural Reviews*, 1980, **4**, e53.

Akashi M. and Nishida E., Involvement of the MAP kinase cascade in resetting of the mammalian circadian clock, 2000, Genes & Development, 14, 645-649.

Balsalobre A, Brown SA, Marcacci L, Tronche F, Kellendonk C, Holger M. Reichardt H.M., Schutz G. and Schibler U., Resetting of circadian time in peripheral tissues by glucocorticoid signaling, *Science*, 2000, **289**, 2344–2347.

Balsalobre A., Marcacci L. et and Schibler, Multiple signaling pathways elicit circadian gene expression in cultured Rat-1 fibroblasts, *Science,* 2000, **10**, 1291–1294.

Balsalobre A., Damiola F. and Schibler U., A Serum Shock Induces Circadian Gene Expression in Mammalian Tissue Culture Cells, *Cell*, 1998, **93**, 929–937.

Hara R., Wan K.K., Wakamatsu H., Aida, R., Moriya, T., Akiyama, M., et al., 2001. Restricted feeding entrains liver clock without participation of the suprachiasmatic nucleus. *Genes to Cells*, **6**, 269e278.

Hirota T., Kon N., Itagaki T., HoshinaN., Okano T. and Fukada Y., Transcriptional repressor TIEG1 regulates Bmal1 gene through GC box and controls circadian clock work, *Genes to Cells*, 2010, **15**, 111–121.

Kornmann, B., Schaad, O., Bujard, H., Takahashi, J.S., Schibler, U.. System-driven and oscillator-dependent circadian transcription in mice with a conditionally active liver clock, *PLoS Biology,* 2007, **5**, e34.

Leise T.L., Wang C.W., Gitis P.J. and Welsh D.K., Persistent Cell-Autonomous Circadian Oscillations in Fibroblasts Revealed by Six-Week Single-Cell Imaging of PER2::LUC Bioluminescence, *Plos ONE*, 2012, **7**, e33334.

Nagoshi E., Saini C., Bauer C., Laroche T., Naef F. and Schibler U., Circadian Gene expression in individual fibroblasts: cell-autonomous and self-sustained oscillators pass time to daughter cells, *Cell*, 2004, **119**, 693–705.

Peret, J., Macaire, I., Chanez, M., 1973. Schedule of protein ingestion, nitrogen and energy utilization and circadian rhythm of hepatic glycogen, plasma corticosterone and insulin in rats, *Journal of Nutrition*, 1973, **103**, 866e874.

Yagita K., Tamanini F., van der Horst G.T.J. and Okamura H., Molecular mechanisms of the biological clock in cultured fibroblasts, *Science*, 2001, **292**, 278-281.

Yamazaki S., Numano R., Abe M., Hida A., Takahashi R. Ueda M., Gene D. Block G.D., Sakaki Y., Menaker M. and Tei H., Resetting central and peripheral circadian oscillators in transgenic rats, *Science*, 2000, **288**, 682-685.

CHAPTER 5

Microfluidic technology for circadian study on a chip

In this chapter, we will describe the results about the circadian clock of cell culture within microfluidic environment. We will discuss how different operative parameters typical of microfluidic cell culture such as, the frequency of medium delivery or metabolite perturbation, could affect circadian synchronization. We will also analyze circadian synchronization heterogeneity over all microfluidic culture chambers. Finally, this chapter will provide a clear evidence of the potential of using microfluidic technology in circadian study.

5.1 Circadian gene expression on a chip by RT-PCR

We first asked whether it is possible to synchronize the circadian gene expression of cell culture within a microfluidic environments.

This microfluidic application is not straightforward. As reported in Chapter 3, the ratio between medium volume and cell volume is 20 times smaller in microfluidic cell culture chamber than in conventional Petri dish. This high reduction of extracellular volume is actually electing different biological and cellular phenomena; for instance, consumption of metabolite by cell culture will strongly

decrease the level of metabolite in the media, as well the cytokines releases from the cell will fast accumulated at higher concentration within microfluidic (Giulitti G. et al., 2013).
Both fast metabolite deprivation and cell release products accumulation could strongly affect circadian clock.

With this in mind, the synchronization protocol for the circadian entrainment was adapted from the protocol used for *in vitro* cell culture in a Petri dish, described in § 4.2. The synchronizing perturbation was applied to a confluent culture of human fibroblasts integrated into the microfluidic technology. The platform used for this experiment, widely described in § 3.2, is a multi-channel device that allows performing parallel cell culture conditions with a low degree of complexity.
The dexamethasone shock (1 mM) was applied at t=0 and in the following 48 hours the total mRNA, extracted from each channel, was isolated from cells for performing make qRT-PCR Analysis. Three mRNA samples were collected for each time point and qPCR was performed in duplicate.
More details about the mRNA extraction from the microfluidic cell culture chamber and qPCR protocol of small sample are reported in Appendix A2.
The mRNA accumulation profiles (Figure 5.1) show the gene expression of *BMAL1* and *PER2* achieved on a chip.
Consistent with the results obtained in the conventional Petri dish (Figure 4.4), the dexamethasone shock produces robust 24 hrs rhythms of gene expression also in human fibroblasts integrated in microfluidic channels.
The small volume (less than 10 uL) characterizing the microfluidic devices has not precluded the circadian synchronization of cell culture, demonstrating the microfluidic technology is feasible approach in biology, comparable to the traditional cell culture approach.

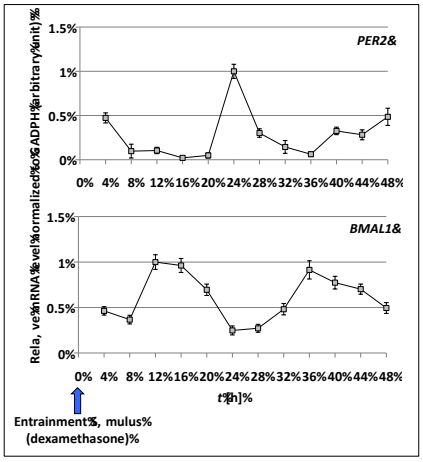

Figure 5.1: Temporal profiles of clock gene expressions, Bmal1 and Per2, in human fibroblasts, after the synchronization (t=0) with dexamethasone. The mRNA level of clock genes was normalized to housekeeping gene (GADPH) expression. Values represent the mean ± SD (n = 3 per time point).

5.2 Circadian gene expression by bioluminescence imaging

Because the qRT-PCR analysis is time consuming and it requires multiple sampling to provide dynamic profile of gene expression, we integrated a cellular system with luciferase readout within the microfluidic platform.

This approach allows on the one hand increasing the amount of data collected in high temporal resolution and on the other hand enabling to dynamically manipulate the cellular microenvironment by integration of liquid handling system; this latter aspect allows to perform biochemical system perturbation while detecting gene expression dynamic through imaging analysis.

The experimental setup used in this part of the work (described in § 3.2), is made up of two parallel microfluidic chambers connected to a syringe pump, all integrated into an apparatus of bioluminescence detection based inverted microscope equipped with super high sensitive CCD camera.

The cells were seeded in the microfluidic chip, at the precise density of 200 cell/mm^2, 24 h before the bioluminescence acquisition running and kept in incubator (37 °C, 5% CO2 and 95% humidity).

Before to place the sample on the microscope stage for real-time imaging, the inlets of each chamber were connected to the syringe pump (Cavro Pump XLP 6000- Tecan) by teflon tubes, filled with sterile medium in order to perfuse the cells during the days; the medium contained 1 mM of luciferin substrate. Every protocol and detail about cell integration and long-term culture on a chip are reported in Appendix A2.

A heated lucite chamber custom-engineered to fit around the microscope stage, kept the cells at constant 36 °C; the absence of CO2 was buffered by 350 mg/L of sodium bicarbonate 10 mM of HEPES; the proper humidity was kept covering the bottom of the Petri dish, containing the microfluidic platform with 1mL of PBS 1X.

The microscope rested in antivibration table in a dark and windowless room. After focusing carefully with brief-field illumination, we eliminated stray light by covering the microscope with a back lucite box, darkening the acquisition room completely.

Light from the sample was collected by 10x objective and transmitted directly to the cooled CCD camera mounted on the bottom port of the microscope. We used the Series 600s camera made by Spectral Instruments, containing a black-thinned CCD thermoelectrically cooled to -90 °C with a rated quantum efficiency of ~92% at 560 nm.

Adapting the microfluidic technology to this very sensitive equipment was not simple, we needed to perform several preliminary experiments ($n=10$) to optimize all those critical parameters, such as cell density, humidity control, CO_2 buffer, flow rate and darkness around the sample, in order to acquire specific high quality luminescence signal.

The figure 5.2 shows a time-lapse of the circadian behavior of a *Per2*::Luc mouse cell line (# 128 clone) derived from *Per2*::Luc knockin mice.

The intensity variation of photons emission from the cells corresponds to the different levels expression of *Per2*.

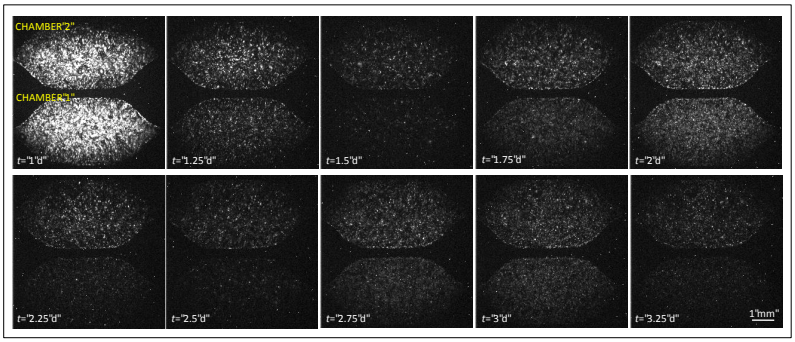

Figure 5.2: Time-lapse of bioluminescence images, at F=1/6 h^{-1} (frequency of medium delivery within the microfluidic cell culture chamber), of immortalized fibroblasts cell line derived from *Per2*::Luc knockin mice, showing circadian rhythms of luminescence 10 x .

5.2.1 Influence of the medium delivery frequency in the clock synchronization

The possibility to implement different protocols of medium delivery, by remote control of the liquid handling system, allowed to investigate the effects of different occurrence frequencies of a entrainment signal on the circadian expression of the cells.

It was used a serum shock (10% FBS), contained in the culture medium, as entrainment signal (Balsalobre A. et al, 1998).

Two different protocols of circadian synchronization (Figure 5.3A) were imposed to two independent parallel chambers, tuning the frequency of medium delivery:

- medium change every 24 h (F=1/24 h^{-1});
- medium change every 1 h (F=1 h^{-1}.)

The medium flow rate of 3uL/min ensures the minimal stress to the cells, that conserve a healthy morphology for all experiment duration.

The bioluminescence images of both cell culture chambers were acquired every 30 min by CCD camera for 7.5 days.

Figure 5.3B shows the daily profiles of the raw bioluminescence signals (without background subtraction) correlated to *Per2* expression for the two different conditions of the circadian entrainment imposed.

The temporal oscillation of the *Per2*:luminescence signals were obtained as the average of the luminescent intensity on the entire culture chamber by imaging processing (Matlab Software- Appendix A3).

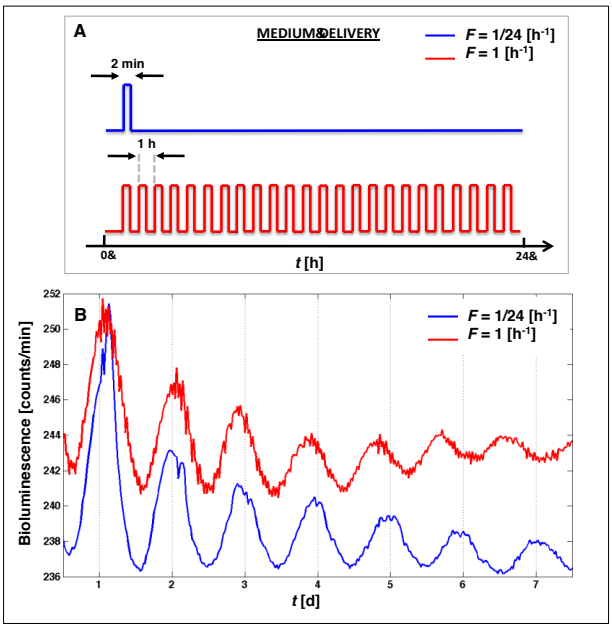

Figure 5.3: A) Schematic representation of the two different protocols of medium delivery imposed by microfluidic approach. B) *Per2*::luminescence signal monitored during the two different medium delivery (F=1/24 h^{-1} and F=1 h^{-1}), for 7.5 days.

The results of Figure 5.3 are in a way surprising. One could be expected that each medium change delivered to the microfluidic cell culture chamber it could results in cell culture resynchronization. This expectation is consistent with the experimental observation of conventional circadian experiments, in which the temporal variation of circadian gene expression is studied after an only one pulse of serum, provided to the culture by medium change.

However, Figure 5.3 clearly shows that circadian clock is maintained regardless of the frequency of medium delivery.

In order to deeply analyze differences between the two experimental conditions, the circadian parameters (period, amplitude damping and phase shift) were

evaluated by baseline correction on row data and fitting with polynomial curve by LumiCycle Software. The Figure 5.4 shows an example of circadian oscillation before and after fitting and the baseline subtraction. Major details of luminescence imaging and signal were described reported in § 4.2).

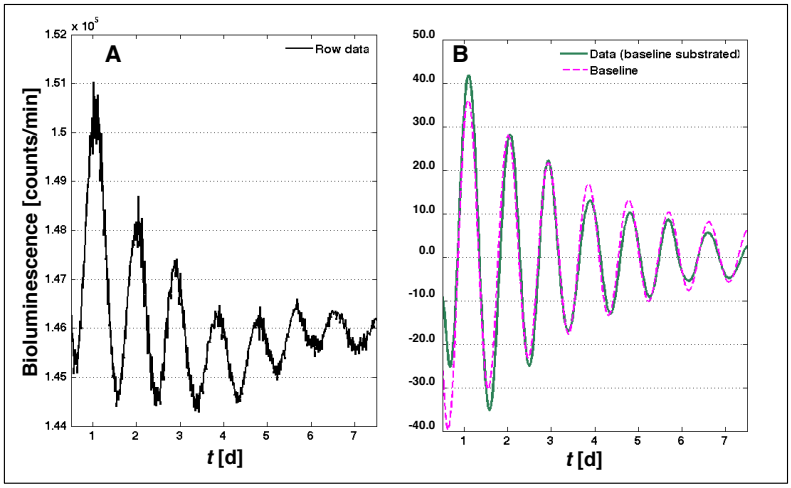

Figure 5.4: An example of bioluminescence processing. *A*) Raw data. (*B*) Data after baseline correction.

Moreover, in order to better characterize the uniformity of circadian behavior overall the cell culture within microfluidic environments, the average of the luminescent signal was calculated on 9 different regions of interest, 32x32 pixel, for each chamber (insert of Figure 5.5). It is worth to underline that a possible upstream down stream differential biological behavior could be take place.

For each ROI was calculated the average intensity frame by frame. The signals, thus obtained, before to be manipulated for the following circadian analysis, were baseline subtracted, as shown in Figure 5.5.

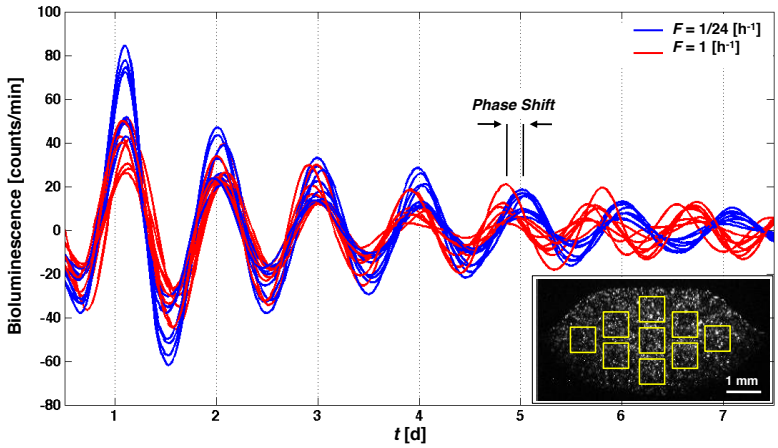

Figure 5.5: *Per2*::Luc bioluminescencepatterns of the two different medium delivery imposed (F=1/24 h^{-1}, F=1/h^{-1}); the signal was calculated as average intensity of bioluminescence integrated in the time of 9 ROI 32x32 pixel, as shown in the insert).

A first qualitative observation shows evident differences in circadian behavior between the two entrainment conditions.

A quantitative analysis is necessary to better understand the role of entrainment frequency on the period, amplitude and phase of circadian gene expression.

The period can be obtained as the time difference peak-to-peak of the circadian gene oscillation or by interpolation function provided from the LumiCycle software.

There is a significant difference ($p < 0.001$) in term of period between the two different protocols of circadian clock synchronization.

In particular the culture 'entrained' once per day has a circadian rhythm with a period of 23.7 ± 0.1 h (n=9), whereas the other one shows a period of 22.5 ± 0.1 h (n=9); the low values of standard deviation evidences the robustness of intrinsic and self-sustained circadian rhythms that characterize the peripheral clocks.

The comparison between the two period values leads to conclude that more frequent medium deliveries seem to cause decrease in the period.

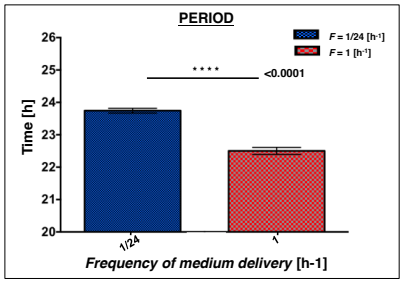

Figure 5.6: : Comparison of period values between the two conditions of medium delivery.

A quantification of peak amplitude was performed for both conditions (Figure 5.7).

It is interesting to see that there is a difference ($p<0.01$) only for the first peak, comparing the two condition of medium change; this result is consistent with the gradual lack of significant phase clustering because of desynchronization among individual cellular oscillators.

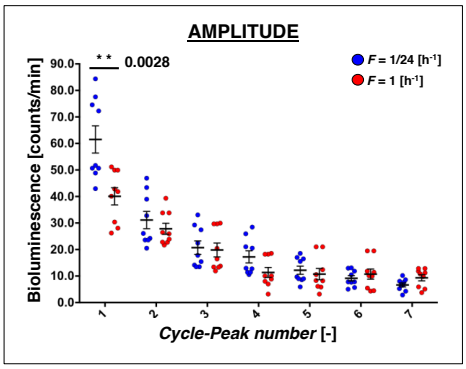

Figure 5.7: Temporal evolution of the peak amplitude for both conditions of medium delivery.

The last circadian parameters analyzed was the shift phase (Figure 5.8).

We already noted that the two *Per2* temporal variation begin with small phase shift that continuously increase up to the end of the experiment.

It seem evident that the entrainment frequency of 1 h-1 produces a negative phase shift compared to the frequency of 1/24 h-1; in particular frequent medium changes (F= 1 h-1) provide a phase delay of circadian gene expression in the range [0.1 ± 0.3, 0.9 ± 0.4] h for the first three days, that becomes more significant from the 4th day to the end of experiment, varying in the range of [2.0 ± 0.6, 9.0 ± 0.6] h.

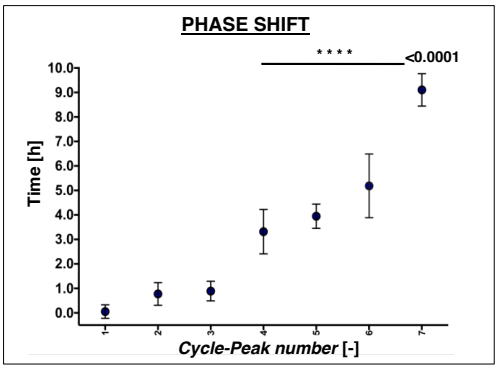

Figure 5.8: Phase shift, calculated as absolute value of different peak-to-peak time between the two medium conditions delivery.

5.2.2 Spatial distribution of circadian rhythms

The lack of significant phase clustering by the end of the experiment suggests an absence of functional coupling among individual cellular oscillators, which seem to drift freely out of phase over the course of the experiment without influencing one another's rhythms.

In order to investigate whether there is some correlation between the synchrony damping and the spatial positions, we mapped some region of the culture chamber in horizontal and vertical directions.

Figure 5.8 shows luminescence intensity from different ROIs.

Each horizontal line represents a pixel space of luminescence image, with elapsed time plotted left to right.

In particular it was mapped the horizontal circadian behavior, running in time a vertical ROI (8x8 pixel) at the center of chamber, viceverca for the vertical behavior.

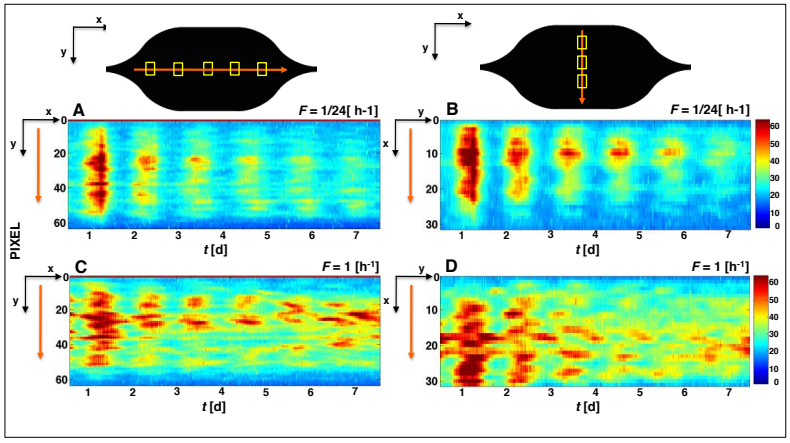

Figure 5.99: Heat-map of *Per2* bioluminescence; each line represents a single ROI, taken along the horizontal or vertical direction of chamber, with elapsed time plotted left to right.

The color-maps show that the frequency of 1/24 h^{-1} ensured a homogenous distribution of the luminescence signal in both horizontal and vertical directions, proving a sorted circadian behavior.

Conversely the frequency of 1 h^{-1} was able to keep a good organization until to the 2 days, after that the circadian gene expression became irregular in both the directions.

Constant delivery of medium (frequency of 1 h^{-1}) is actually resulting in high concentration of exogenous factors for the entire 24 h cycle (quasi-steady-state conditions). On the other hand, frequency of 1/24 h^{-1} ensures high concentration of exogenous factors only right after the medium change; concentration of exogenous factors will decrease by cellular consumption and uptake. Intuitively, these two different hypothetical experimental conditions only partially reproduce physiological glucose fluctuations observed *in vivo*.

The first case (frequency of 1 h^{-1}) maintains constant high level of glucose concentration without the typical oscillatory day/night behavior, on the other

hand, the second case (frequency of 1/24 h^{-1}) has oscillatory behaviors but with unknown dynamic.

With these considerations in mind, we designed new experiments in which we compare to different condition in which the cyclic glucose perturbation has a 12 h phase shift.

5.3 Cyclic glucose perturbation within microfluidic device

As proof of concept we performed an experiment for studying the variation of circadian gene expression by metabolic cycles.

This experiment has the same rationale of those described § 4.3, with the advantage being able to analyze the circadian behavior also during the stimulation phase.

In particular we wanted to test the effect of alternate cycles of low (2mM) and high (20 mM) glucose concentration, delivered with a flow rate of 3 uL/min and at the frequency of 1 h^{-1}, on circadian gene expression.

The two different cycles of glucose perturbation imposed are:

1. cyclic 12 h High glucose medium pulse – 12 h Low glucose medium (HL 12h);
2. cyclic 12 h Low glucose medium pulse – 12 h High glucose medium (LH 12h).

This experiment was monitored for almost 3 days and the *Per2* luminescence is shown in Figure 5.10.

The signals represent the average intensity of bioluminescence, time integrated, di 9 ROIs, (32x32) pixel, for each chamber, after baseline subtraction.

128 Per2::Luc

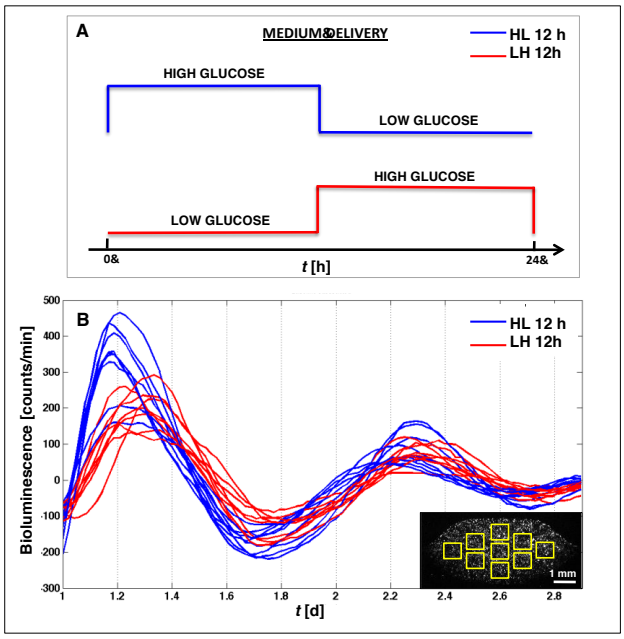

Figure 5.10: A) Schematic representation of the two different protocols of medium delivery imposed by microfluidic approach. B) *Per2*::luminescence signal monitored during the two different medium delivery (HL12h, LH 12h), for 3 days.

For a complete characterization of circadian behavior it was performed a quantification of period, amplitude and phase shift.

The period, shown in Figure 5.11, does not exhibit significant difference between the two protocols of stimulation. The HL-12h 'entrained' culture has a period of 24.0 ± 0.4 h (n=9) while LH-12h 'entrained' culture of 23.4 ± 0.6 (n=9).

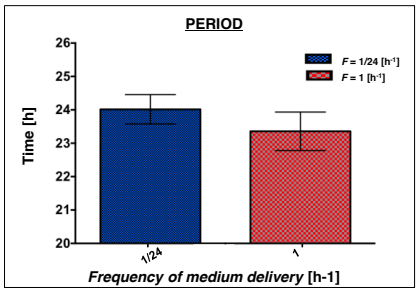

Figure 5.11: Comparison of period values between the two conditions of medium delivery.

The quantification of peak amplitude was performed for both conditions (Figure 5.12); the HL-12h seems being able to synchronize the cell culture more than the LH-12 h protocol ($p< 0.01$); this is gradually damped by the second day, obtained peak amplitude comparable between both conditions.

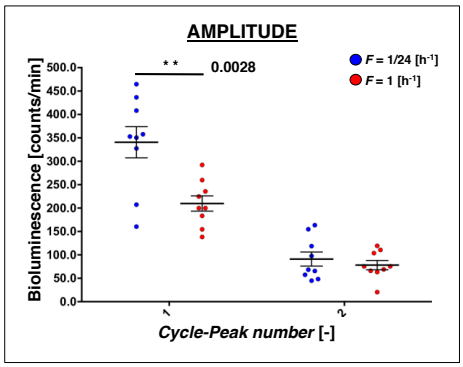

Figure 5.12: Temporal evolution of the peak amplitude for both conditions of medium delivery.

The phase shift (Figure 5.13) between the two conditions was also valuated, showing that the LH-12h exhibits a positive phase shift of 2.5 ± 0.4 h ($p<0.0001$) in the first peak and of 1.2±0.6 h ($p<0.05$) in the second peak.

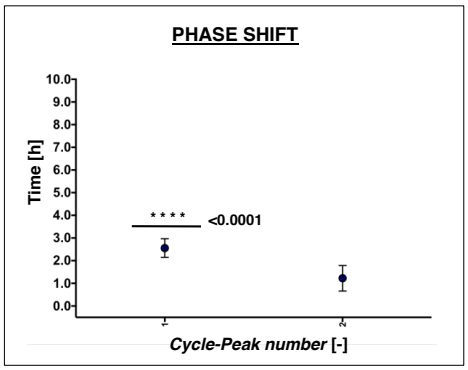

Figure 5.13: Phase shift, calculated as absolute value of different peak-to-peak time between the two medium conditions delivery.

These results show that microfluidic cyclic glucose perturbations within microfluidic device result in oscillatory circadian clock gene expression without substantially difference between the two different conditions.

This result suggests that the glucose only acting on the amplitude of the initial oscillation but, alone, it does not override the initial clock synchronization.

5.4 Conclusions

In this chapter, first of all a clear experimental evidence that circadian synchronization is possible within a microfluidic environments was provided.
It is worth to highlight that, so far our knowledge this is a first example of circadian clock detected in microfluidic for mammalian cell culture.
Moreover, targeted experiments (one experiment is long 10 day) were produced to analyze the effect of medium delivery on circadian clock within the microfluidic environment. The effect of media supply was more evident in the phase shift, suggesting that using high frequency medium delivery the composition of entrainment factor within the media should be accurately controlled. Analysis about spatial homogeneity of circadian synchronization overall microfluidic culture chamber provide useful information on optimal condition to obtain uniform cell culture synchronization.
Finally, we provide a proof of concept that we could also perform cyclic metabolite stimulations within the microfluidic environment while simultaneously recording circadian gene expression. This technological achievements open completely new perspective in circadian study.

From scientific point of view, these latest microfluidic results are very encouraging. In particular, it seems straightforward that the use of cyclic glucose and insulin perturbations, as suggested from the results of chapter 4 obtained using conventional methodology, will be next step.

In this perspective, the number of experimental combinations required for properly studding simultaneous metabolic and hormonal perturbation is exponential growing; for instance the main variables to be considered are: frequency of medium delivery, glucose and insulin concentrations, period of stimulation, number of cyclic perturbation within 24h.

With this in mind, it was considered unfeasible to continue on using the microfluidic platform B (multichannel platform with off line liquid handling) described on chapter 3. On the other hand, the microfluidic platform C

(multichannel platform with online liquid handling), specifically designed for parallel independent biological experiments, will be the perfect solution. We demonstrate the feasibility of the microfluidic platform C for long-term biological experiment and circadian study with this platform are now ongoing.

References

Balsalobre A., Damiola F., Schibler U., A serum shock induces circadian gene expression in mammalian tissue culture cells, *Cell*, 1998, **93**, 929–937.

Giulitti G., magrofuoco E., Prevedello L. and Elvassore N, Optimal periodic perfusion strategy for robust long-term microfluidic cell culture, 2013, Lab on a Chip, 13, 4430-4441.

CHAPTER 6

Conclusion and perspective

The study of circadian rhythms is a complex problem, which has a high social impact. Dysfunction of circadian rhythms has strong effects on human health and many clinical studies show that circadian disruption may have great implication in metabolic syndrome or obesity. This is not surprising if we think that many metabolic processes, such as glucose and cholesterol metabolism, are directly regulated by the circadian clock; the most important function of the circadian system is to maintain energy homeostasis by anticipating changes in the external environment and preparing the internal molecular environment to respond to these changes. On the other hand, the metabolic signals send feedback to the circadian system, modulating the phase, amplitude and period of circadian oscillators of the peripheral tissues. Therefore, how the environmental conditions or human behavior affects the clock is of fundamental importance for maintain healthy life-style.

Whereas cell-autonomous molecular clock in mammals is known to be generated by two interlocking transcription/translation feedback loops (TTFL) that function together to produce robust 24 h rhythms of gene expression, the mechanism of clock synchronization and its correlation with behavioral conditions is still unknown.

The general aim of the thesis is developing an *in vitro* model that resembles the cyclic dynamic fluctuations of metabolites and hormones (i.e. glucose, insulin), and even circadian related pathological alteration, at which the peripheral tissues are exposed in vivo.

The correlation between metabolite and hormone fluctuations and the circadian oscillators on cell culture derived from peripheral tissues, were specifically evaluated. The results clearly show how oscillatory perturbation of glucose and insulin together could affect some aspects of the circadian behavior. These results are quite important in the context of this thesis because they are actually confirming that the hypothesis of metabolic perturbation on circadian rhythms could be relevant in peripheral tissue.

Moreover, the circadian experiments using conventional technology show that the lacking of simultaneous perturbation/recording systems and the low level of automation in the conventional cell culture methods represent a strong limitation to further progress in circadian field.

As innovative technological tool, we identified the microfluidic technology for its capacity of delivering periodic extracellular chemical stimuli that could mimic the pulsatile nature of in vivo signaling systems.

In this perspective, three types of microfluidic platforms suitable for robust *in vitro* model for study of circadian rhythms were developed: i) single independent channel for fast biological validation; ii) multiple channel chip with off-line liquid handling for biological validation of cyclic perturbations; iii) large scale integration chip with on line liquid handing for multiple parallel independent biological experiments exposes to cyclic perturbations.

All microfluidic platforms have been developed in order to obtain devices as simple and easy-to-use as possible, while maintaining the following capability: long-term cell culture integration, accurate dynamic perturbation by chemical stimulus and quantitative analysis of circadian targets. These latter points were deeply investigated by developing to different molecular methods suitable for quantitative analyzing the temporal oscillatory behavior of the circadian genes circadian analysis, qPCR and luciferase reporter gene assay.

First of all a clear experimental evidence that circadian synchronization is possible within a microfluidic environments was provided; it is worth to

highlight that, so far our knowledge this is a first example of circadian clock detected in microfluidic for mammalian cell culture.

Targeted experiments (one experiment is long 10 day) were produced to analyze the effect of medium delivery on circadian clock within the microfluidic environment. The effect of media supply was more evident in the phase shift, suggesting that using high frequency medium delivery the composition of entrainment factor within the media should be accurately controlled. Analysis about spatial homogeneity of circadian synchronization overall microfluidic culture chamber provide useful information on optimal condition to obtain uniform cell culture synchronization.

We also provide a proof of concept that we could also perform cyclic metabolite stimulations within the microfluidic environment while simultaneously recording circadian gene expression.

Altogether, the results reported in this thesis have the potential to open a new perspective in circadian study. From technological point of view, the simultaneous cyclic perturbation of cell culture and gene expression recording will allow to perform high sensitive screening on potential entrainment factors.

In particular, as demonstrated in this thesis work using conventional technology, the use of cyclic perturbations with glucose and insulin in the same time could synchronize peripheral cells.

The number of experimental combinations required for properly studding simultaneous metabolic and hormonal perturbation is exponential growing; for instance the main variables to be considered are: frequency of medium delivery, glucose and insulin concentrations, period of stimulation, number of cyclic perturbation within 24h.

With this in mind, it was considered unfeasible to continue on using simple microfluidic platform such as the multichannel platform with off line liquid handling. On the other hand, the microfluidic platform with multichannel platform with online liquid handling, specifically designed for parallel independent biological experiments, will be the perfect solution. We already demonstrate the feasibility of this microfluidic platform for long-term biological experiment and circadian study with this platform are now ongoing.

As mentioned above, the molecular correlation between entrainment factors and circadian clock of peripheral tissues is still largely unknown. The dissection of mechanisms and isolation of specific factors will be almost impossible using human individuals or even animal model.

The microfluidic technology could offer a unique opportunity to explore the correlation between entrainment factors and human behavior. Alternatively to screening relevant entrainment factors with a series of multiple parallel experiments, it would be possible to use directly serum samples collected from human individual at different time of the day. This experimental strategy it would be feasible just because typical microfluidic experiments are based on the consumption of few microliter of medium per day.

In order to provide the proof of concept of this idea, we collect plasma sample from 12:12 LD (12 h Light- 12 h Dark) entrained mice at ZT=3 h and at ZT= 15 h, corresponding to starvation phase and to iperglicemia peak, respectively.

This condition, as reported in figure 6.1, could be correlated to high glucose and high insulin at ZT=3 and low glucose and low insulin for ZT=15.

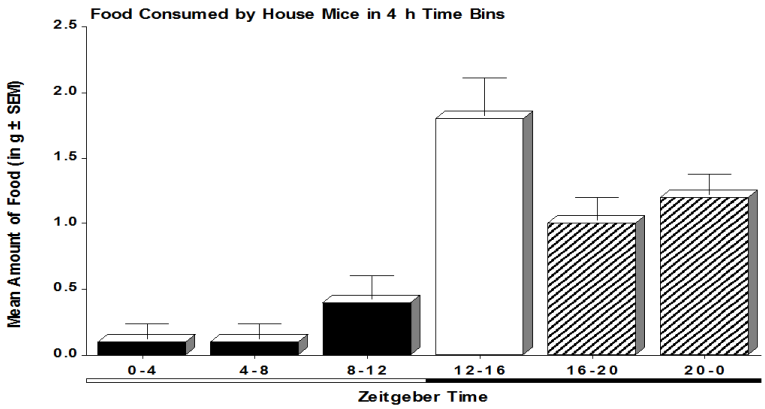

Figure 6.1. Daily profile of food consumed by 12:12 LD (12 Light :12 Dark) entrained mice.

Figure 6.2 shows Fibroblasts-Per2 luminescence resulting by synchronization with two different sera derived from plasma of 12:12 LD (12 h Light- 12 h Dark) entrained mice. Surprisingly, the post-prandial condition (corresponding to

iperglicemia peak) is a strong entrainment of circadian clock. In contrast, the plasma sample collected at starvation phase seems to have minimal influence on circadian clock.

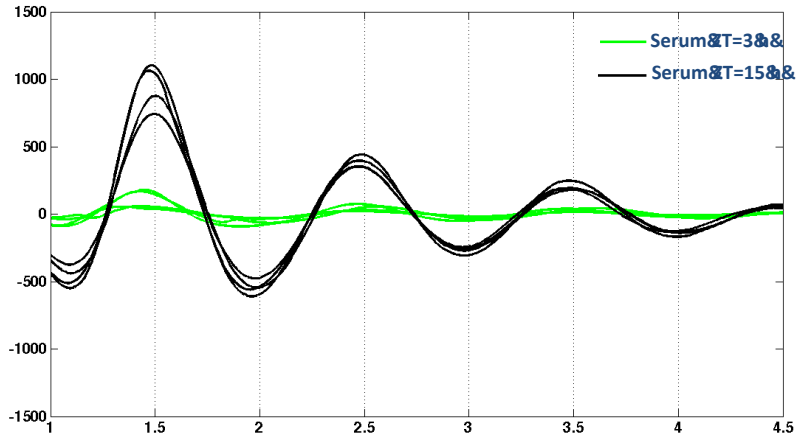

Figure 6.2. Fibroblasts-Per2 luminescence resulting by synchronization with two different sera derived from plasma of 12:12 LD (12 h Dark- 12 h Light) entrained mice. ZT=3 corresponds at starvation phase, whereas the ZT= 15h corresponds to iperglicemia peak.

These preliminary results show that the plasma collected from animal models contains information about the behavior of the animal. The development of *ad hoc* microfluidic technology cold be effective used to identify specific entrainment factor.

These microfluidic approaches offer a unique possibility that is not possible with conventional technology.

Appendix A1

Microfabrication

In this Appendix, the material and methods of the protocols used for the designing and fabrication of single or multi layer mold and chip.

A1.1 Soft lithography

Soft lithography is the most used technique to fabricate silicon-based devices that use replica molding of elastomeric materials to produce microfluidic devices
The first step in multi layer soft lithography is mold making.

Mold Making
This mold……..

At the end of these operations, molds contain the relief of the wanted microfluidic device. The thickness of the resist used during mold making determines the channel height on the further microfluidic device. It is obvious that this step is very crucial for the entire process and the minimum imperfection will be reflected on the following operations.
For molding making can be used two different type of photoresist, negative and positive.
In general a negative resist is a type of photoresist in which the fraction of the resist that is exposed to light becomes polymerized and more difficult to dissolve.

Therefore, the negative resist exposed to the light stays on the surface, and the developer solution removes only the unexposed fraction.

A positive resist behave in just the opposite way: the fraction of the photoresist that is exposed to light becomes soluble to the photoresist developer. The exposed resist is then washed away by the developer solution, leaving windows of the bare underlying material. Only the fraction of the photoresist that is unexposed continues to remain insoluble to the developer (Figure A1.1).

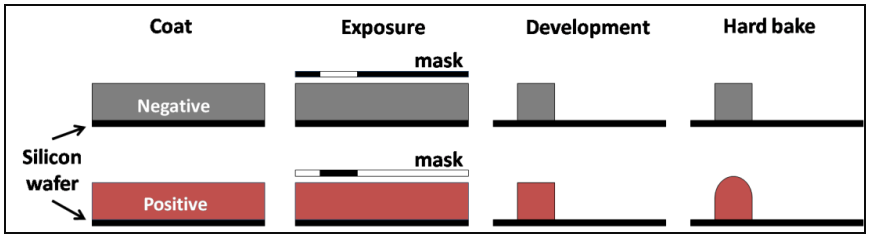

Figure A1.1: differences in exposure mask and hard bake for negative and positive photoresist. In the negative photoresist only the fraction exposed to the light (white in the mask) crosslink, the remain resist will be dissolved by the solvent. During hard bake the positive resist re-flow and the geometry from square becomes round.

For manufacturing the microfluidic device in this thesis we used SU8, as negative resist, that involves thickness about 5 to 200 um, and SPR, as positive resist, that involves thickness about 5 to 45 um. The thickness of the resist on the substrate used is determined by the type of resist and the spin speed used during the coating process (further details on general thickness will be found on the specific photoresist datasheets). The lowest aspect ratio of structure is 1.10 (height: width): structures with lower aspect ratios are prone to collapse.

The process to produce molds can be classified in subsequently steps:

- Substrate cleaning and treating
- Photoresist coating
- Pre-expose bake
- Exposure
- Post-expose bake
- Development
- Hard bake

The steps are followed in total for the negative resist, instead for the positive there is a little change.
One of the more frequent issues is imperfections due to not perfect cleaning, and adhesion problems due to wet surface. Before coating, the substrate must be clean with solvent and dried with clean air and heat. For the positive resist the substrate treatment with HDMS (hezadymetilsilazane) improve adhesion at the substrate.

The photoresist coating is made with a spin coater, in which spin speed, acceleration and length determine the thickness.

The pre-exposure bake (PEB) consists in 2-3 baking steps: for the negative resist at 65°C and 95°C followed to the expose. In this step the solvent starts to evaporate and the polymer improve mechanical properties before exposure. For the positive resist there are 2 bakes during the entire process and time and temperature can vary from 90°C to 105°C with the thickness. In general, lesser is the temperature longer is the bake time and stronger will be the polymer adhesion. Before the exposure the positive resist needs to be rehydrated, to reduce the strength induced by the solvent evaporation. It is achieved at room temperature in the dark. During light exposure there is geometry transfer by chemical reaction due to photoresist properties through an overlaying specific mask placed between the light and the photoresist. There is selective exposure on the mold by these transparency films printed with high resolution: the masks used for negative resist contain the inverse (the "negative") of the pattern to be transferred; the positive masks, therefore, contains an exact copy of the pattern which has to remain on the wafer.

Exposure time depends with the resist thickness: increasing in thickness involve to increasing in exposure energy and therefore in exposure time. In general the energy required is lesser for the negative photoresist than for the positive one, in order to 10-20 times. Since the exposure time required for positive resist is very long, it could generate overheating and consequently it can damage the surface. A multiple cyclic exposure can be used to avoid overheating, alternating short

exposure time with delay time. They can be repeated until the total energy amount is transferred to the positive resist.

For the negative photoresist an additional 2 step bake follows the exposure at 65°C and 95°C; this improve the polymerization due to the light and increase mechanical properties to the structure before the development.

Development is a very tricky step. Length and shake are two important parameters to control in the process and they depend from the resist thickness. Shake decrease the development time, reducing issues connect to over-development. Longer development time can damage the polymer and generate modified structure

The last step is hard baking, in which the polymer is baked at high temperature to complete the crosslink and increase resistant and hardness. For the positive this step is very important because it causes the reflow and therefore the obtaining of round channels. After reflow the polymer is very strong and hard and cannot be solved anymore by solvent. The reflowing must be done very slowly, due to not damage the channels. After reflow the channels blow up a little bit and it has to be considered during design.

A1.2 Multi-layer chip fabrication

PDMS is a popular material for microfluidic applications due to its chemical resistance, low cost and rapid fabrication.

Using PDMS material in the last decay, an extension of soft lithography, called multilayer soft lithography, has been proposed [5, 6]. With this technique active microfluidic devices have been built, generating the new automation era for microfluidic chip and the development of mLSI, integrating microvalves and pumps.

In general a basic multilayer microfluidic device is composed of two PDMS layers: the layer that contains channels for flowing liquid is called flow layer (FL), and the other one is called control layer (CL).

Before to pour PMDS, the molds are treated with silanized reagent that makes the PDMS not stackable to the mold. PDMS is a silicon-based organic polymer; it's

optically clear, and, in general, is considered to be inert, non-toxic and non-flammable. PDMS consist of two components: the base and the cure agent. The manufacture recommendation is to use these two components in the weight ratio 10:1 ("ON RATIO"). For application regarding valves technology and multilayer PDMS chip, the ratio between the two PDMS layer (CL and FL) has been modified in order to make multilayer PDMS structures using thermal bonding. In multilayer soft lithography the bond of multiple PDMS layers is a necessary condition that has to be achieved during fabrication.

Moreover the two layers have to be allocated in a precise position in which the control channels create the valve areas in the right point over the flow channels. To achieved this, in the design process some marks have been added at the edge of the chip and in the center of the pattern. These marks help the operator during the alignment process in the fabrication. Thermal bonding it has been preferred for mLSI (microfludic large scale integration) because it is more yielding during alignment: it isn't a one shot process (as plasma bonding) and the operator has more time to ensure the best alignment condition. This technique is called "OFF RATIO" due to the modified ratio of the two layers from 10:1. One PDMS layer is made at high ratio (5:1) and the other one at low ratio (20:1); the two layers are partially cured before put in contact. A followed bake create an irreversible bonding at the interface due to rapid diffusion of the catalyst from the rich layer to the poor layer (about 10-40 μm).

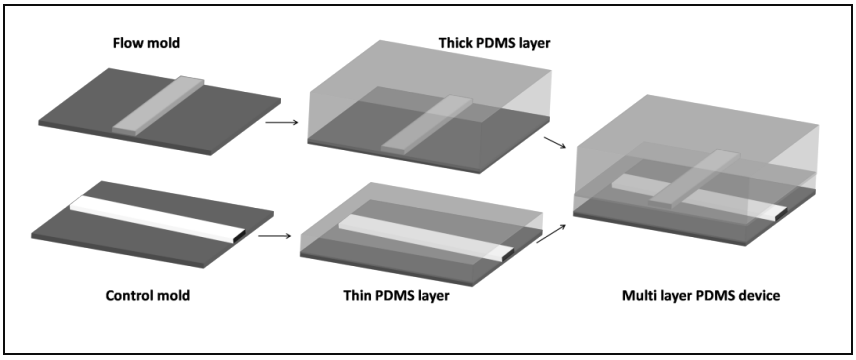

Figure A1.2*: Multi layer PDMS chip is made by more than 1 PDMS layer in which the bond is ensure usually by plasma or by off ratio PDMS curing. In Thermal bonding, partially cured PDMS layer are aligned and placed in contact before put them together in oven to complete the curing*

and ensure the bond. Therefore with plasma bonding the surfaces are treated with plasma and made in contact. Strong covalent bonds are guaranteed.

The ability to create valves is achieved by interjection channels in two PDMS layers separates by a thin PDMS membrane. A valve is created by the thin membrane deflection that separates the two channels: when the control channel is pressurized a complete sealing is created. The thin membrane is formed by a thin PDMS layer spun over the mold: the PDMS height over the pattern determines the thickness of the membrane. The most important parameter that has to be evaluated at the end of the making process is the valve minimum closing pressure that is the minimum pressure applied to the control that can deflect all the membrane's valve on the chip, creating a complete sealing in the valve region. This pressure must be guarantee during its use. The thickness of the membrane is the only constraint that could be adjust during chip making to improve the valve sealing during operations. Thicker is the membrane stronger is the valve, but higher will be the pressure that has to be applied to deflect the membrane, increasing the risk of breaking chip. Thinner membrane is preferred but the better choice is a compromise between robustness and workability: usually it is achieved with a 10-20 μm membrane. Actually the most important parameters for the sealing are the valve cross section and the high of the flow channels. In general higher is the flow channel higher is the closing pressure, but this parameter has to be chosen during mask design and mold making. Also the shapes of the flow channels are important: round flow channels help the membrane deflection during sealing comparing with square flow channels.

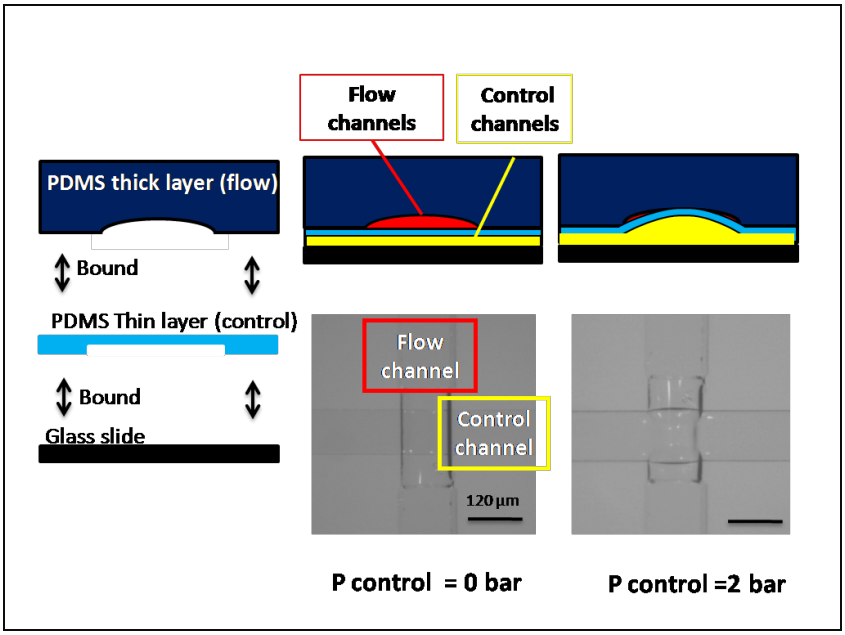

Figure A1.3: A microfluidic valve is created when two channels are overlapped and separated by a thin membrane. When the control channel is pressurized the membrane deflects and there is sealing of the channel placed over.

Two types of valves can be fabricated: if the control lines is under the flow channels it has been made a "push up" valve, in which the membrane is deflected up into the flow channels. Therefore, if the control line is up the flow channels it has been made a "push down" valve. There is a standard geometry for the flow channels and control channels for both valves type to ensure sealing. In general higher closing pressure is required for push down valves. The specific application has to be considering during the process design due choosing the right layers configuration. It's not possible use 2 molds that were produced for push up valves to make push down valves.

In the OFF RATIO technique the thin layer is made in PDMS 20:1 ratio, therefore, the thick layer in PDMS 5:1 ratio.

For making the devices used in this thesis we used PDMS Sylgard 184 (Dow Corning), that ensures no toxicity to the mammalian cell culture.

When microfluidic devices are ready, they are bonded to a resistant substrate that is usually a glass slide via plasma bonding. Devices sealed to glass are rated to

approximately a lower pressure before delamination than the devices sealed with a thin layer of PDMS over the glass slide. In this case delamination is not achieved up to 2 bars.

Multi layer chip can be made also in the 10:1 ratio to reduce cure agent massive use. For mammalian cells it may avoid some toxicity problems due to high partially uncured PDMS when a different ratio from 10:1 is used. In this case thermal bonding cannot be used. Alternatively irreversible plasma bonding can be adapted easily for alignment of simple geometry where precision is not so important.

The ratio used for making the three different layer of the Platform C described in tha Chapter 3 are:

- 5:1 ratio (base:cure agent) for FL (Flow Layer)
- 20:1 ratio for CL (Control Layer)
- 10:1 ratio for chambers layer CHL (Chamber Layer).

All the layers have been partially cured at 60 °C before peeling, cutting and punching: 45 minutes for FL, 60 minutes for CL and 70 minutes for CHL. After alignment, other 2 hours at 80 °C completed the curing. The chip has been finally bonded on large glass slip covered with a thin 20:1 PDMS layer by plasma activation.

A1.3 Mold Making Materials

A1.3.1 Reagents and Substrates

100 mm silicon wafer, orientation any, material type CZ silicon, dopant any, thickness min 400-600 um, resistivity 0-100 ohm cm, FrontSideFinished polished, BackSide Etched; (MCR Microsystems, Germany).

Photoresist: SPR 220-7 (Dow Corning), SU8 2005 (Microchem), SU8 2010 (Microchem), SU8 2025 (Microchem), SU8 50 (Microchem)

Developer: MF319 developer (Dow Corning), SU8 developer (Microchem)

Solvent: Ethanol (Sigma), Isopropanol (Sigma), Methanol (Sigma), Acetone (Sigma)
1,1,1,3,3,3 hexamethyl-disilazane (HDMS), reagent grade 97% (Sigma)

A1.3.2 Equipments and Other

Spin coater (Laurell WS-400b-6npp/lLITEHOR)
programmable hot plate (Torreypines scientific)
Rocking shaker (Reliable scientific inc)
Karl suss alignment
Karl suss UV intencity meter- model 1000
Olympus TCH microscope ergolux (Olympus)
White nitril gloves and clothes for clean room facilities (cover shoes, hairnet, bunny suit/frock, booties)
Flat bottom and straight sides glass tank 125x75 (VWR)
Wafer tweezers
120 mm Petri dishes

A1.4 Mold procedure

A1.4.1 Flow Mold

The flow mold is made by 3 photoresist layers.

E.4.1.1 First layer, rounded channels

1 Clean wafers
Rinse wafers with acetone, then methanol, then distilled water (DI) (using squirt bottle), blow dry with pressure clean air. Dry on hotplate at T>100C for at least 15 min
2 Treat with HMDS
Place the wafer in a closed chamber with an open container of HDMS for at least 10 min

3 Spin photoresist 1st layers with SPR-220-7

Place wafer onto spinner chuck and apply vacuum; pour 5 ml of SPR-220-7 on wafer. Use 7 steps spin program:

Step number	Time [sec]	Speed [rpm]	Acceleration [rpm/sec]
1	10	0	0
2	70	200	200
3	15	200	400
4	45	200	1000
5	10	700	1000
6	30	400	2000
7	5	800	5000

Let wafer sit on a flat level surface, covered with Petri dish for 10 min or less if de-wetting is observed on edges

4 Soft bake photoresist 1st layer

2-steps soft baking on 2 hotplates, covered with Petri dish leaving an air gap for solvent to escape while soft baking. Use 2 steps bake:

Step number	Temperature [°C]	Time [min]
1	65	5
2	90	40

Remove wafer from 90°C slowly, rising the wafer a millimeters every few seconds

5 Resist rehydration

let wafer sit in closet petri dish, wrapped in aluminum foil at room temperature for at least 3 hours (overnight is also good)

6 Exposure

Prepare mask and place into Karl suss mask aligner. Choose exposure parameters and expose wafer: parameters: soft contact; Intensity:9mW/cm2; Time 14sec x 19, 25 sec pause

7 Develop MF-319 developer

place wafer in MF-319 developer and continuously agitate the solution time for 10-15 min. Rinse with DI water by filling agitation, and pouring out for 6 times.

8 Measure profile

Measure photoresist height in profilometer: expected photoresist thickness: 15-20 um (depending on place on the wafer)

9 Hard baking & reflow

Reflow on hotplate, covering with petri dish. Hard bake recipe: leave at 65C for 1hr, then from 65C to 190 using 10C/hr ramp. Set timer to 15hrs and use an auto off.

10 Measure profile

Measure photoresist height in profilometer: expected photoresist thickness: 27-32 um (depending on place on the wafer)

A1.4.1.2 Second layer, square channels

1 Clean wafers

Rinse wafers with acetone, then methanol, then distilled water (DI) (using squirt bottle), blow dry with pressure clean air. Dry on hotplate at T>100C for at least 15 min

2 Spin photoresist SU8-50

Place wafer onto spinner chuck and apply vacuum. Pour 5 ml of SU8-50 on wafer. Use 2 steps spin program

Step number	Time [sec]	Speed [rpm]	Acceleration [rpm/sec]
1	10	500	100
2	50	2000	260

Let wafer sit on a flat, level surface, covered with petri dishes for 10 min.

3 Soft bake photoresist

3-steps soft baking on 2 hotplates:

Step number	Temperature [°C]	Time [min]
1	65	5
2	95	15
3	65	2

Cover wafers with glass petri dish leaving an air gap for solvent to escape while soft baking. Remove wafer from 95C and from second 65C bake slowly, rising the wafer a millimeters every few seconds

4 Exposure

Prepare mask and place into karl suss mask aligner. Align mask to rounded channels on the wafer and chose exposure parameters. Recipe: soft contact; Intensity: 9mW/cm2; Time:22sec

5 Post Exposure Bake

3-steps soft baking on 2 hotplates

Step number	Temperature [°C]	Time [min]
1	65	2
2	95	5
3	65	2

cover wafers with glass petri dish leaving an air gap for solvent to escape while soft baking. Remove wafer from 95C and from second 65C bake slowly, rising the wafer a millimeters every few seconds

6 Develop SU8 developer

place wafer in SU-8 developer and continuously agitation solution for 2 min-2.5min. Rinse wafer with lots of isopropanol (using squirt bottle). Blow dry with clean pressurized air.

7 Measure profile

measure photoresist height in profilometer: expected photoresist thickness: 47-51 um (depending on place on the wafer)

8 Hard bake

Place the wafers on hotplate, covering with petri dish. Hard bake recipe: leave at 65C for 2 min, then from 65C to 160 using 120C/hr ramp. Set timer to 2 hours and use an auto off.

A1.4.2 Control Mold

A1.4.2.1

1 Clean wafers

rinse wafers with acetone, then methanol, then distilled water (DI) (using squirt bottle), blow dry with pressure clean air. Dry on hotplate at T>100C for at least 15 min

2 Spin photoresist SU8 2005

place wafer onto spinner chuck and apply vacuum. Pour 5 ml of SU8 2005 on wafer. Use 1 steps spin program

Step number	Time [sec]	Speed [rpm]	Acceleration [rpm/sec]
1	400	3000	400

let wafer sit on a flat, level surface, covered with petri dish for 5 min.

3 Soft bake photoresist

3-steps soft baking on 2 hotplates:

Step number	Temperature [°C]	Time [min]
1	65	2
2	95	5
3	65	2

cover wafers with glass petri dish leaving an air gap for solvent to escape while soft baking. Remove wafer from 95C and from second 65C bake slowly, rising the wafer a millimeters every few seconds

4 Exposure

Expose the wafer without masks: all the polymer is exposed to the UV light. Recipe: soft contact; Intensity: 9mW/cm2; Time:18sec

5 Post Exposure Bake

3-steps soft baking on 2 hotplates

Step number	Temperature [°C]	Time [min]
1	65	2
2	95	6
3	65	2

cover wafers with glass petri dish leaving an air gap for solvent to escape while soft baking. Remove wafer from 95C and from second 65C bake slowly, rising the wafer a millimeters every few seconds

A1.4.2.2 Second layer, square channels

1 Spin photoresist SU8-2025

place wafer onto spinner chuck and apply vacuum. Pour 5 ml of SU8 2025 on wafer. Use 1 step spin program

Step number	Time [sec]	Speed [rpm]	Acceleration [rpm/sec]
1	80	3000	130

let wafer sit on a flat, level surface, covered with petri dish for 10 min.

2 Soft bake photoresist

3-steps soft baking on 2 hotplates:

Step number	Temperature [°C]	Time [min]
1	65	2
2	95	5
3	65	2

cover wafers with glass petri dish leaving an air gap for solvent to escape while soft baking. Remove wafer from 95C and from second 65C bake slowly, rising the wafer a millimeters every few seconds

3 Exposure

prepare mask and place into karl suss mask aligner. Choose exposure parameters and expose wafer. Recipe: soft contact; Intensity: 9mW/cm2; Time:18sec

4 Post Exposure Bake

3-steps soft baking on 2 hotplates

Step number	Temperature [°C]	Time [min]
1	65	2
2	95	5
3	65	2

cover wafers with glass petri dish leaving an air gap for solvent to escape while soft baking. Remove wafer from 95C and from second 65C bake slowly, rising the wafer a millimeters every few seconds

5 Develop SU8 developer

place wafer in SU-8 developer and continuously agitation solution for 2.5 min-3min. Rinse wafer with lots of isopropanol (using squirt bottle). Blow dry with clean pressurized air.

6 Measure profile

measure photoresist height in profilometer: expected photoresist thickness: 19-21 um (depending on place on the wafer)

7 Hard bake

Place the wafers on hotplate, covering with petri dish. Hard bake recipe: leave at 65C for 2 min, then from 65C to 160 using 120C/hr ramp. Set timer to 2 hours and use an auto off.

A1.4.2.3 Third layer, chamber layer

1 Clean wafers

rinse wafers with methanol (using squirt bottle), blow dry with pressure clean air. Dry on hotplate at T> 65°C for at least 15 min

2 Spin photoresist SU8-2025

place wafer onto spinner chuck and apply vacuum. Pour 5 ml of SU8 2025 on wafer. Use 2 steps spin program

Step number	Time [sec]	Speed [rpm]	Acceleration [rpm/sec]
1	20	500	130
2	50	1500	300

let wafer sit on a flat, level surface, covered with petri dishes for 10 min.

3 Soft bake photoresist

2-steps soft baking on 2 hotplates:

Step number	Temperature [°C]	Time [min]
1	65	5
2	95	7

cover wafers with glass petri dish leaving an air gap for solvent to escape while soft baking. Remove wafer from 95C and from second 65C bake slowly, rising the wafer a millimeters every few seconds

4 Exposure

prepare mask and place into karl suss mask aligner. Align mask to square channels on the wafer and chose exposure parameters. Recipe: soft contact; Intensity: 9mW/cm2; Time:18sec

5 Post Exposure Bake

2-steps soft baking on 2 hotplates

Step number	Temperature [°C]	Time [min]
1	65	1
2	95	6

cover wafers with glass petri dish leaving an air gap for solvent to escape while soft baking. Remove wafer from 95C and from second 65C bake slowly, rising the wafer a millimeters every few seconds

6 Develop SU8 developer

place wafer in SU-8 developer and continuously agitation solution for 1 min. Rinse wafer with lots of isopropanol (using squirt bottle). Blow dry with clean pressurized air.

7 Hard bake

Place the wafers on hotplate, covering with petri dish. Hard bake recipe: leave at 65C for 2 min, then from 65C to 160 using 120C/hr ramp. Set timer to 2 hours and use an auto off.

8 Measure profile

measure photoresist height in profilometer: expected photoresist thickness: 45-47 um (depending on place on the wafer)

A1.5 Chip Making Materials

A1.5.1 Reagents and Substrates

Chloromethylsilane (C 72854-500ml Sigma Aldrich)

Sylgard 184 Dow corning kit (base and cure agent)

Glass slide: Brain Research laboratories n 1 thickness 48x60

VWR micro slides 25x75 (cat n 48300-025)

VWR micro slides 50x75 cat 48300-050

A1.5.2 Equipments and others

PDMS Mixer (Thinky AR-250)
spic coater (Laurell WS-400b-6npp/lLITEHOR)
Vacuum system (vacuum pump and crystallization tank)
Stereomicroscope Nicon SMZ1500
Convective Oven (VWR model NO 1350 FM)
Punch machine (Schmidt technology press and camera)
Plasma Machine
Cutter
White tape
Wafer tweezers
Al foil
TX 1109 Non waven wipers Technicloth II
TX 1010 Vectro Alpha 10, Vectro Sealed-border wipers
Petri dishes 150x15 mm (VWR 25384-326 and 25384-302 100x15mm)

A1.6 Chip procedure

1 Coating

Molds are placed under vapor of chlorotrimethylsylane for 10-20 minutes. Then , they are cleaned with pressurized dry air and placed in clean, covered petri dishes.

2 PDMS preparation: Sylgard 20:1

Prepare 20 g of PDMS 20:1 (base:cure agent): weight base and cure agent under hood; mix for 2 minutes following degassing for 3 minutes.

3 PDMS preparation: Sylgard 5:1

Prepare 50 g of PDMS 5:1 (base:cure agent): weight base and cure agent under hood; mix for 2 minutes following degassing for 3 minutes.

4 Control Layer coating

Place the mold onto spinner chuck and apply vacuum. Pour 10 ml of PDMS 20:1 on the center of the mold. Use a 1 step program:

Step number	Time [sec]	Speed [rpm]	Acceleration [rpm/sec]
1	75	2200	133

Let on a flat surface for 90 minutes inside a closed petri dish.

5 Degassing

Put the FL mold in a foil vessel and cover the mold with the uncured 5:1 PDMS. Degas until bobbles disappear.

6 First curing

Bake at 60°C for 45 minutes the CL and for 35 minutes the FL.

7 Flow layer chip casting

Peel, cut and punch (20G) the FL chip and clean the surface with tape.

8 Alignment

Align the FL on the CL under stereomicroscope. Check all markers and valves intersection. No bubbles have to be present.

9 Thermal Bonding

Bake the 2 aligned layers together at 60°C for 15 minutes and then at 80°C for 90 minutes.

10 Two-layers chip casting

Cut, peel and punch (20G) the two layers chip. Remove the eventual thin membrane on the chamber. Clean the surface with tape.

CHL casting

11 PDMS preparation: Sylgard 10:1

Prepare 80 g of PDMS 10:1 (base:cure agent): weight base and cure agent under hood; mix for 2 minutes following degassing for 3 minutes.

12 Degassing

Put the CHL mold in a foil vessel and cover the mold with the uncured 10:1 PDMS. Degas until bobbles disappear.

13 Curing and casting

Bake at 60°C for 3 hours, then peel, cut and punch with a 4 mm puncher to make the hole for biopsies insertion.

14 Plasma bonding

Clean the surface with tape. Treat the CHL and the 2-layers chip with plasma for 35 sec at 70W. Align under the microscope to center the chambers with the holes in the CHL. Put in the oven for at least 2 hours (better overnight).

A1.8 Automation

Automation is achieved by valve control with custom software. All the valves in the chip are driven by miniature pneumatic solenoid valves (24V, CKD Corporation) which are in turn controlled by electronic unit for the generation of digital signal (NI USB-6501, National Instruments) connected to the USB port of a computer. The electronic unit is plugged to a 24V transformer. There is also a system composed of rechargeable battery to guarantee charge during relocation, for example from the incubator to the microscope in another room (up to 15 minutes declared).

Each solenoid valve can switch more valves in the chip between atmospheric pressure (on-chip valve open) and 250 kPa (on-chip valve closed). Custom software developed using Labview® (National Instruments) operates the chip. This software permits fully automated and unattended operation of the system during an experiment.

[1] Younan Xia and George M. Whitesides, Soft lithography,Annual Review of Materials Science Vol. 28: 153-184, DOI: 10.1146/annurev.matsci.28.1.153

[2] Melin and Quake, Microfluidic large-scale integration: the evolution of Design rules for Biological Automation.

[3] Hu and Li, Multiscale phenomena in microfluidics and nanofluidics, Chemical Engineering Science, volume 62, Issues 13, July 2007, 3443-3454

[4] Sollier et al., Rapid prototyping polymers for microfluidic devices and high pressure injections, Lab Chip, 2011, 11, 3752

[5] Thorsen et al, Microfluidic Large Scale Integration, Science 2002, vol 298, 380-384

[6] Marc A. Unger, *et al.* Monolithic Microfabricated Valves and Pumps by Multilayer Soft Lithography, *Science* 288, 113 (2000); DOI: 10.1126/science.288.5463.113

[7] Seok Woo Lee and Seung S. Lee, Shrinkage ratio of PDMS and its alignment method for the wafer level process, Microsyst Technol (2008) 14:205–208, DOI 10.1007/s00542-007-0417-y

Appendix A2

Biological protocols

A2.1 Cell Culture integration in the microfluidic device

All fibroblasts culture used in this work (HFF, #128 Per2::Luc) were expanded in tissue culture 10 mm dishes with proliferation medium: Dulbecco Modified Eagle Medium (DMEM, Sigma-Aldrich), 10% Fetal Bovine Serum (FBS, Life Technologies), 1% Penicillin-Streptomycin mix (Life Technologies). Before reaching the confluence, cells were trypsinized with Trypsin-EDTA 0.25% (Life Technologies) and replated either in new dishes or into the microfluidic chip.

Before cell seeding, microfluidic chip was sterilized by autoclave processing. After its sterilization, it is moved into a 35 mm Petri dish under sterile hood and injected with cold 25 ug/mL fibronectin (Sigma Aldrich), 25 ug/mL in PBS 1X; the fibronectin coating is kept at room temperature for 1 hour and is removed by washing microfluidic chamber with culture medium. A cells suspension was then prepared in order to obtain a cell seeding density of 200 cell/mm^2 and injected in the chip. The bottom of the dish was covered with 1 ml of PBS 1X, in order to maintain proper humidity. The cells were kept in incubator at 37°C, 5% CO_2 for 3 to 5 hours, until they adhered to the bottom glass of the chip. After their adhesion, the lateral wells of the microfluidic chip were filled with proliferating medium and cells maintained in the incubator.

Medium was then changed every 24 h, by adding new medium in the lateral wells and rapidly perfusing it inside the chambers with the help of a hand held pipette. This protocol allowed to have confluence cell culture after 4 to 5 days from seeding.

A2.2 Circadian synchronization of a cell culture

Two different protocols of synchronization were used in this thesis, by dexamethasone and serum shock; the same procedures were applied in static an microfluidic condition.

Synchronization by dexamethasone shock

A shock of dexamethasone (10 nM) was applied to the confluent cell layer for two hours, then washed twice with PBS 1X. The cells were kept in a FBS-free medium until the end of the experiment.

Synchronization by serum shock

This protocol involves just a medium change with 10% FBS medium after a wash with PBS 1X. The cells were kept in 10% FBS medium for all experiment duration.

After imposing one of these protocols, the circadian gene expression was analysed by Real-Time PCR or luciferase reporter assay.

A2.3 Extraction of mRNA sample

Extraction from microfluidic channel

A lysis buffer, RT-qPCR iScriptTM Sample Preparation Reagent (BIO-RAD), was used for extracting the mRNA sample from the microfluidic channels. Because this buffer was designed to degrade the cytoplasmic membrane while leaving intact nuclear membrane, just the cytoplasmic RNA was extracted, while the genomic DNA remains within the nuclei.

Before the extraction, the cells must first be washed gently with cold PBS 1X twice. 10 uL of iScript was injected in microfluidic channel and left for 1 minute at room temperature.

All reagent was collected, without disturbing the cell pellet, in a 0.2 mL RNase-free tube kept on ice. mRNA was stored at -80 ° C.

Extraction from Petri dish

The mRNA extraction from cell culture seeded in Petri dish involves two step: the isolation by Tryzol and the purification by chloroform.

The mRNA contained in 3.5 mm dish was isolated in 1 mL of Tryzol for 5 min a room temperature. The samples were collected in 1.5 mL tube and kept at -80°C or immediately processed for the following purification.

Chloroform (200 uL per 1 mL of Tryzol) was added and incubated for 15 minutes on ice.

The sample was centrifuged at 12000g for 25 min at 4 ° C; after centrifugation, the mixture was separated into a phase that contains phenol and chloroform, an interphase, and a transparent aqueous phase on the top.

The aqueous phase was collected, taking care not to remove the phases underlying in a RNase free tube previously put on ice.

Ethanol (70 %, prepared with RNase free H2O and previously filtered with filters from 0:20 pM) was added and left at room temperature.

After a centrifugation at 12000g for 25 min at 4 ° C, the mRNA pellet was formed and the surnatant was sucked. The mRNA was diluited in 100 uL of RNA free water and was quantified.

A2.4 Retrotranscription

The reverse transcription reaction is the synthesis of a cDNA molecule from an RNA mold, catalyzed by the enzyme reverse transcriptase.

To perform the reverse transcription was used High Capacity cDNA Reverse Transcription Kit (Applied Biosystems), which contains all the reagents necessary to obtain single-stranded cDNA of high quality even starting from very small amounts of RNA mold, up to 0.02 g. The trigger for the enzyme is given by random primers.

A single reaction mix (Table A2.1) was prepared, for being apportioned into individual RNase-free tubes to which are added 2 L of mRNA extracted.

RT mix (20 uL total)	
RNA free water	12 uL
10x RT Buffer	2 ul
10X Random Primers	8.4 uL
25X dNTP Mix (100 mM)	0.8 uL
Mtultiscrible Reverse Transcriptase	1uL
RNA	2 uL

Table A2.1: Retrotranscription reaction performed with High Capacity cDNA Reverse Transcription Kit (Applied Biosystems). The volume of 20 ul is the volume of the single reaction for sample.

The RT-sample mixes were loaded in a thermocycler that imposes diverse temperature cycles (Table A2.2). The final product of the reaction is the cDNA, that could be kept at 20 °C or processed for the following Real-Time PCR.

	Step 1	Step 2	Step 3	Step 5
Temperature [°C]	25	37	85	4
Time [min]	10:00	120:00	5:00	

Table A2.2: Temperature cycles imposed during the retrotranscription.

A2.5 Real-Time qPCR

The analysis of genes PER2 and BMAL1 was carried out by Real Time quantitative PCR following RNA extraction and reverse transcription to cDNA. To perform quantitative PCR was used the kit TaqMan® Gene Expression Assays (Applied Biosystems), which involves the use of fluorescent probes for the detection and quantification of an amplification product specific. The probes and primers for cDNA gene Per2, Bmal1 and GAPDH are designed and tested by the manufacturer, so they specificity and efficiency certified. The probes are equipped with a molecule MGB which further increases the specificity.
The reaction mix for single sample of cDNA is reported in Table A2.3.

Reaction Mix for each probe (20 uL total)	
2X TaqMan Gene Expression Master Mix	10 uL
TaqMan Gene Expression Assay	1 ul
RNase & DNase-free water	7 uL
cDNA	2 uL

Table A2.3: Reaction mix performed with TaqMan® Gene Expression Assays (Applied Biosystems). The volume of 20 ul is the volume of the single reaction for sample.

The temperature cycles imposed are reported in Table A2.4.

			40 Cycles	
	Step 1	Step 2	Step 3	Step 5
Temperature [°C]	50	95	95	60
Time [min]	2:00	10:00	0.15	1:00

Table A2.2: Temperature cycles imposed during the Real-Time PCR.

Appendix A3

Bioluminescence reporter assay

A3.1 Development a luciferase reporter cell line

Development of a stably transfected luciferase reporter gene assay requires two step:

- production of the luciferase reporter plasmid by virus production
- integration of genic material in the cell line by infection.

A3.1.1Virus production:

According to protocol cpmb, chapter 16.21, 16.22.

The protocol below described the procedures, day by day, of the virus production used for stable transfection in order to obtain a Bmal1::Luc reporter cell line.
This virus can be integrated in both human and mouse cell culture.

Day 0

- The day before the infection split 293T cells to 10 cm dishes so that they are semi-confluent the day of transfection; usually a confluent plate split 1:6 (up to 1:10) the day before transfection is about correct (aim at 30-50% confluence on the day of transfection). Big Petri Plates should contain 8ml DMEM/10%FCS/1%pennicillin-streptomycin-*glutamine*. Be careful when handling the dishes, 293T cells do not adhere very well: pipet slowly and against the walls of the dish.
- Incubate 293T over night

Day 1

- Make a solution per plate with:

  Backbone (coding) plasmide (BLUFpuro): 15 mg

  pSPAX2 (RNA pol. and packaging plasmid): 1 0 mg

  pMD2G (coat plasmid): 6 mg

  [$CaCl_2$] 2.5M, filter-sterilized 100 ml

  DNAs freee H_20: 500 ul

  The structure of the backbone plasmid is reported at the end of this Appendix.

- Vortex
- In 4-10ml (also 50 ml) polypropylene tube, place 0.5ml HeBS 2X per plate.
- Take a sterile pipette, put it in the tube containing HeBS 2x, and make bubbles of the air and at the same time take the solution made before with a pipette and pour it drop by drop while letting slip the bubbles on the sterile pipette. Vortex immediately during 5 seconds (=>don't to make more than two tubes at the same time). A fine white translucent precipitate should form.
- Let rest 20 min at room temperature
- Add dropwise 1 ml of the translucent solution per plate. Mix precipitate and medium by rocking plate back and forth, as for spreading cells

Day 2

- After 24 hours of incubation in standard incubator, change medium:
- Rinse cells carefully with 5ml of PBS 1X
- Replace medium with 10ml fresh medium containing 200ml of Hepes 1M

Day 3

- After 24 hours, harvest supernatant

Day 4

- After 24 hours harvest again medium, pool it with the one harvested on day 3 and concentrate the virus
- Plates of 293T can now be discarded
- Spin supernatant at 500 rpm for 10 minutes to pellet debris
- Filter the supernatant through filters with 0.2-0.4mm of diameter, to remove eventual 293T cells detached from the plate

Concentrate the virus using ultracentrifugation:

- Ultracentrifuge at 80000G 4'C, 90 minutes. In rotor 70Ti: 28000 rpm (it is 80695 G)

Dilute the virus:

- Remove the supernatant to a new tube
- Add 1/10 of initial volume (using the removed supernatant) to have 10x virus
- Pipet up and down to suspend the virus
- Aliquot the virus (1 ml aliquot) and store at -80°C.

HeBS 2X:	
NaCl	0.283M,
HEPES acid	0.023M
Na_2HPO_4	1.5mM
pH 7.05	

pH of HeBS is absolutely critical. 7.05 is ideal, less than 7.0 or more than 7.1 is useless. Use Fluka Buffer tablets pH 7.0 to calibrate pH meter. Calibrate three times. Store at -80°C.

Check the pH of the solutions of HeBS.

A3.1.1 Infection

The day before infection, split confluent cells 1:4 in 35 mm dishes. The cell heve to be 40-50% confluent the day of infection.

The day of thrasfetion, remove the medium and add drop by drop warmed viral surnatant.

For increase the infection rate, add polybene 1 ug/mL final concentration, immortalizzated cells, protamine sulfate 8 ug/mL final concentration, for primary cells.

Change to fresh surnatant after 12-24 h, replacing fresh culture media after 2 wash of PBS 1X.

At the third day after the transfection, start the selection of the cells with selectin medium by adding 1 mg/mL of puromycin (Sigma Aldrich).

Split the cells in selection medium twice to be sure that all the cells are selected. Cultivate the cells in selecting medium for at least 2 weeks.

A3.2 Long-term circadian rhythms recording

LumiCycle and Imaging recording medium

All media used during the recording phase are high-glutamine (2 mM, Sigma Aldrich) Dulbeccos Modified Eagles Medium (Sigma Aldrich), that contain different concentrations of glucose [25 mM: 2mM] according to the purpose of experiment.

Because the equipment for luminescence detection (LumiCycle and microscope) are controlled in temperature but not in CO2, we add 350 mg/L of sodium bicarbonate (Sigma Aldrich) and Hepes 10 mM (Sigma Aldrich), for buffering the CO2 concentration.

B27 supplement (2%, Life Techologies) or fetal bovine serum (10%, Life Techologies) was used as serum. Because phenol red reduces light signal penetration, the culture media should not contain phenol red. The medium must be sterilized by filtering. Luciferin (final concentration 0.1 mM, beetle luciferin, potassium salt, Sigma Aldrich) should be added just before the luciferase activity assay. The medium should be warmed at 37° before being used.

A2.3 Imaging analysis

The bioluminescence images were acquired by SI Image SGL B software (Spectral Instrument).

After removing the outliers and adjusting the contrast by NIH ImageJ Software, the bioluminescence images were processed by a Matlab program.

This program processed all images acquired by frame by frame, dividing them in ROIs, whose pixel number can be modulated, depending on detail degree of interest (Figure A3.1-A3.2).

Using large ROI allows to investigate a population behavior than the small those that enable to see single-cell details.

For each ROI was calculated the average intensity of luminescence integrated in the time, by implementation of Matlab function mean.

These signals thus obtained were processed with LumiCycle Sofware for the baseline subtraction and the calculation of circadian parameters (period, amplitude and phase).

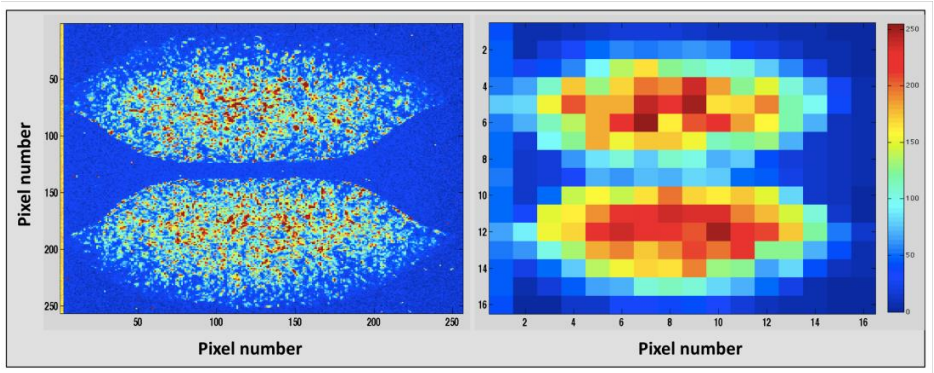

Figure A3.1: Image processing. The initial image [256x256] pixel was divided in 256 ROIs [16x16] pixel. For each ROI was calculated the average intensity of luminescence.

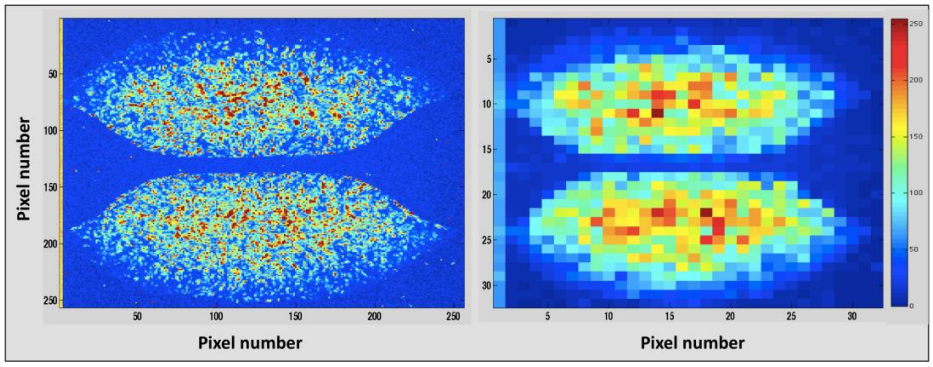

Figure A3.2: : Image processing. The initial image [256x256] pixel was divided in 1024 ROIs [16x16] pixel. For each ROI was calculated the average intensity of luminescence.

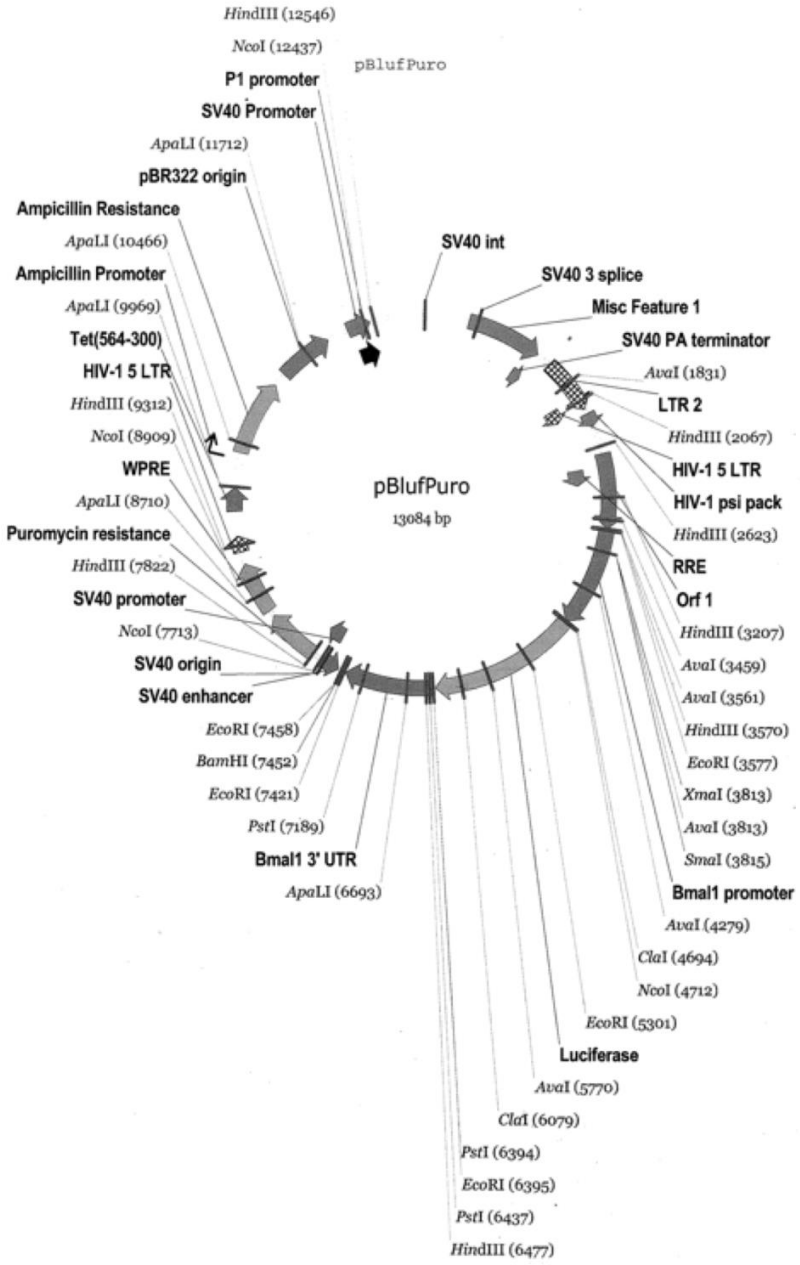
pBlufPuro
13084 bp
HindIII (12546)
NcoI (12437)
P1 promoter
SV40 Promoter
ApaLI (11712)
pBR322 origin
Ampicillin Resistance
ApaLI (10466)
Ampicillin Promoter
ApaLI (9969)
Tet(564-300)
HIV-1 5 LTR
HindIII (9312)
NcoI (8909)
WPRE
ApaLI (8710)
Puromycin resistance
HindIII (7822)
SV40 promoter
NcoI (7713)
SV40 origin
SV40 enhancer
EcoRI (7458)
BamHI (7452)
EcoRI (7421)
PstI (7189)
Bmal1 3' UTR
ApaLI (6693)
SV40 int
SV40 3 splice
Misc Feature 1
SV40 PA terminator
AvaI (1831)
LTR 2
HindIII (2067)
HIV-1 5 LTR
HIV-1 psi pack
HindIII (2623)
RRE
Orf 1
HindIII (3207)
AvaI (3459)
AvaI (3561)
HindIII (3570)
EcoRI (3577)
XmaI (3813)
AvaI (3813)
SmaI (3815)
Bmal1 promoter
AvaI (4279)
ClaI (4694)
NcoI (4712)
EcoRI (5301)
Luciferase
AvaI (5770)
ClaI (6079)
PstI (6394)
EcoRI (6395)
PstI (6437)
HindIII (6477)

Appendix A4

High temporal resolution detection of patient-specific glucose uptake from human ex-vivo adipose tissue on chip

Zambon Alessandro, Zoso Alice, Gagliano Onelia, Magrofuoco Enrico, Gian Paolo Fadini, Angelo Avogaro, Mirto Foletto, Quake Stephen, Elvassore Nicola

My contribution is concerning the design and development of the automation and of the user-friendly interface of multilayer microfluidic platform; I also participated to the fabrication of all components and external devices for the chip management and the relative calibration and validation.

A4.5 ABSTRACT

Human tissue *in vitro* models on-chip are highly desirable to dissect the complexity of physio-pathological *in vivo* response because of their advantages compared to traditional static culture systems in terms of high control of microenvironmental conditions, including accurate perturbations and high

temporal resolution analyses of medium outflow. Human adipose tissue (hAT) is a key player in metabolic disorders, such as Type 2 Diabetes Mellitus (T2DM). It is involved in the overall energy homeostasis not only as passive energy storage, but also as an important metabolic regulator.

Here, we aim at developing a large scale microfluidic platform for generating high temporal resolution of glucose uptake profiles, and consequently insulin sensitivity, under physio-pathological stimulations in *ex vivo* adipose tissues from non-diabetic and T2DM individuals.

A multi-scale mathematical model that integrates fluid dynamics and intra-cellular insulin signaling pathway description was used for assisting microfluidic design in order to maximize measurement accuracy of tissue metabolic activity in response to perturbations. An automated microfluidic injection system was included on chip for performing precise dynamic biochemical stimulations. The temporal evolution of culture conditions could be monitored for days, before and after perturbation, measuring glucose concentration in the outflow with high temporal resolution. As a proof of concept for detection of insulin resistance, we measured insulin-dependent glucose uptake by hAT from non-diabetic and T2DM subjects, mimicking the post-prandial response. The system presented thus represents an important tool in dissecting the role of single tissues, such as hAT, in the complex interwoven picture of metabolic diseases.

A4.2 INTRODUCTION

In vitro biological and physio-pathological studies, drug testing and therapy development demand robust systems that not only reproduce human tissue response with high fidelity, but also mimic the *in vivo* stimulating dynamic environment and monitor the resulting biological response[1].

On-chip *in vitro* models have several advantages respect to conventional cultures in well. The microfluidic culture microenvironment can be accurately controlled at the micro-scale due to the laminar flow therein[2]. Furthermore, microfluidic large-scale integration systems couple the advantages of miniaturization with those of automatic and temporally controlled fluid handling[3], making possible precise biochemical stimulations with high temporal resolution. Finally, being perfused systems, the culture outflow can be analyzed for on-line biological response monitoring without perturbing culture conditions[4].

A biopsy-derived human tissue culture is currently the most faithful *in vitro* model of human physiology[1], because it preserves cell-cell and cell-matrix interactions within the native three-dimensional architecture. Traditionally, tissue cultures are maintained in static wells with poor spatial and temporal control of the cellular microenvironment[5]. Metabolic measurements are performed therein with limited temporal resolution, given the high perturbation induced at every medium collection[6]. Recently, Iori *et al* developed a large-scale perfused system for hAT co-culture with hepatocytes and endothelial cells[7]. However, cultures were stopped after 48 h, with only three time points for measurements of metabolic activity.

Ex vivo culture of a freshly-isolated tissue within a microfluidic device adds to the traditional *in vitro* model the above-mentioned advantages of tight culture control, tissue accurate temporal stimulation, and on-line readout. In addition, being a perfused system, on-chip culture enhances mass transport throughout the whole tissue volume, avoiding internal necrosis. Lastly, miniaturization increases experimental throughput and decreases the amount of biological material required.

A limited number of tissue cultures have been performed within microfluidic systems, mainly using animal cells[1], because of human tissue scarce availability. However, few human microfluidic *ex vivo* models were reported for islets[8], liver[9],

brain[10], and heart slices[11]. Considering the high rate of failure in the drug discovery pipeline, especially occurring at the last stages of clinical trials, human disease modeling *in vitro* is becoming the new frontier[12], encouraged by the recent breakthrough discovery of induced pluripotent stem (hiPS) cells[13]. However, using hiPS to model diseases that develop over decades, such as T2DM, is currently prevented, although attempts to recapitulate in short-term at least the effects of ageing are under investigation[14]. Thus, using primary tissues from patients affected by late-onset diseases is currently the most reliable choice. Human adipose tissue (hAT) plays an important role in T2DM and, more generally, in metabolic disorders[15–17]. Rather than being a mere energy storage, it is actively involved in organ cross-talk[18,19]. With respect to other tissues, hAT is also more easily available from both non-diabetic and T2DM patients. To the best of our knowledge, no adipose tissue *ex vivo* cultures have been performed in microfluidics. On the other hand, hAT investigations under static conditions have been focused on different aspects, such as metabolic activity, adipokine and hormone release[20–22]. Static cultures of hAT showed good preservation of gene expression and adipocyte function for up to 1 week[23].

In this work, we present the development of a microfluidic chip for *ex vivo* hAT long-term culture that includes an automated system for precise dose-time stimulation and quasi-on-line glucose monitoring. A multi-scale mathematical model allowed a signaling-pathway-based design of the culture micro-chamber and operating conditions to maximize measurement accuracy. The fluidic configuration was designed in order to decouple normal culture conditions and perturbation analyses. The system proved suitable for long-term *ex vivo* culture of hAT. Technical variability of measurements was minimized allowing a robust high-throughput study of single-patient biopsy-derived samples. Due to the perfused culture conditions, measurements could be performed continuously at high temporal resolution without disruption of the tissue culture. Glucose concentration could be tracked for several days, without using radio-tracers[24] or fluorescent probes[25], to closely mimic physiological *in vivo* conditions. As a proof of concept, the differential response of hATs derived from healthy and T2DM patients was investigated applying a step stimulation of insulin under normal or high-glucose conditions.

A4.3 EXPERIMENTAL SECTION

Mathematical model. A two-dimensional (2D) multi-scale mathematical model has been developed to describe medium fluid dynamics, mass transport of glucose and insulin, and intracellular insulin signaling pathway. The model adapts a previously published model of a three-dimensional cell culture on a scaffold[26], to a 2D culture system with a different geometry. Figure 1A describes the configuration of the setup, and the physical and biological processes modeled. The culture chamber is a cylinder with diameter D, which hosts a hAT sample of height H_b. The chamber has an inlet and an outlet given by a 3.5-cm long channel, with rectangular section of 100-μm height and 40-μm width. For modeling purposes the system was sub-divided into two regions: the medium and the tissue domains (Figure 1A). Within the first one, mass transport of insulin and glucose occurs by both convection and diffusion, while in the tissue domain only diffusion takes place along with processes of insulin and glucose consumption by cells. This cellular uptake was included in the model by describing the insulin signaling pathway, which involves insulin internalization and, after a phosphorylation cascade, glucose entrance into the cells by active transport. Specifically, fluid dynamics was described by Navier-Stokes equation for incompressible fluids, molecular diffusion by Fick's law, and glucose and insulin consumption by combining a model of the insulin signaling pathway[27], reduced as previously described[26,28], with a Michaelis-Menten kinetic model[29]. Results are reported in terms of outlet glucose concentration normalized by the concentration at the inlet. The model was numerically solved by finite element method (FEM) using COMSOL Multiphysics 4.3 (Comsol Inc.). More details are reported in Supporting information (Extended methods, Table S-1).

Microfluidic platform. An automated microfluidic chip was produced by standard photo- and soft-lithography techniques[30] (Figure 2A). It is composed of three polydimethylsiloxane (PDMS, Sylgard 184, Dow Corning) layers: a flow layer, a biopsy sample insertion layer, and a control one. The flow layer includes 8 independent culture chambers, each equipped with an injection system, which allows a biochemical stimulus to be inserted very closely to the culture chamber inlet, and independent inlet and outlet channels of 50-μm height and 170-μm width for medium distribution. Each culture chamber is a 3-mm diameter cylinder

that can contain a 1-2 mm high tissue sample (Figure 2B). An array of hexagonally spaced PDMS micro-posts of 50-µm diameter and 115-µm center-to-center spacing, are located at the top surface of each chamber. The injection system is composed of a 20-cm long serpentine, with rectangular section of 100-µm width and 50-µm height, for a total volume of approximately 1 µL (Figure 2C). The serpentine has dedicated inlet and outlet for easy off-line refill. The sample insertion layer is a 6-8 mm high PDMS layer that contains 4-mm diameter holes at culture chamber positions (Figure 2B). After hAT sample insertion, each hole is sealed by conical polypropylene caps, having a flat base aiding sample positioning against the micro-post array. The caps are made using a 1/8-in fitting luer (Cole Parmer) filled with PDMS. The control layer, fabricated according to Zambon et al.[4], includes a network of control channels that actuate a peristaltic micro-pump[31] near medium inlet and a system of pneumatic micro-valves for controlling medium or stimulus delivery to each culture chamber with high temporal resolution (Figure 2A). More details are included in Supporting information (Extended methods, Figure S-1, Table S-2).

Automation. Control channels were connected via Tygon® tubes (ID 0.02", Cole Parmer) and filled with distilled water. During operation, each tube was internally pressurized (P=250 kPa) to close a specific set of normally-open micro-valves by miniature pneumatic solenoid valves (M3MAO, CKD Corporation), which are controlled by an I/O device (USB 6008, National Instruments) connected to a USB port of a computer. The electronic unit was plugged to a 24-V transformer. The system was equipped with a rechargeable battery to guarantee long-term functioning also during repositioning or emergency outage. A custom software was developed in LabVIEW® (National Instruments) to automatically manage chip operations. Specific subroutines were implemented to assist all the phases for the organ culture in microfluidics (preliminary valve test, chip de-bubbling, feeding, and insulin stimulation). Cell culture medium was placed inside vials (Cryovial, Greiner Bio-one) that were pressurized at 70 kPa by compressed air. When on-chip valves were open, medium could flow due to this positive pressure, useful for fast fluid changes and channel rinsing steps. When a precise flow rate was required, medium movement was controlled by using the on-chip peristaltic micro-pumps. An image of the complete experimental setup is shown in Figure S-

2. Pump calibration was performed before the experiments (Figure S-3), as previously reported[31].

hAT sample collection and preparation. Samples of visceral adipose tissue were collected from individuals undergoing surgery (sleeve gastrectomy or routine abdominal surgery) at the University Hospital of Padova (Italy). Subjects provided informed consent to the procedure and for collection of the sample to be used for research purposes. Collection and storage of biological samples was approved by the local Ethical Committee. Patients' age varied between 34-80 year and body mass index (BMI) between 24-54 kg/m^2. Of 16 patients, 50% were female. More details are reported in Table S-3.

hAT *in vitro* culture protocol was adapted from literature[32]. After isolation, each biopsy was maintained in 5 mL of Dulbecco's Modified Eagle Medium (DMEM) with 5-mM glucose (Life Technologies) for up to 3 h at room temperature. Then, each biopsy was washed with phosphate buffer saline (PBS, Life Technologies) and cut into 3-mm diameter slices with the aid of a sterile punch (Miltex) and a scalpel. Each slice was weighted and put in a 48-well plate with 300 μL of 5-mM glucose DMEM. At least 18 h of static culture were required for culture adaptation before microfluidic integration or control experiments in static wells. After this period, hAT glucose consumption rate was estimated by measuring its concentration in 1 μL of culture medium using FreeStyle Lites glucometer and strips (Abbott Diabetes Care).

hAT microfluidic integration. DMEM having 4 and 7-mM glucose concentration were obtained by mixing 25-mM glucose and glucose-free DMEM (Life Technologies) in different ratios. Before use, medium was conditioned in a biological incubator (37°C, 5% CO_2, 95% relative humidity) in a Petri dish for at least 2 h. Prior to biopsy sample integration in microfluidics, PDMS culture chambers and flow channels were conditioned with medium at 1-μL/min flow rate for at least 1 h by means of a syringe pump (Harvard Apparatus). Medium perfusion was then stopped for sample insertion. Each experiment was performed with at least three parallel chambers filled with hAT slices having similar weight and glucose consumption under static conditions. The chambers were then closed and pressurized at 40 kPa for few hours to dissolve bubbles possibly introduced during sample insertion. Then, medium perfusion was started keeping the

microfluidic platform in a biological incubator during culture. For exploratory experiments at different flow rates ($\dot{V}$ =0.025-0.6 µL/min), medium delivery was performed via a syringe pump (Harvard Apparatus) equipped with 250-µL Hamilton Glass syringes. Once selected an optimal flow rate of 0.1 µL/min, the integrated micro-pumps within the chip were used. For stimulations, a 100-nM human recombinant insulin (Sigma Aldrich) solution was used in 4- or 7-mM glucose DMEM, pre-loaded in the injection system. hAT slices were removed from the microfluidic system at the end of culture for further characterization. During control static culture experiments, the sample was maintained in a well, medium replaced every 3 days, and glucose concentration measured daily.

Glucose measurement. Glucose concentration at the outlet of the culture chamber, G_{OUT}, was measured to derive hAT glucose uptake performing a mass balance on the whole culture system[4]. For sampling, outlet tubes were removed from the microfluidic chip and replaced by a 22G dispensing needle for medium collection[4]. Medium samples of 0.6-µL volume were analyzed off-line using FreeStyle Lites glucometer and strips (Abbott Diabetes Care) to measure glucose concentration G_{OUT}. The effect of medium evaporation during culture in the microfluidic chip was corrected by keeping, as a control, a microfluidic chamber without any hAT sample inside and measuring glucose outlet concentration[4]. Glucometer measurements were initially validated by Gas Chromatography Mass Spectrometer (Agilent 5973) with a DB5ms Column (122-5532 J&W) using standard procedures.

Biological analyses. hAT characterization at the end of culture was performed after tissue extraction from the microfluidic chip. To evaluate tissue viability, standard MTT test was performed on samples immediately after isolation and at the end of the culture period. 20 to 40-µm thick hAT cryosections were obtained after embedment in OCT®. Subsequently, hematoxylin and eosin (H&E, Bio-Optica) and Masson trichrome (Bio-Optica) staining were performed on the obtained slices. After staining, slices were mounted in HI-MO (Lab-Optica).

A4.4 RESULTS AND DISCUSSION

The development of a physiologically relevant *in vitro* model mandates important prerequisites for the precise readout of information. Two of the most critical are the long-term stability of the tissue culture, and the availability of a correlated and significant benchmark. Furthermore, even starting from a patient's biopsy of human tissue, collecting data instructive for physio-pathological applications demands the simultaneous spatio-temporal control of biochemical stimulations and time-resolved detection of the induced metabolic target physiological perturbation. These essential requirements can be satisfied by a properly designed micro-perfused system. Design criteria of the microfluidic tissue-chamber geometry should take into account the role played by experimental and operative variables, such as biopsy-derived sample size and flow rate. For instance, a high residence time (given by the ratio of microfluidic chamber volume to medium flow rate) will result in stronger medium perturbation in the chamber as a consequence of cellular activity, but at the expenses of a limited time resolution of the measured response in the outflow. Whereas a low residence time leads to inevitably undetectable inlet/outlet variations.

Multi-scale model-based culture chamber design. To proper design the microfluidic chamber, we took advantage of multi-scale mathematical modeling, as a means to theoretically investigate the effect of the most important experimental and operative variables (Figure 1A). We simulated a 100-nM insulin-pulse perturbation lasting 15 minutes, as an exacerbation of what occurs *in vivo* during post-prandial conditions, and evaluated the effect on glucose concentration at the outlet of the culture chamber (Figure 1B and C). Outlet glucose concentration is directly correlated to glucose uptake in the chamber, and its experimental measurement would allow the study of tissue response following a stimulation.

By the model, we first studied the influence of chamber geometry (Figure 1B). Specifically, we varied sample and chamber heights within experimentally meaningful ranges. Results show that a thinner sample (H_b=1 mm) gives a faster response, i.e. it reaches the minimum of outlet concentration in a shorter time; whereas a thicker sample (H_b=2 mm) produces a larger overall concentration variation after stimulation respect to the initial basal level. Insulin transport within

the tissue domain is governed only by interstitial diffusion, which is slow compared to cell glucose uptake rate, and it is the limiting step in the overall process. Thus, insulin penetration into the thinner sample occurs more rapidly because a shorter distance needs to be covered. However, the double uptake-volume of the thicker sample consumes a quantity of glucose that is higher, although less than the double because of the transport limitations mentioned. Therefore, in the experiments, sample height (H_b) was chosen as a trade-off between rapidity and amplitude of response.

A positive height of the chamber inter-layer (H_c) has a negative effect on tissue response, in terms of rate of glucose uptake and overall consumption (Figure 1B). When sample surface is not in direct contact with medium flow channel ($H_c>0$), a gradient of glucose concentration establishes in in the chamber inter-layer, because insulin (fast) transport by convection is less efficient in this region (Figure S-4). This result highlights the importance of experimentally positioning the tissue sample as close as possible to the flow channel, with the consequent difficulty of avoiding channel clogging or sample partial wash-out.

Then, we investigated the effect of flow rate in the system (Figure 1C), a parameter directly related to medium residence time in the culture chamber. The higher the flow rate, the lower is the outlet glucose concentration drop following an insulin pulse, down to the point of becoming practically undetectable. However, at very low flow rates ($\dot{V} < 0.025$ μL/min) the amount of glucose provided by the flow becomes the limiting factor for glucose uptake, irrespective of insulin presence (Figure S-5).

Experimental microfluidic platform. The microfluidic culture chamber represents the core of the platform. The mathematical model results instructed the choice of important parameters, but other practical considerations were also taken into account, such as access for sample insertion, device robustness, uniform distribution of medium. For easy hAT sample insertion into the chamber, a vertical opening was provided, and sealed by a flat cap during perfused culture (Figure 2B). In the medium channel, in correspondence to the chambers, an array of circular micro-posts was included (Figure 2B). This technical expedient ameliorates the homogeneous distribution of medium on the surface of the sample reducing the formation of dead volumes, gives support to the sample avoiding its

partial wash-out or its clogging of the flow channel, and also prevented sample floating, allowing turning the device upside-down for ease of optical observation. The overall microfluidic platform includes eight culture chambers to increase experimental throughput and parallel culture control (Figure 2A).

A patient-specific *in vitro* model should include not only the tissue itself, through the ability of performing long-term culture, but also a means of giving precise and modulated physiological stimuli. Thus, the experimental setup also includes an injection system near the entrance of each chamber, where a biochemical stimulus, such as insulin-containing medium, can be loaded and automatically delivered to the chamber with precise timing and concentration profile, minimizing delay and axial dispersion (Figure 2C). The shape of the stimulus can be customized by changing stimulus duration, flow rate, repeating the stimulation several times, or performing a step stimulation. The injection system is connected to a reservoir that allows fresh loading of perishable chemicals, inserted few minutes before injection, avoiding thermo-sensitive degradation. The injection system was validated with food dyes and fluorescent tracers in order to simulate a drug pulse delivery (Figure 2C and D). The system demonstrated suitability to perform precise stimulation into the chamber with high spatio-temporal resolution (Figure 2C). Specific validation experiments were performed integrating *ex vivo* hAT. Medium homogeneous distribution in the chamber was verified by means of a fluorescein solution, first in a simplified version of the microfluidic chip (Figure S-6), then within the final setup both in absence and presence of a hAT sample inside (Figure 2D). We observed a uniform distribution of the fluorescent tracer inside the chamber, aided by the presence of the micro-post array. hAT sample was tracer-soaked, with the most porous regions showing a higher fluorescence intensity.

Microfluidic platform validation. Within our setup, hAT maintained high viability after one-week culture. No significant differences were observed between static and microfluidic cultures, and compared to the corresponding freshly isolated biopsy (Figure 3A). Thus, we confirmed that long-term hAT cultures can be successfully performed, as was previously found under static conditions[33], and for the first time we extended this result to a microfluidic system. Moreover, tissue morphology from H&E stain (Figure 3B) and Masson

trichrome (Figure S-7) did not show significant differences between static or microfluidic conditions after 8 days of culture, even compared to the tissue morphology immediately after surgery.

The maintenance of metabolic activity during culture was measured using 3 samples from the same hAT biopsy and detecting glucose concentration at the outlet of the culture chamber (Figure 3C). A low G_{OUT} means a high glucose uptake, at fixed flow rate (0.025 µL/min). After one day of sample adaptation to culture conditions, glucose concentration at the outlet was constant for the next 4 days, confirming high metabolic tissue activity in microfluidics. We verified that a 24-h adaptation period was needed also under static culture conditions (data not shown).

After confirming hAT viability, normal morphology, and accurate response in terms of glucose consumption, we investigated the effect of flow rate on glucose outlet concentration, starting from low (0.025 µL/min) to high values (0.6 µL/min). Figure 3D shows outlet glucose profile at increasing flow rates, monitored at maximum time resolution, i.e. medium was continuously collected and analyzed every 0.6 µL eluted. This measurement was repeated for 4 samples derived from the same hAT biopsy. Consistently, glucose concentration profile was maintained for different samples with low variability. At low flow rates, glucose concentration drop between inlet and outlet was large, with high signal-to-noise ratio. On the other hand, a high flow rate increased measurement time resolution, up to one measurement per minute for the highest flow rate investigated (0.6 µL/min). Thus, we chose a flow rate of 0.1 µL/min for further analyses with insulin stimuli, which guaranteed both high temporal resolution and a glucose concentration drop sufficiently detectable to capture differences in glucose uptake under stimulation.

We also obtained consistent data analyzing the steady-state G_{OUT} value at different flow rates (Figures 3E and F). Figure 3E shows the results of these measurements with a special focus on the temporal robustness of the methodology. Three samples derived from the same hAT biopsy were repeatedly analyzed during 3 successive days and showed remarkable reproducibility both in time and between samples. These important data had a positive impact in demonstrating robustness and high-throughput experimental feasibility, key

parameters for a robust *in vitro* physiological analysis. We also compared the experimental data with model results, which were in good agreement, and demonstrating the suitability of our mathematical model for experimental design (Figure 3F). From data in Figure 3F and knowing sample weight, we calculated glucose uptake as a function of flow rate, by a mass balance approach[4] (Figure 3G). Uptake depends on flow rate because of different glucose availability. It follows a Michaelis-Menten-like kinetics, approximately reaching a plateau at high flow rates ($\dot{V} > 0.4$ μL/min).

Figure 3D-G were obtained using different samples derived from the same patient's hAT biopsy. Overall, data show high reproducibility and make possible using the same biopsy for parallel studies with different conditions and biochemical stimulatory cues. We also observed a fair reproducibility of data using samples from different patients (Figure 3C and S-8). These results are particularly promising for the use of our system to discriminate between a healthy and pathological phenotype.

hAT *in vitro* model for insulin resistance measurement. Once we had demonstrated the capability to ensure long-term culture, reliable readout and biological analysis, we focused our investigation on an advantageous application of our system for the physiological hAT field. hAT is a complex organ and its role in metabolic activity and disorders such as T2DM is an important field of investigation[17]. We applied our system for the obtainment of proof-of-concept data related to insulin effect on glucose uptake after a long stimulation. We evaluated the effect of an insulin step on outlet glucose concentration during hAT cultures exposed to normal or post-prandial physiologic glucose concentrations. We focused on discriminating between a healthy and a T2DM phenotype, by using hAT biopsies taken from patients in either state. Our goal was to determine differences in glucose uptake from insulin-stimulated and non-stimulated biopsies, thus to relate the profile to diabetic or healthy patients. Since we had previously observed some inter-patient variability, we expected differences in readout of outlet glucose concentration even within the same category of patients, and we performed each experiment with an internal control using samples from the same hAT biopsy.

We performed two sets of experiments. In the first one, we stimulated both healthy and diabetic samples with a 100-nM insulin step (Figure 4A and B), maintaining the same basal glucose concentration (G_{IN}=4 mM) during the whole duration of the experiment. In this condition, as expected[7], we did not observe differences in outlet glucose concentration in healthy and diabetic patients, compared with their respective unstimulated controls. In the second set of experiments, we stimulated hAT samples with a 100-nM insulin step overlapped to a step of glucose concentration, from basal to high (G_{IN}=7 mM), mimicking the trend of a post-prandial phase (Figure 4C and D). hAT biopsy from a healthy patient showed a significant decrease in outlet glucose concentration from the insulin-stimulated chamber respect to the non-stimulated one (Figure 4C and S-9). Thus, as expected, insulin triggers glucose uptake at high-glucose concentration. On the other hand, for the diabetic patient-derived biopsy, no evidence of differences in glucose uptake between stimulated sample and control was apparent (Figure 4D). A progressive reduction of glucose uptake was also observed during the persistent post-prandial-like state. These data, even if derived from a limited number of patients, are promising for *in vitro* studies of insulin sensitivity and they represent a proof of concept for its applicability.

A4.5 CONCLUSIONS

Taking advantage of microfluidic large-scale integration systems, we developed an on-chip tissue culture platform that could be advantageously used to maintain *ex vivo* hAT for several days, without loss of viability and typical morphology. Although hAT has the advantage of being more accessible in comparison to other tissues, this miniaturized culture system can be readily applied also to other tissue types of interest.

This microfluidic system requires only approximately 10-mm^3 tissue, but allows the robust measurement of glucose uptake with high temporal resolution, due to the high surface-to-volume ratio and the properly defined geometrical and operative conditions. In particular, the design of the culture chamber took advantage of a multi-scale mathematical model, not only describing the fluid dynamics in the system, but also the intra-cellular signaling processes leading to insulin-stimulated glucose uptake. Thus, high-accuracy and repeatable

measurements were achieved with samples taken from the same patient's biopsy, and sensitivity was sufficient to discriminate the biological patient-to-patient variability.

The injection system was designed to maximize precision and controllability of the biochemical stimulations. In this work, as a proof of concept, a single step of insulin stimulation was performed, but more elaborated dynamics are also possible to fully explore the complexity of the biological response. Actually, the intracellular network architecture and its dynamic behavior are better investigated through system perturbations[34].

The availability of hAT from normal patients and those affected by T2DM made possible to show the feasibility of studying hAT insulin resistance *in vitro* with high accuracy. We measured glucose as the main target molecule of interest, but other compounds sampled from the outflow can be equally analyzed, for example by Gas Chromatography Mass Spectrometry or other enzymatic assays. Thus, the micro-culture system we developed represents a springboard for future studies of insulin resistance *in vitro*, effectively dissecting the role of a single tissue in the large scenario of metabolic diseases.

ACKNOWLEDGMENT

This research work was supported by Progetto di Eccellenza CA.RI.PA.RO. and the European Foundation for the Study of Diabetes; O.G. thanks CA.RI.PA.RO Foundation for supporting PhD fellowship.

REFERENCE

(1) Luni, C.; Serena, E.; Elvassore, N. *Curr*. *Opin*. *Biotechnol*. **2014**, *25*, 45–50.

(2) Squires, T. M.; Quake, S. R. *Rev*. *Mod*. *Phys*. **2005**, *77*, 977–1026.

(3) Gómez-Sjöberg, R.; Leyrat, A. A.; Pirone, D. M.; Chen, C. S.; Quake, S. R. *Anal*. *Chem*. **2007**, *79*, 8557–8563.

(4) Zambon, A.; Zoso, A.; Luni, C.; Frommer, W. B.; Elvassore, N. *Integr*. *Biol*. **2014**, *6*, 277–288.

(5) Resau, J. H.; Sakamoto, K.; Cottrell, J. R.; Hudson, E. A.; Meltzer, S. J. *Cytotechnology* **1991**, *7*, 137–149.

(6) Martin, I.; Wendt, D.; Heberer, M. *Trends Biotechnol*. **2004**, *22*, 80–86.

(7) Iori, E.; Vinci, B.; Murphy, E.; Marescotti, M. C.; Avogaro, A.; Ahluwalia, A. *PLoS ONE* **2012**, *7*, e34704.

(8) Wang, Y.; Mendoza-Elias, J.; McGarrigle, J.; Nourmohammadzadeh, M.; Wang, Q.; Li, Z.; Rady, B.; Feng, F.; Qi, M.; Lo, J.; Eddington, D.; Oberholzer, J. *Micro Nanosyst*. **2013**, *5*, 216–223.

(9) Wagner, I.; Materne, E.-M.; Brincker, S.; Süßbier, U.; Frädrich, C.; Busek, M.; Sonntag, F.; Sakharov, D. A.; Trushkin, E. V.; Tonevitsky, A. G.; Lauster, R.; Marx, U. *Lab*. *Chip* **2013**, *13*, 3538–3547.

(10) Huang, Y.; Williams, J. C.; Johnson, S. M. *Lab*. *Chip* **2012**, *12*, 2103–2117.

(11) Cheah, L.-T.; Dou, Y.-H.; Seymour, A.-M. L.; Dyer, C. E.; Haswell, S. J.; Wadhawan, J. D.; Greenman, J. *Lab*. *Chip* **2010**, *10*, 2720–2726.

(12) Engle, S. J.; Puppala, D. *Cell Stem Cell* **2013**, *12*, 669–677.

(13) Takahashi, K.; Tanabe, K.; Ohnuki, M.; Narita, M.; Ichisaka, T.; Tomoda, K.; Yamanaka, S. *Cell* **2007**, *131*, 861–872.

(14) Miller, J. D.; Ganat, Y. M.; Kishinevsky, S.; Bowman, R. L.; Liu, B.; Tu, E. Y.; Mandal, P. K.; Vera, E.; Shim, J.; Kriks, S.; Taldone, T.; Fusaki, N.; Tomishima, M. J.; Krainc, D.; Milner, T. A.; Rossi, D. J.; Studer, L. *Cell Stem Cell* **2013**, *13*, 691–705.

(15) Scherer, P. E. *Diabetes* **2006**, *55*, 1537–1545.

(16) Bjørndal; Rndal, B.; Burri, L.; Staalesen, V.; Skorve, J.; Berge, R. K. *J*. *Obes*. **2011**, *2011*, e490650.

(17) Donath, M. Y.; Shoelson, S. E. *Nat*. *Rev*. *Immunol*. **2011**, *11*, 98–107.

(18) Li, F. Y. L.; Cheng, K. K. Y.; Lam, K. S. L.; Vanhoutte, P. M.; Xu, A. *Acta Physiol*. **2011**, *203*, 167–180.

(19) Rosen, E. D.; Spiegelman, B. M. *Cell* **2014**, *156*, 20–44.

(20) Trujillo, M. E.; Lee, M.-J.; Sullivan, S.; Feng, J.; Schneider, S. H.; Greenberg, A. S.; Fried, S. K. *J. Clin. Endocrinol. Metab*. **2006**, *91*, 1484–1490.

(21) Fain, J. N.; Madan, A. K.; Hiler, M. L.; Cheema, P.; Bahouth, S. W. *Endocrinology* **2004**, *145*, 2273–2282.

(22) Fried, S. K.; Bunkin, D. A.; Greenberg, A. S. *J. Clin. Endocrinol. Metab*. **1998**, *83*, 847–850.

(23) Cigolini, M.; Smith, U. *Metabolism*. **1979**, *28*, 502–510.

(24) Virtanen, K. A.; Peltoniemi, P.; Marjamäki, P.; Asola, M.; Strindberg, L.; Parkkola, R.; Huupponen, R.; Knuuti, J.; Lönnroth, P.; Nuutila, P. *Diabetologia* **2001**, *44*, 2171–2179.

(25) Speizer, L.; Haugland, R.; Kutchai, H. *Biochim. Biophys. Acta BBA - Biomembr*. **1985**, *815*, 75–84.

(26) Magrofuoco, E.; Elvassore, N.; Doyle, F. J. *Biotechnol. Prog*. **2012**, *28*, 833–845.

(27) Sedaghat, A. R.; Sherman, A.; Quon, M. J. *Am. J. Physiol. - Endocrinol. Metab*. **2002**, *283*, E1084–E1101.

(28) Luni, C.; Doyle, F. J. *Int. J. Robust Nonlinear Control* **2011**, *21*, 1730–1741.

(29) Olefsky, J. M. *J. Clin. Invest*. **1976**, *57*, 842–851.

(30) McDonald, J. C.; Duffy, D. C.; Anderson, J. R.; Chiu, D. T.; Wu, H.; Schueller, O. J. A.; Whitesides, G. M. *Electrophoresis* **2000**, *21*, 27–40.

(31) Unger, M. A.; Chou, H.-P.; Thorsen, T.; Scherer, A.; Quake, S. R. *Science* **2000**, *288*, 113–116.

(32) Smith, U. *J. Clin. Invest*. **1974**, *53*, 91–98.

(33) Carswell, K. A.; Lee, M.-J.; Fried, S. K. In *Human Cell Culture Protocols*; Mitry, R. R.; Hughes, R. D., Eds.; Methods in Molecular Biology; Humana Press, 2012; pp. 203–214.

(34) Ideker, T. E.; Thorsson, V.; Karp, R. M. In *Pacific Symposium on Biocomputing*; 2000; Vol. 5, pp. 302–313.

Figures and captions

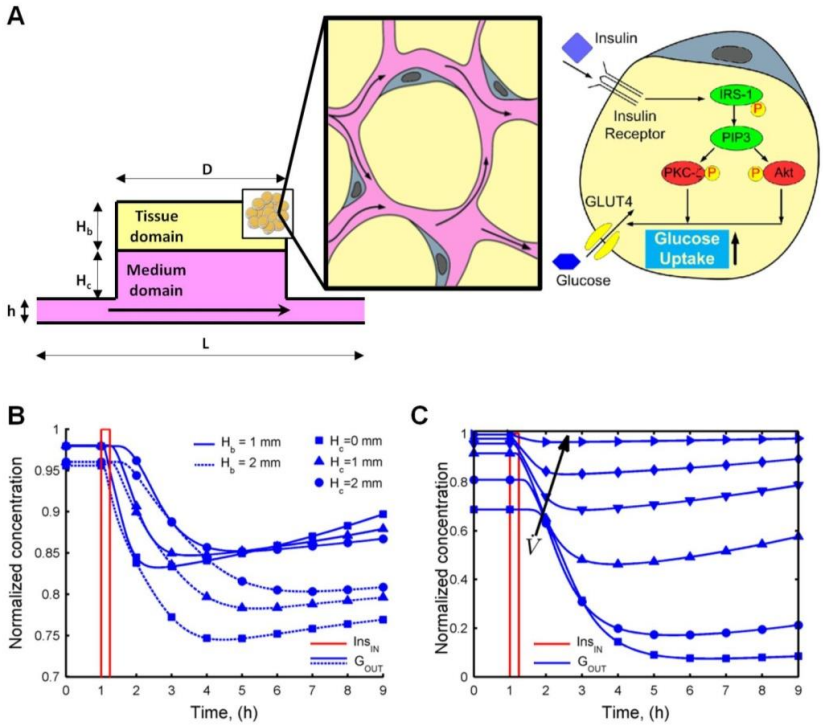

Figure 1. Multi-scale model-based design of the microfluidic culture chamber and definition of the operating conditions. (**A**) Schematic representation of the three scales simulated, from larger to smaller: the culture chamber geometry, including a tissue domain, where hAT biopsy sample is positioned, and a medium domain, where medium flows by convection; the tissue architecture, formed by a cluster of cells separated by interstitial spaces occupied by medium; and the single-adipocyte intracellular insulin signaling pathway resulting in glucose uptake. (**B**) Simulated effect of sample and culture chamber heights on the mean normalized glucose concentration profile at the outlet of the chamber, following a 100-nM insulin pulse stimulation of 15 min at the inlet (red line). Flow rate, 0.1 µL/min. (**C**) Simulated effect of medium flow rate on the mean normalized glucose concentration profile at the outlet of the culture chamber after an insulin pulse at the inlet as in (B). H_b, 1 mm; H_c, 0; $\dot{V}$, 0.005, 0.01, 0.025, 0.05, 0.1, 0.5 µL/min increasing in the direction indicated by the black arrow.

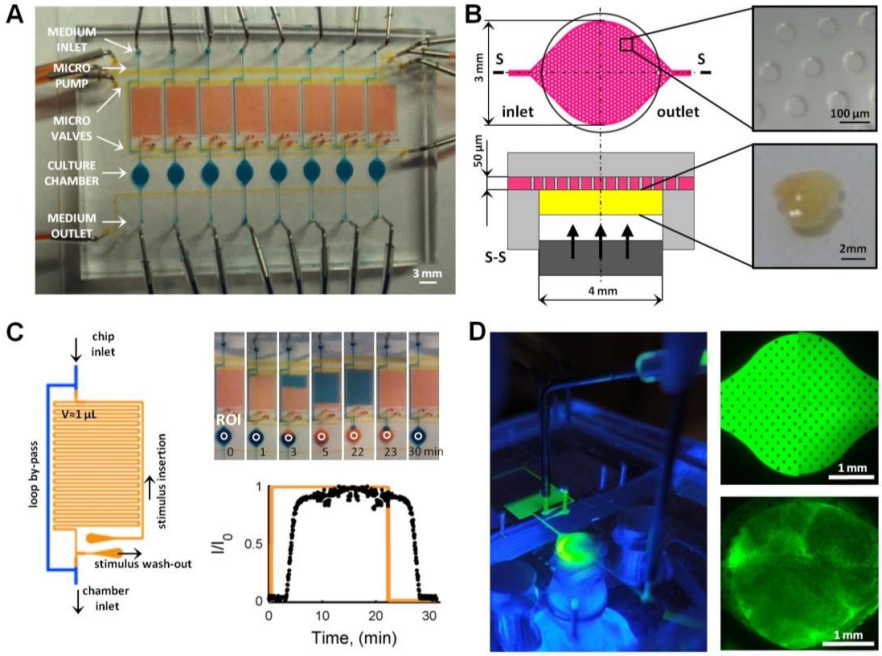

Figure 2. Experimental microfluidic setup validation and optimization. (**A**) Image of the multi-layer microfluidic platform including 8 independent culture chambers (blue), each with its dedicated injection system (orange). Medium channels used during non-stimulatory conditions are shown in blue, and control channels in yellow. (**B**) Optimized configuration of the culture chamber (top view and section) where an array of micro-posts provide stable and precise placement of hAT sample. A representative hAT sample is also shown. (**C**) Design of the injection system used for biochemical stimulation delivery at the entrance of the culture chamber. Validation of this system functionality by filling the chamber with different food dyes: image sequence and quantitative comparison between theoretical and actual concentration profile in the indicated ROI after a pulse. I/I_0, red intensity in the indicated ROI, normalized by its maximum value during a pulse. (**D**) Insulin pulse stimulation into the culture chamber by the automated injection system, using a fluorescent tracer in the insulin-containing medium. The homogeneous distribution of the tracer in the chamber, without and with a hAT sample, is shown.

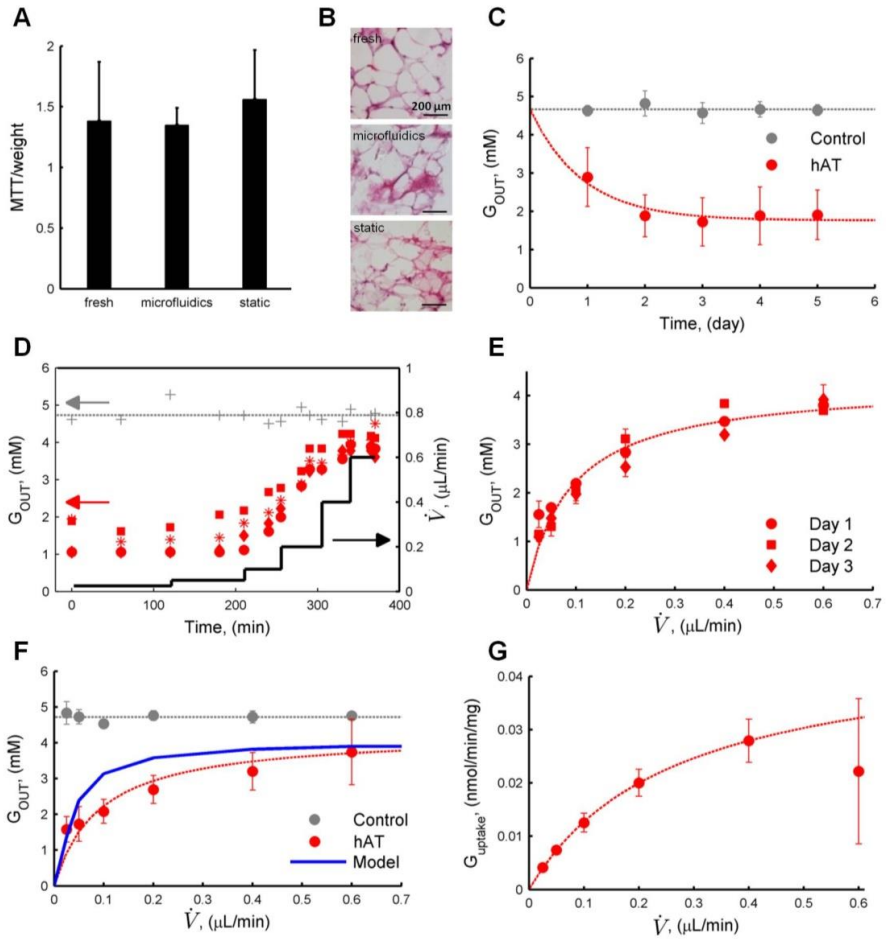

Figure 3. Validation and characterization of the microfluidic system during culture of hAT biopsy-derived samples from healthy patients. (**A**) MTT viability test (normalized by sample weight) of hAT samples from the same patient biopsy either freshly isolated, or after 7-day culture in a static well or a microfluidic chamber, as indicated. Error bar, standard deviation (n≥4). Patient no. 10 (Table S-3). (**B**) Hematoxylin and eosin staining of hAT samples from the same patient biopsy, analyzed immediately after isolation (top), cultured for 7 day in a microfluidic chamber (center), or in a static well (bottom). Patient no. 5 (Table S-3). (**C**) Glucose concentration at the outlet of the chamber where hAT samples were cultured for 6 days (flow rate, 0.025 µL/min). Control refers to measurements at the outlet of a culture chamber without biological sample inside. Error bar, standard deviation (n=3). Patient no. 1 (Table S-3). (**D**) Glucose concentration at the chamber outlet measured at increasing flow rates (0.025-0.6 µL/min). Sampling was performed continuously (medium was analyzed every

0.6-µL volume eluted). Data were obtained from 4 hAT samples (red) and a control (gray). (**E**) Steady-state measurements of outlet glucose concentration at different flow rates. Measurements were repeated using the same hAT cultures during 3 consecutive days. Error bar, standard deviation (n=3). (**F**) Steady-state measurements of outlet glucose concentration at different flow rates using different hAT samples and control chambers. Error bar, standard deviation (n=4). Corresponding results obtained by the mathematical model are also shown. (**G**) Calculated glucose uptake, G_{uptake}, from data in (F) as a function of medium flow rate, normalized by hAT sample weight. The data point at 0.6 µL/min was excluded from Michaelis-Menten fitting because of its high standard deviation. (**C-G**) G_{IN}, 4 mM. (**D-G**) Patient no. 2 (Table S-3).

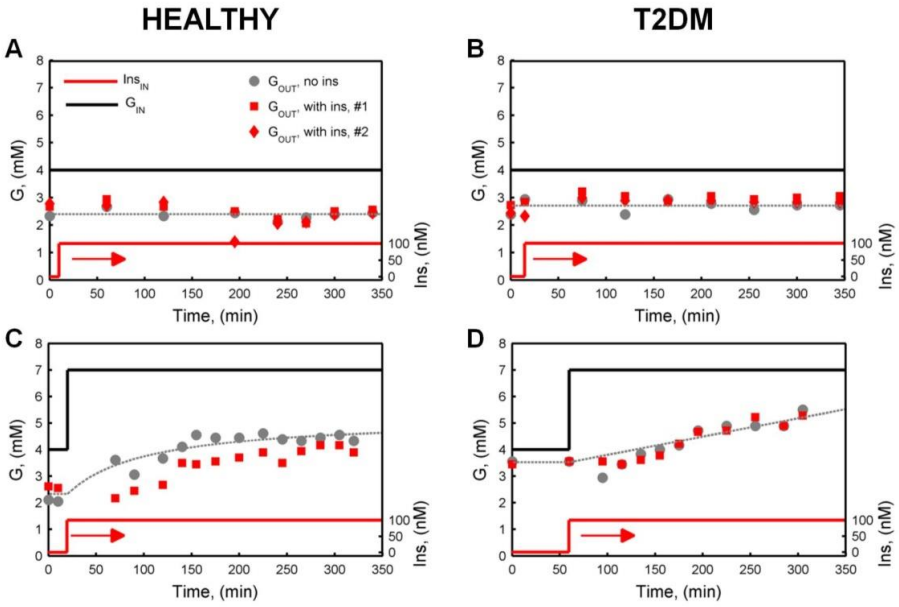

Figure 4. Response to insulin and glucose concentration of hAT samples from healthy and T2DM patients. (**A-B**) Effect of an insulin-step stimulus on glucose concentration at the outlet of the culture chamber. (**C-D**) Same as (A-B) with the simultaneous increase of glucose inlet concentration. Measurements taken at day 3 after microfluidic integration. $\dot{V}$ =0.1 µL/min. (**A, C**) Patient no. 6; (**B**) Patient no. 4; (**D**) Patient no. 9 (Table S-3).

Appendix A5

High-throughput reprogramming and differentiation on chip

This Appendix is extract from the work entitled “high-throughput reprogramming and differentiation on chip” with the following authors: C. Luni, S. Giulitti, E. Serena, L. Ferrari, A. Zambon, O. Gagliano, G. G. Giobbe, S. Knöbel, A. Bosio, F. Michielin, N. Elvassore.

My contribution is concerning the design and development of the multilayer microfluidic platform, the fabrication of all components and external devices for the chip management and the relative calibration and validation. This microfluidic technology is was specifically designed and developed for long-term biological cell culture that also required high frequency (mostly, on daily bases) biochemical perturbations. These features it makes the technology suitable for circadian application as well for cellular reprograming.

First of all, we decide to test the feasibility of the automatized microfluidic platform developed in this thesis for cellular reprograming because this biological process does not require bioluminescence-imaging acquisitions.

A5.1 Abstract

Human induced pluripotent stem cells (hiPSC) represent a limitless source of patient-specific and disorder-specific functional differentiated cells. Massive parallel production of hiPSCs fosters the establishment of large-scale population studies while considering human genetic diversity and polymorphisms. Here, we

downscaled to microliter volume a feeder-free reprogramming process through transient expression of non-integrating modified mRNAs. Taking advantage of intrinsic properties of microfluidics, we improved the exogenous factors delivery and we shaped the endogenous extracellular microenvironment activating pro-pluripotency pathways. We achieved highly efficient reprogramming (up to ~40%) from human somatic cells within an automated microfluidic chip. Notably, the non-integrating reprogramming strategy enabled unbiased differentiation on chip into functional cardiomyocytes and hepatocytes, immediately after hiPSC derivation. This five-week microliter reprogramming-differentiation opens the perspective for large-scale population studies.

A5.2 Introduction and Motivation

The discovery of human induced pluripotent stem cells (hiPSC) opened a new frontier for the *in vitro* derivation of human functional cells and tissues[1]. Since hiPSCs can be derived from easily accessible somatic cells, they represent a very interesting source for patient-specific and disorder-specific studies and applications. Human medical conditions are characterized by marked genetic heterogeneity, far greater than previously appreciated[2], raising implications for development of molecular treatments and their appropriate use in individual patients. To recapitulate the complexity and variety of human genetics and polymorphisms, the massive production of hiPSCs could represent a unique tool to obtain differentiated functional tissues for large-scale population studies and multiplex assay (Fig. 1a)[3,4].

Delivery of reprogramming factors, either by viral vectors or biomolecules, is critical to induce highly efficient conversion of somatic cells. Footprint-free strategies, like modified mRNAs (mmRNAs), allow the efficient production of hiPSCs preserving genomic integrity, but require daily transfections due to high mmRNA turnover.

Microfluidic devices are particularly suitable for controlling cell culture microenvironment because, in their laminar flow regime, molecules are transported in a relatively predictable manner through microchannels[5]. They also have other advantages such as ease of automation and unmatched minimum requirements of reagents due to their microliter-scale volume (Fig. 1b).

Soluble microfluidic culture microenvironment differs from that in conventional culture systems because of the high ratio of culture surface to medium volume[6]. Thus, it offers new opportunities to shape the cellular niche[7], taking into account that self-organized spatial gradients finely regulate the balance between differentiation and maintenance of pluripotency[8,9].

Here, we down-scaled reprogramming and subsequent differentiation of human cells within a microfluidic platform, also reducing the time requirements of the overall process (Fig. 1c), towards the final aim of increasing the production throughput of patient-specific functionally differentiated cells (Fig. 2a). We finally provide a proof of concept of one-step reprogramming and differentiation for highly parallel production of patient-specific functional cells.

A5.3 Results

Main requirements for the micro-scale culture technology are the ability to sustain long-term cell culture, efficiently and accurately deliver the reprogramming transcription factors, and provide a permissive microenvironment for highly efficient reprogramming. According to a mmRNA reprogramming protocol reported in literature having efficiency of up to 2.6%[10], we designed the culture chambers as microchannels of approximately 27 mm^2 (Fig. 2b), a surface sufficient to obtain up to about 10 hiPSC colonies from less than 300 cells using 250 μL of medium totally. This microfluidic experimental setup will provide enough biological material to perform biomolecular analyses using previously optimized protocols[6,11] and it has already been tested in multiple other human cell culture experiments by our group[6,11,12].

To verify whether the microfluidic environment could sustain long-term cell culture, we optimized the biofunctionalization of the silicon chip surface enabling human fibroblast culture for up to 40 days. Optimal performances were obtained with a covalently bonded gelatin coating that we selected for all subsequent experiments (Extended Data Fig. S1).

We then tested if we could efficiently perform mmRNA transfections within the microfluidic channels by delivering a mmRNA encoding for a nuclear-targeted green fluorescent protein (nGFP). mmRNA delivery resulted to be not only feasible, but also particularly efficient in microfluidics compared to a control in a

standard well, with up to 80% of $nGFP^+$ cells after a low-dose single transfection (Fig. 2c and Extended Data Fig. S2). These data were confirmed with different transfection reagents and after multiple transfections (Extended Data Fig. S2). We optimized mmRNA delivery as for transfection duration and mmRNA concentration: two variables that we found, both experimentally and by mathematical modeling (Extended Data Fig. S3), to strongly affect transfection efficiency (Fig. 2d) and mmRNA distribution within the cell population (Fig. 2e). The efficient mmRNA-mediated induction of protein expression in microfluidics was also confirmed in early reprogramming phase quantifying KLF4 and OCT4, two major players in driving cell mesenchymal-epithelial transition and pluripotency establishment[13,14], respectively (Fig. 2f and Extended Data Fig. S3). Thus, our microfluidic system proofed to be technically suitable to host the reprogramming process.

Encouraged by the effective protocol for long-term culture and the high-efficiency transfection, we developed a new microfluidic platform that, in contrast to our previous prototype[6,11,12], now provides increased automation options and a completely computer-assisted closed system. The main unit of this new configuration is a multilayered chip, built on top of a microscopy glass slide where cells grow in adhesion on a functionalized PDMS surface for long-term cell cultures (Fig. 2b and Extended Data Fig. S4). An external multi-port pump (with nano-liter accuracy) and an on-chip valve system are remotely controlled to distribute cells, medium and other reagents throughout the platform (Supplementary Video 1), with each cell culture chamber working independently.

We previously showed that hiPSC colonies can be seeded and cultured in microfluidics with maintenance and stabilization of pluripotency[6]. To determine whether the microfluidic environment is permissive during all stages of reprogramming, we downscaled a reprogramming protocol (using mmRNAs encoding for OCT4, SOX2, KLF4, c-MYC, NANOG, and LIN28) we had used in a six-well plate with efficiency up to 2.6% on human fibroblasts. The micro-scale process development was instructed by our previous results on *nGFP* mmRNA transfections, balancing transfection efficiency and cell mortality (Fig. 2c). By adding *nGFP* mmRNA during reprogramming, we verified the sustained delivery efficiency of daily transfections (Extended Data Fig. S3) and the emergence of

nGFP$^+$ epithelial-like cells (Fig. 2g). In 5 days cells were extensively E-CAD$^+$ (Extended Data Fig. S5), and in less than 2 weeks stable hiPSC colonies with typical morphology could be identified in the channels (Fig. 2h and 2i).

From our experimental observations, seeding density plays an important role in obtaining a balance between death and proliferation during reprogramming. We found an optimal cell seeding density of 10 cell/mm^2 (Fig. 2j) for maximizing the number of TRA-1-60$^+$/NANOG$^+$ colonies (Fig. 2k and Extended Data Fig. S5), and we further optimized the biofunctionalization strategy by reducing gelatin-coating amount, subsequent aspecific adsorption and unwanted cell migration throughout silicone surface. Under these conditions, we obtained up to 44 colonies per channel (16 as average), with a hiPSC onset as early as 7 days after beginning of reprogramming; all channels showed multiple colonies (Fig. 2k, Extended Data Fig. S5, and Supplementary Video 2). Thus, in microfluidics, the maximum reprogramming efficiency with a feeder layer was 16% (5.9±4.2%), which is much higher than we and others obtained in a conventional multi-well plate (up to ~3% under normoxia conditions)[10]. Protocol optimization towards a feeder layer-free system is an important step forward in controlling the reprogramming process and closer to clinical-grade hiPSCs. However, in these conditions the balance between cytotoxicity induced by reprogramming factor delivery and target cell proliferation becomes even more critical. Accurate control of microenvironmental conditions within the microfluidic platform allowed consistent reprogramming of fibroblasts in feeder-free conditions (Fig. 2j and Extended Data Fig. S6) with efficiencies up to 38%. Finally, we demonstrated that the microfluidic system is also suitable for reprogramming non-fibroblast cell types, such as urine-derived renal epithelial cells (Extended Data Fig. S7).

We verified the pluripotency of the hiPSC colonies obtained in microfluidics, first by *in situ* characterization (Fig. 3h, Extended Data Fig. S5, and S8), then after single-colony extraction from the microfluidic chip (Extended Data Fig. S9) and subsequent expansion (Fig. 3a-d, Extended Data Fig. S8, and Supplementary Video 3). Furthermore, microfluidic hiPSC colonies were able to give rise to cells from the three germ layers after differentiation either in monolayer or *via* embryoid bodies (Fig. 3e-g). Thus, microfluidic colonies demonstrated their pluripotency *de facto*.

We further asked whether microfluidics could substantially shape the culture environment to boost the reprogramming process, or if the higher reprogramming efficiency we obtained in microfluidics compared to the control multi-well plate were only attributed to the more effective exogenous transcription factor delivery.
To this end, we performed a microarray analysis selecting four colonies both from the microfluidic system and from a parallel reprogramming experiment in well plates. Each colony was split into two halves: the one half (p0) was used for total RNA extraction, the other one was further expanded in feeder-free conditions for 3 passages (p3) in well plates before total RNA extraction (Extended Data Fig. S9). Bioinformatics analyses highlighted differences between gene expression profiles of p0 colonies derived in microfluidics and in well plates (Fig. 3i and Supplementary Spreadsheet 1), which were abolished after the 3-passage expansion.
Functional annotation analysis highlighted enrichment in multiple gene ontology (GO) categories of genes differentially expressed between p0 μF and p3 μF, and between p0 μF and p0 well (Supplementary Spreadsheet 2). The most significant are related to the extracellular space and receptor-mediated signaling pathways (Fig. 3j). In particular, the TGF-β pathway, which is strongly involved in hiPSC stabilization[15,16], resulted as one of the most significant pathways affected by the microfluidic environment (Supplementary Spreadsheet 2). Microarray data showed a much higher expression of multiple TGF-β-related pathway components in freshly isolated microfluidic colonies with respect to both microfluidic colonies expanded in well plates and colonies initially obtained in a conventional well, suggesting this pathway superfamily is highly activated in the microfluidic system (Fig. 2j). Nonetheless both well and microfluidic colonies cluster together with other human pluripotent cell samples obtained from public repositories (Extended Data Fig. S9), suggesting that the microfluidic colonies obtained are still within the range of variability between different pluripotent clones.
To validate a possible perturbation of soluble microfluidic microenvironment by cell-released factors, we investigated the conditioned medium during reprogramming. In particular, since TGF-β pathway superfamily acts through multiple extra-cellular activating and inhibitory ligands, we analyzed the activation of TGF-β pathway transcription factors SMAD2/3[16]. A SMAD2/3 luciferase-reporter cell line evidenced that TGF-β-free reprogramming media

collected from the microfluidic system during reprogramming more strongly activated luciferase expression (Fig. 3k), supporting the hypothesis of strong accumulation of cell-secreted TGF-β pathway ligands that activate pro-pluripotency SMAD2/3.

Thus, besides higher mmRNA delivery efficiency, a different soluble microenvironment could contribute to the enhanced reprogramming efficiency. However, a short expansion in a conventional system highlights that microfluidic-derived hiPSC modify their gene expression profile resembling hiPSCs derived under standard conditions.

To fully exploit the potential of the microfluidic platform in providing high-throughput patient-specific *in vitro* models of human tissues, we asked if we could differentiate the freshly obtained hiPSCs into functional cells, without prior expansion. We have recently developed a method for successful differentiation of human pluripotent stem cells within a microfluidic chip into the three germ layers through accurate regulation of extrinsic environments and balance between exogenous and endogenous, cell-secreted, factors [6]. We started all differentiation protocols 48 h after the last mmRNA reprogramming transfection to ensure using transgene-free colonies.

First we found that, by sole introduction of an aspecific differentiation medium, freshly formed hiPSCs changed morphology resembling different cell types (Fig. 4a). RT-PCR confirmed the presence of cells expressing markers of the three germ layers within each channel (Fig. 4b), although this analysis could not exclude that the expression of the three-germ layer markers were derived from different colonies within the same channel.

To improve the selectivity of differentiation towards a specific cell type, we performed three sets of parallel experiments, each directing the obtained microfluidic colonies towards a single early germ layer. Consistently in 10 parallel experiments, we obtained a robust and remarkable selectivity towards the specifically induced germ layer, in all three cases (Fig. 4c).

Although a single hiPSC colony can be extracted from the microfluidic system for conventional differentiation, the full potential of the microfluidic technology is achieved with an integrated process of reprogramming and differentiation that increases the throughput of subsequent studies. As cardiac and hepatic tissues are

involved as main targets or side effects of a number of tested drugs, we focused on directed differentiation towards these two phenotypes.

As a proof-of-concept that freshly obtained hiPSC colonies could be successfully differentiated, without any intermediate process of expansion, we applied our previously developed protocols for efficient differentiation into cardiomyocyte- and hepatic-like cells in microfluidics[6]. We pooled the colonies reprogrammed in microfluidics and seeded them at a higher density in new microfluidic channels before starting the cardiac and hepatic protocols. With this one-passage protocol, we confirmed our previous data obtaining cardiomyocytes showing remarkable troponin-T expression and sarcomeric organization. In parallel, we obtained polygonal-shaped hepatocyte-like cells expressing CK18, and occasionally poly-nucleated cells. These cellular phenotypes were obtained as early as 35 and 36 days from the day of fibroblast seeding for reprogramming, respectively (Fig. 4d).

Finally, we asked whether we could differentiate primary hiPSCs in microfluidics into a specific cell fate without prior passaging to achieve the maximum throughput of this technology. Within the same channels where cells were reprogrammed, we performed either the hepatic or cardiac differentiation protocols. In the former case, after 15 days, extensive morphologically differentiated areas were present and we characterized the cells obtained for their functional maturation (Fig. 4e). Cells were $CK18^{+}$ and albumin-positive and showed remarkable glycogen storage ability. Cardiac differentiation was tested by PCR and revealed cell positivity to markers of advanced cardiac maturation: FLK-1, NKX-2.5, and cTNT (Extended Data Fig. S10).

Thus, a one-step process of reprogramming and differentiation within a microfluidic chip was obtained, allowing the automated production of functional hepatocyte- and cardiomyocyte-like cells starting from fibroblasts in 36 and 35 days, respectively, within the same device (Fig. 4f).

A5.4 Conclusion

In this study, we reprogrammed human fibroblasts and derived functional tissue-specific cells within a high-throughput microfluidic platform through a robust one-step process. This technology opens a new perspective in generating tissue-on-chips from hiPSC for extensive screening studies, overcoming the issues

related to the limited availability of human primary cell sources and process costs. Although recent advances in genome-editing technologies make possible the artificial introduction of genetic variability *in vitro*, they still cannot handle the wide variety of genetic backgrounds, including possibly multi-factorial idiopathic diseases, present in the human population, as only few *loci* can be modified at once[17].

The specific characteristics of the microfluidic culture environment not only turned out to enhance process efficiency, but also ensured a robust performance due to automation and tight control of the soluble microenvironment under reproducible laminar flow conditions. The use of this technology is not restricted to the specific application presented, but rather allows population studies in a broader sense[18,19]. For example, in cases where a primary cell source of a specific tissue is available, a screening study can be accomplished within the microfluidic platform taking advantage of the possibility to perform precise dynamic stimulations. Tight control over extrinsic and intrinsic cell microenviroment establishes microfluidics as a tool to trigger cellular self-specification, promote hiPSC stabilization and impose targeted differentiation.

This study made an important step forward to ultimately exploit the translational potential of hiPSCs[18,19]. Further mimicking of organogenesis *in vitro* and developing in-line functional assays will provide scientific and technological cues to establish pluripotent stem cells in biomedicine.

A5.5 Methods

Cell culture. Human foreskin BJ fibroblasts (Miltenyi Biotec) were cultured in Dulbecco's modified Eagle Medium (DMEM, Life technologies) supplemented with 10% fetal bovine serum (FBS, Life Technologies). HFF-1 fibroblasts (ATCC) were cultured in DMEM with 15% FBS. Renal epithelial cells (RE) were isolated and expanded from a healthy 28-year old donor in RE medium (Lonza) as previously described[20]. Inactivated human newborn foreskin fibroblasts NuFF-RQs (AMS Biotechnology) were seeded on 0.2% type-A gelatin (Sigma-Aldrich) at 260 cells/mm^2 in DMEM with 10% FBS, in case of use as a feeder layer for reprogramming and for Pluriton medium (Stemgent) conditioning.

hiPSC were mechanically passaged on mytomicin-treated mouse embryonic fibroblasts (MEF, Millipore) with daily changes of hiPSC medium (DMEM/F12, 20% knockout serum replacement, 1% NEAA, 1% glutamine, 1% β-mercaptoethanol (all Life Technologies), 20 ng/ml b-FGF (Peprotech). Alternatively, freshly derived hiPSC were directly cultured in feeder-free medium StemMACS^{TM} iPS-Brew XF (Miltenyi Biotec) or transferred from MEF without any adaptation. hiPSC were passaged every 3-4 days on vitronectin XF treated plates using gentle cell dissociation reagent (both Stemcell Technologies). All cell lines were cultured at 37 °C and 5% CO_2 atmosphere.

Microfluidic platform. Microfluidic platforms were fabricated according to standard soft-lithographic techniques and molded in poly-dimethylsiloxane (PDMS), as previously described[11,12]. Briefly, Sylgard 184 (Dow Corning) was cured on a 200-µm-thick patterned SU-2100 photoresist (MicroChem) in order to obtain a single PDMS mold with multiple independent channels. The PDMS mold was punched and sealed on a 75 x 25 mm microscope glass slide (Menzel-Glaser) by plasma treatment. Channels were rinsed with isopropanol and distilled water to check proper flow, before autoclaving. A syringe step-motor pump (Cavro, Tecan) was used to periodically control medium flow rate into the microfluidic channels at 120 µL/min for 5 s. 0.5 ID Tygon tubings (Cole-Parmer) and 21G stainless-steel needles were used to connect the microfluidic channels to the pump head.

Microfluidic platform with integrated medium distribution system. Multilayer soft lithography was used to fabricate this type of microfluidic platform, composed of a 3-layer PDMS chip[21,22]. Transparent photomasks were printed at 8000 dpi. A 4-inch silicon wafer (Siegert) was used for molding. Control mold was made by SU8 2050 (Microchem), obtaining 45 µm square channels. Flow mold had 45 µm round channels made by SPR 220-7 (Dow Corning); to avoid unintentional cross-section valves, 90 µm square channels have been made over the previous by a second SU8 2100 layer. Culture channel mold has 220 µm square section made by SU8 2100. Every mold was previously coated for 1 hour at room temperature with chlorotrimethylsilane vapors (Sigma-Aldrich). Sylgard 184 (Dow Corning) was mixed at 5:1 ratio (base:cure agent) for the flow layer (FL), 20:1 ratio for the control layer (CL) and 10:1 ratio for the cell culture layer (CCL). All layers were partially cured at 333 K before peeling,

cutting and punching: 45 minutes for FL, 60 minutes for CL and 70 minutes for CCL. After alignment, another 2 hours at 353 K completed the curing. The PDMS chip was finally bonded by plasma activation on a large glass slip (75 x 50 mm, Ted Pella) covered with a thin (<0.5 mm) 20:1 PDMS layer.

The microfluidic platform was fully assisted by an automated medium delivery and distribution system into the culture channels. A periodic 120 µL/min perfusion for 5 s was controlled twice a day by Cavro pumps (Tecan) and a lab-made software interface written in Labview (National Instruments). The experimental setup is shown in Fig. 2B and Extended Data Fig. S4.

Surface coating in microfluidic setup. After autoclaving and before cell seeding, microfluidic culture channels were treated for surface functionalization. Extracellular matrix proteins were either adsorbed or chemically bound to the silanized glass bottom of each channel to provide a durable coating for cell culture (Extended Data Fig. S1). For the adsorbed substrates either fibronectin (Fn, 10 µg/mL, Sigma-Aldrich) or type-A pork gelatin (Gel, 0.1% and 0.6%, Sigma-Aldrich) were incubated within the microfluidic channels for 1 h at 37 °C before rinsing with DPBS. For glass silanization, surface was treated either with a 5% water solution of (3-aminopropyl)-triethoxysilane (APTES, Sigma-Aldrich) for 20 minutes, or a 0.3% ethanol solution of 3-(trimethoxysilyl)-propyl methacrylate (TMSPMA, Acros Organics) for 5 minutes. Covalent bonding of adsorbed Gel on APTES was obtained treating with 0.5% v/v glutaraldehyde for 10 minutes. Covalent bonding of Gel on TMSPMA was obtained treating Gel with methacrylic anhydride (Sigma-Aldrich) in PBS buffer for 1 h at 60 °C to produce an acrylate-reactive variant (GelMA). A TMSPMA-GelMA bonding was performed for 15 minutes by adding 0.1% ammonium persulphate and N,N,N',N'-tetramethylenethylenediamine (Sigma-Aldrich) prior to GelMA (0.1% or 0.6%) injection within each channel. After surface biofunctionalization, channels were extensively rinsed with DPBS prior to cell seeding. In multilayered platforms (Extended Data Fig. S4), the distribution layer was functionalized by directly incorporating 0.3% TMSPMA in the PDMS before curing.

Reprogramming. For technological validation, an mmRNA encoding for nuclear GFP (StemMACS Nuclear eGFP, Miltenyi Biotec) was used alone, carried into the cells by different transfection reagents: RNAiMAX (RiM, Life Technology), Stemfect (SF, Stemgent), and StemMACS Transfection Reagent (SM, Miltenyi

Biotec), according to the transfection protocols below. Comparisons of transfection efficiencies, between microfluidics and wells, and between different transfection reagents, were carried out with the same cell density. SF was used if not specified. SM was used for feeder-free protocols.

hiPSCs were generated via mmRNA-mediated reprogramming, adapting the protocols reported in literature for feeder[23] and feeder-free[24] hiPSC derivation, from multiple cell sources: human foreskin BJ and HFF-1 fibroblasts, and urine-derived renal epithelial cells (RE).

For reprogramming with a feeder layer, NuFF-RQs were seeded at day -2. At day -1, the reprogramming target fibroblasts (either BJ or HFF) were seeded at different densities (5, 10, and 26 cell/mm^2) in DMEM with 10% FBS. At day 0, 2 h prior to the first mmRNA transfection, medium was switched to Pluriton reprogramming medium (Stemgent) supplemented with B18R interferon inhibitor (eBioscience) at a final concentration of 200 ng/mL.

The transfection mix was prepared according to the manual of the StemMACS mRNA Reprogramming Kit (Miltenyi Biotec) pooling two solutions: the first obtained diluting 5X 100 ng/µL mmRNA of OCT4, SOX2, KLF4, c-MYC, NANOG, LIN28, and nGFP, with stoichiometry 3:1:1:1:1:1:1, in transfection buffer solution, and the second diluting 10X transfection reagent in transfection buffer solution. The two solutions were mixed in 2:1 volume ratio (RiM and SF) or 3:1 (SM), and the final solution was incubated for 15 min (RiM and SF) or 20 min (SM). Where not specified, SF transfection reagent was used.

Transfections using the final mmRNA solution were started at day 0 and daily repeated for at least 12 days. In well, the final mmRNA solution was added drop-wise gently rocking the plate, 4 hours prior to daily medium changes with B18R-supplemented Pluriton medium. In microfluidics, the final mmRNA solution was added to different percentages of B18R-supplemented Pluriton medium, pipetted inside a reservoir and automatically perfused inside each channel. Fresh B18R-supplemented Pluriton was added to the reservoir and automatically perfused after the transfection period and 12 h thereafter.

To compensate for progressive NuFF death during reprogramming, NuFF-conditioned B18R-supplemented Pluriton medium was used from day 6. Pluriton medium was conditioned daily with 4 ng/mL b-FGF on a separate NuFF culture.

At the end of the transfection series, hiPSC were cultured for two days in Pluriton medium without B18R. Few experiments were stopped at this point for performing immunofluorescence analysis and determining reprogramming efficiency, defined as the ratio of the number of TRA-1-60^{+} colonies to the number of target cells seeded. Otherwise hiPSC colonies were picked and passaged as previously described. Microfluidic hiPSC colonies were collected either by coring the rubber of the microfluidic chip with a biopsy punch or by a preferential detachment using a high flow rate corresponding to a shear-stress of 25 Pa [25], as shown in Extended Data Fig. S9.

Feeder-free reprogramming was performed solely seeding BJ, HFF or RE cells at day -1 and using B18R-supplemented Pluriton medium for the whole duration of reprogramming. RE cells were also kept in RE medium during the first 5 days of reprogramming transfections, and were additionally transfected with 45 nM hsa-miR-372 on day -1 and 4 of the mmRNA reprogramming protocol.

TRA-1-60^{+} colonies obtained in microfluidics were catalogued as hiPSC with progressive numbering and labeled thereafter.

Immunofluorescence and colorimetric assays. Immunofluorescence analysis was performed either in conventional wells or microfluidic channels with the same protocols. Cells were fixed in 4% (w/v) paraformaldehyde (Sigma-Aldrich) for 10 min and stained with primary antibodies in 5% goat serum with 0.1% (v/v) Triton-X-100 (Sigma-Aldrich). Membrane markers were stained without cell permeabilization. Primary antibodies: OCT4 and SSEA-4 (Santa Cruz), NANOG (Reprocell), TRA-1-60 and TRA-1-81 (Millipore), SOX2 (Novus Biologicals); AFP and BRACHYURY-T (Sigma-Aldrich), β-III-TUBULIN (Abcam), CK18 (GeneTex), ALBUMIN (R&D). Alexa488 or Alexa594 conjugated rabbit or mouse secondary antibodies were used (Life technologies). Nuclei were stained with Hoechst 33342 (Life Technologies). Images were acquired with a DMI6000B fluorescence microscope with motorized stage (Leica Microsystems). The alkaline phosphatase (AP) assay was performed either by a live AP-kit in KnockOut DMEM (both Life Technologies) with a 45-minute incubation, or after cell fixation by AP-staining kit II (Stemgent) with a 10-minute incubation of the staining solution. Glycogen storage analysis was performed by periodic acid-Schiff (PAS) staining (Sigma-Aldrich) following manufacturer's specifications.

Image analysis. Image analysis was performed as previously described[12]. Briefly, pairs of images of Hoechst 33342 stained nuclei and $nGFP^+$ cells were analyzed using the software MATLAB R2012b (The MathWorks). HOECHST images were binary transformed for nuclei localization, after contrast adjustment and morphological filtering. In the detected nuclei positions, mean nGFP fluorescence intensity was evaluated. A background correction was performed to account for differences in cell substrates and in image acquisition conditions. A threshold of fluorescence intensity was chosen to discriminate between nGFP positive and negative cells. Images were taken at 10X magnification for quantification of $nGFP^+$ cells, and 20X for quantification of single nucleus fluorescence intensity.

Stochastic model. A mathematical model was developed to describe the transfection process of nGFP-encoding mmRNA at different concentrations (from 0.48 to 20 pg/100 cell in microfluidics) and transfection durations (1, 2, and 4 h). The model is in the form of a stochastic simulation algorithm to capture the discrete nature of mmRNA-containing vesicles and cells (Extended Data Fig. S3). Cells are described as a two-dimensional partially adsorbing boundary layer at the bottom of the culture volume. In each simulation, they are randomly positioned within a regular square grid of 1 mm^2, on the cartesian plane xz. The grid spacing, Δx and Δz, was fixed at 57.7 μm, corresponding to the side of a square having the same area as the average cell, determined experimentally. In the experiments we observed that BJ cells, seeded at a density of 250 cell/mm^2, reached a density of 300 cell/mm^2 after 24 h, when transfection occurred, and of 600 cell/mm^2 after another 24 h, when nGFP images were taken. Thus, we simulated the transfection process at 300 cell/mm^2 and assumed that proliferation rate was not affected by cell transfection.

The stochastic model is discrete both in time and space. A vesicle in position $\big(x(t), y(t), z(t)\big)$, in a time interval Δt will jump to the neighbor position on the lattice with probability $P_{jump} = D\Delta t / \delta^2$[26], where δ, equal to 10 μm, is the lattice spacing and the capture boundary layer[27]. Δt, the time interval simulated, is arbitrary as long as the inequality $2D\Delta t \square \ \delta^2$ holds, where D is the diffusion coefficient of vesicles in medium. D was estimated to be 10^{-12} m^2/s by Stokes-Einstein equation:

$$D = \frac{k_B T}{6\pi\mu R} \qquad (1)$$

where k_B is Boltzmann constant, T absolute temperature (310.15 K), μ medium viscosity (691.6 10^{-6} Pa·s[28], approximated by water property), and R the vesicle radius assuming a spherical shape (approximately 300 nm[29]).

Named y the direction perpendicular to the plane of cell culture, the boundary condition at $y = 0$ (the cell plane) was defined as partially adsorbing: a vesicle is adsorbed with probability $P_{ads} = c_{RNA} k \delta$ and reflected otherwise, where c_{RNA} represents the vesicle concentration in the bulk, and k is a positive constant that describes the reactivity of the boundary and is the only parameter fitted ($1.4 \cdot 10^3$ μm^2/pg), using experimental data collected in microfluidics at an nGFP mmRNA concentration of 16 pg/100 cell. Thus, the overall probability a vesicle enters a cell at the boundary is given by two contributions, the probability of reaching the boundary and the probability of adsorption:

$$P_{transf} = P_{jump} \cdot P_{ads} = \frac{kD\Delta t}{\delta} \qquad (2)$$

provided a vesicle is at distance δ from the boundary at the previous time point simulated.

As the characteristic time of adsorption at the surface is much longer than the diffusion characteristic time in the medium bulk, we simulated the process within the capture boundary layer, assuming the medium bulk plays as an infinite source of vesicles. The model was solved using Matlab software (version R2012b).

RT-PCR and qPCR analyses. Microfluidic channels were first perfused with D-PBS, then with iScript (Bio-Rad) for total RNA extraction. The solution was left in the channels for 2 min before collection. Total RNA was isolated with the RNeasymini kit (Qiagen), treated with DNase (Life Technologies), and quantified using NanoDrop spectrophotometer. RNA (0.1 μg) was reverse transcribed into cDNA (Life Technologies). The list of primers used is available in Supplementary Table 1. PCR was performed with Platinum Taq polymerase (Life Technologies). Electrophoresis was perfomed in a 2% (w/v) agarose gel with SYBR Green (Life Technologies). qRT-PCR was performed with TaqMan gene expression assay probes (Life Technologies) according to manufacturer's instructions. Reactions were performed on ABI Prism 7000 machine and results were analyzed with ABI

Prism 7000 SDS software. GAPDH expression was used to normalize Ct values of gene expression, and data were shown as relative fold change to control cells, using the delta-delta Ct method.

Western blotting analysis. Whole cell lysate was obtained by solubilization of cells in 10 µL of 5% deoxycholic acid (DOC, Sigma-Aldrich) and Complete protease inhibitor (Roche). PAGE was performed with 4-12% NuPAGE polyacrylamide gels and MOPS buffer (Life Technologies). Proteins were blotted on PVDF membranes (Life Technologies) and detected with Carestream films (Kodak). A 1:1000 dilution of primary antibodies and HRP-conjugated secondary antibodies (mouse, Bio-Rad; rabbit, Life Technologies) were used. Whole cell lysate from HES2 embryonic stem cells was used as OCT4 reference.

TGF-β assay. Cell-conditioned media were collected every 24 h during the reprogramming process. In the microfluidic system this corresponds to mixing the medium collected 3 times/day. To activate latent TGF-β, conditioned media were heat-treated for 5 min at 368 K prior to use. CAGA12 SMAD2/3 reporter HaCaT cell line was obtained from Stefano Piccolo's Lab (Department of Molecular Medicine, University of Padova), cultured in DMEM supplemented with 10% FBS. For luciferase assay, cells were plated in 24-well plates at 90% confluence and incubated overnight in DMEM without serum. Cells were then treated with conditioned media for 10 h, and supplemented with 1 µM TGF-β receptor inhibitor SB431542 (SB, Peprotech) where indicated. Luciferase expression was detected as previously described[30]. Data were normalized on total protein content, determined through Bradford assay.

Karyotype. Q-banded karyotype was performed by the Cytogenetic and Molecular Genetics Laboratory at the University of Brescia (Italy).

Microarray and bioinformatics. 48 hours after last reprogramming mmRNA transfection, four freshly derived colonies of comparable size (~8000 cells) were selected both from the microfluidic system and from a parallel reprogramming experiment in well plates. After a 24-h conditioning in StemMACS iPS-Brew XF medium, each colony was split in two halves: the one half (passage p0) was used for total RNA extraction, the other one was further expanded in feeder-free conditions for 3 passages (p3) in well plates before total RNA extraction from another sectioned colony of comparable size (Extended Data Fig. S9). Each colony was lysed using SuperAmp Lysis Buffer (Miltenyi Biotec) and stored

appropriately according to the instructions of the SuperAmp Preparation Kit. The samples were sent on dry ice to Miltenyi Biotec, where amplification, cDNA quantification using ND-1000 Spectrophotometer (NanoDrop Technologies), evaluation of cDNA integrity using a 2100 Bioanalyzer (Agilent Technologies), and microarray analysis were performed. 250 ng of each of the cDNAs were labeled with Cyanine 3 and hybridized (17 hours, 318.15 K) to an Agilent Whole Human Genome Oligo Microarrays 8x60K v2. Fluorescence signals of the hybridized Agilent Microarrays were detected using Agilent's Microarray Scanner System (Agilent Technologies). Agilent Feature Extraction Software (FES) was used to read out the microarray image files. Extracted signals were analyzed using GeneSpring v12.6 software (Agilent Technologies). Gene expression values were normalized by the 75th percentile shifts, and baseline-corrected to the median of all samples. Differentially expressed genes between pairs of conditions were found using ANOVA with Tukey post-test (significance set at $P<0.05$), combined with a two-fold change expression threshold. Differentially expressed genes were checked for functional enrichment using DAVID bioinformatics database (http://david.abcc.ncifcrf.gov/). Principal Component Analysis (PCA) was performed with variance-based weights, and hierarchical clustering with Euclidean distance and nearest-neighbor linkage clustering method, using MATLAB (version R2012b). Microarray data are available at the National Center for Biotechnology Information Gene Expression Omnibus database under the series accession number GSE59534.

Comparison with microarray datasets deposited in public databases (GEO and Synapse Commons Repository) was performed after selection of relevant samples obtained with similar Whole Human Genome Agilent arrays (GSE50206, GSE42445, syn1447097, syn1449098). Single-batch data normalization was performed as above. Only probes common to all the datasets were taken into consideration, and genes whose detection was compromised in at least one sample were excluded from the analysis. After this filtering procedure, 18479 genes were further processed. Datasets merging was performed after batch-effect removal using an empirical Bayes method implemented in ComBat R-code[31]. PCA was then performed in MATLAB as above.

Aspecific differentiation. *Embryoid bodies (EB).* hiPSC colonies were treated with CTK (0.1 mg/mL collagenase IV, 0.25% trypsin, 0.01 M $CaCl_2$, and 0.2%

KSR in dH2O) for 30 s, mechanically scratched with a serological pipette and resuspended in EB medium (DMEM/F12, 20% knockout serum replacement, 1% L-glutamine, 1% NEAA, β-mercaptoethanol, all Life Technologies). EB were cultured in ultra-low adhesive plates (Corning) for 20 days and then transferred on custom-made PDMS micro-wells with a Matrigel (BD) coated glass bottom. Characterization was performed after 6 days.

Aspecific differentiation in monolayer. EB medium (without β-mercaptoethanol) was used to aspecifically differentiate hiPSC colonies for 6 days. In microfluidics differentiation was performed perfusing the medium every 12 h. In wells medium was changed every 48 h.

Early-germ layer differentiation. hiPSC were differentiated in the following germ-layer-specifing media. *Ectoderm.* DMEM/F12, 1% NEAA, 1 mM L-glutamine, 0.1 mM beta-mercaptoethanol, 20% KnockOUT serum replacement (all Life technologies), 1 uM dorsomorphin. *Mesoderm.* Supplemented StemPro-34 (Life Technologies), 5 ng/mL b-FGF, 2 mM L-glutamine, 50 μg/mL ascorbic acid, 150 μg/mL transferrin, 0.3 ng/mL activin-A, 10 ng/mL BMP-4, 46 μg/mL methyl-thio-glycerol. *Endoderm.* Days 1-2, RPMI, 2% B27 supplement, 100 ng/mL activin-A, 50 ng/mL Wnt3a. Days 3-5, RPMI, 2% B27 supplement, 100 ng/mL activin-A.

Cardiac differentiation. Small molecules were used to promote cardiac differentiation of hiPSC colonies. RPMI with B27 without insulin (cardiac basal medium, CBM, Life Technologies) with 10 mM CHIR99021 and was perfused in microfluidics every 12 h for the first 24 h. Thereafter the medium was changed every 24 h. CBM was used in the following 36 h and CBM with 4 mM IWP-4 in the next 24 h. CBM was then used until cardiac maturation at day 14 from the beginning of differentiation protocol. Medium change in wells was performed only at changes of medium composition as above.

Hepatic differentiation. hiPSC colonies obtained in microfluidics were maintained in StemMACS iPS-Brew XF medium to grow over the channel surface. RPMI-B27 was supplemented with 100 ng/ml activin-A and 0.5 mM sodium butyrate for 3 days. Medium was changed to KO-DMEM, 20% Serum Replacement (both from Invitrogen), 1 mM L-glutamine, 1% NEAA, 0.1 mM b-mercaptoethanol, 1% DMSO (Sigma-Aldrich) for 6 days. Hepatic-like cells were maturated with L15 medium (Sigma-Aldrich) supplemented with 8.3% FBS,

8.3% tryptose phosphate broth, 10 μM hydrocortisone 21-hemisuccinate, 1 μM insulin (all from Sigma-Aldrich) and 2 mM L-glutamine containing 10 ng/ml hepatocyte growth factor and 20 ng/ml oncostatin M (both from R&D) for 6 days. Medium was changed every 12 h in the microfluidic system, and every 24 h in wells.

Statistical analysis. For statistical analyses, single pairwise comparisons were analyzed using Student's t-test with $P < 0.05$ (*), $P < 0.01$ (**) or $P < 0.001$ (***), indicating significance. Multiple comparisons were performed by one-way ANOVA with Tukey post-test, with $P < 0.05$ (*), $P < 0.01$ (**) or $P < 0.001$ (***), indicating significance. Values are expressed by mean and standard deviations (s.d.).

A5.6 Reference

1. Takahashi, K. & Yamanaka, S. Induction of Pluripotent Stem Cells from Mouse Embryonic and Adult Fibroblast Cultures by Defined Factors. *Cell* **126,** 663–676 (2006).
2. McClellan, J. & King, M.-C. Genetic Heterogeneity in Human Disease. *Cell* **141,** 210–217 (2010).
3. Valamehr, B. *et al.* A novel platform to enable the high-throughput derivation and characterization of feeder-free human iPSCs. *Sci. Rep.* **2,** (2012).
4. Xue, Y. *et al.* Generating a Non-Integrating Human Induced Pluripotent Stem Cell Bank from Urine-Derived Cells. *PLoS ONE* **8,** e70573 (2013).
5. Squires, T. M. & Quake, S. R. Microfluidics: Fluid physics at the nanoliter scale. *Rev. Mod. Phys.* **77,** 977 (2005).
6. Giobbe, G. G. *et al.* Integrated multi-stage tissue on a chip generation from human pluripotent stem cells. *Nat. Methods* (Under revision).
7. Lane, S. W., Williams, D. A. & Watt, F. M. Modulating the stem cell niche for tissue regeneration. *Nat. Biotechnol.* **32,** 795–803 (2014).
8. Peerani, R. *et al.* Niche-mediated control of human embryonic stem cell self-renewal and differentiation. *EMBO J.* **26,** 4744–4755 (2007).

9. Warmflash, A., Sorre, B., Etoc, F., Siggia, E. D. & Brivanlou, A. H. A method to recapitulate early embryonic spatial patterning in human embryonic stem cells. *Nat. Methods* (2014). doi:10.1038/nmeth.3016
10. Warren, L. *et al.* Highly Efficient Reprogramming to Pluripotency and Directed Differentiation of Human Cells with Synthetic Modified mRNA. *Cell Stem Cell* **7,** 618–630 (2010).
11. Giulitti, S., Magrofuoco, E., Prevedello, L. & Elvassore, N. Optimal periodic perfusion strategy for robust long-term microfluidic cell culture. *Lab. Chip* **13,** 4430–4441 (2013).
12. Luni, C., Michielin, F., Barzon, L., Calabrò, V. & Elvassore, N. Stochastic model-assisted development of efficient low-dose viral transduction in microfluidics. *Biophys. J.* **104,** 934–942 (2013).
13. Li, R. *et al.* A mesenchymal-to-epithelial transition initiates and is required for the nuclear reprogramming of mouse fibroblasts. *Cell Stem Cell* **7,** 51–63 (2010).
14. Liu, X. *et al.* Sequential introduction of reprogramming factors reveals a time-sensitive requirement for individual factors and a sequential EMT–MET mechanism for optimal reprogramming. *Nat. Cell Biol.* **15,** 829–838 (2013).
15. Maherali, N. & Hochedlinger, K. Tgfβ Signal Inhibition Cooperates in the Induction of iPSCs and Replaces Sox2 and cMyc. *Curr. Biol.* **19,** 1718–1723 (2009).
16. Massagué, J. TGFβ signalling in context. *Nat. Rev. Mol. Cell Biol.* **13,** 616–630 (2012).
17. Sander, J. D. & Joung, J. K. CRISPR-Cas systems for editing, regulating and targeting genomes. *Nat. Biotechnol.* **32,** 347–355 (2014).
18. Neuži, P., Giselbrecht, S., Länge, K., Huang, T. J. & Manz, A. Revisiting lab-on-a-chip technology for drug discovery. *Nat. Rev. Drug Discov.* **11,** 620–632 (2012).
19. Dimmeler, S., Ding, S., Rando, T. A. & Trounson, A. Translational strategies and challenges in regenerative medicine. *Nat. Med.* **20,** 814–821 (2014).
20. Zhou, T. *et al.* Generation of human induced pluripotent stem cells from urine samples. *Nat. Protoc.* **7,** 2080–2089 (2012).

21. Unger, M. A., Chou, H.-P., Thorsen, T., Scherer, A. & Quake, S. R. Monolithic microfabricated valves and pumps by multilayer soft lithography. *Science* **288,** 113–116 (2000).
22. Gómez-Sjöberg, R., Leyrat, A. A., Pirone, D. M., Chen, C. S. & Quake, S. R. Versatile, fully automated, microfluidic cell culture system. *Anal. Chem.* **79,** 8557–8563 (2007).
23. Warren, L. *et al.* Highly efficient reprogramming to pluripotency and directed differentiation of human cells with synthetic modified mRNA. *Cell Stem Cell* **7,** 618–630 (2010).
24. Warren, L., Ni, Y., Wang, J. & Guo, X. Feeder-Free Derivation of Human Induced Pluripotent Stem Cells with Messenger RNA. *Sci. Rep.* **2,** (2012).
25. Singh, A. *et al.* Adhesion strength–based, label-free isolation of human pluripotent stem cells. *Nat. Methods* (2013). doi:10.1038/nmeth.2437
26. Erban, R. & Chapman, S. J. Reactive boundary conditions for stochastic simulations of reaction–diffusion processes. *Phys. Biol.* **4,** 16–28 (2007).
27. Moledina, F. *et al.* Predictive Microfluidic Control of Regulatory Ligand Trajectories in Individual Pluripotent Cells. *Proc. Natl. Acad. Sci.* (2012). doi:10.1073/pnas.1111478109
28. Kestin, J., Sokolov, M. & Wakeham, W. A. Viscosity of liquid water in the range −8 °C to 150 °C. *J. Phys. Chem. Ref. Data* **7,** 941 (1978).
29. Russo, L., Berardi, V., Tardani, F., La Mesa, C. & Risuleo, G. Delivery of RNA and Its Intracellular Translation into Protein Mediated by SDS-CTAB Vesicles: Potential Use in Nanobiotechnology. *BioMed Res. Int.* **2013,** (2013).
30. Inui, M. *et al.* USP15 is a deubiquitylating enzyme for receptor-activated SMADs. *Nat. Cell Biol.* **13,** 1368–1375 (2011).
31. Johnson, W. E., Li, C. & Rabinovic, A. Adjusting batch effects in microarray expression data using empirical Bayes methods. *Biostatistics* **8,** 118–127 (2007).

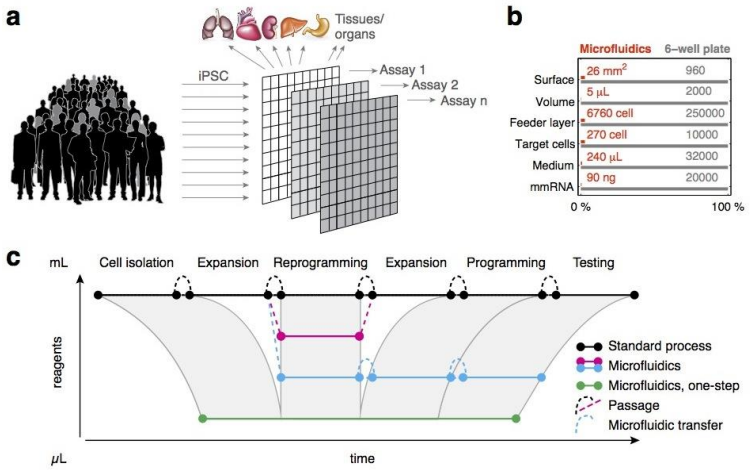

Fig. 1 | Miniaturization of human tissue development *in vitro*. (**a**) Perspective high-throughput derivation of human tissues for biological assays on a population scale. (**b**) Quantitative comparison of resources requirements between reprogramming in a microfluidic channel and in a well of a 6-well plate. (**c**) Progressive down-scaling strategy: from miniaturization of reprogramming, to miniaturization of differentiation, to a fully integrated one-step reprogramming-and-differentiation process.

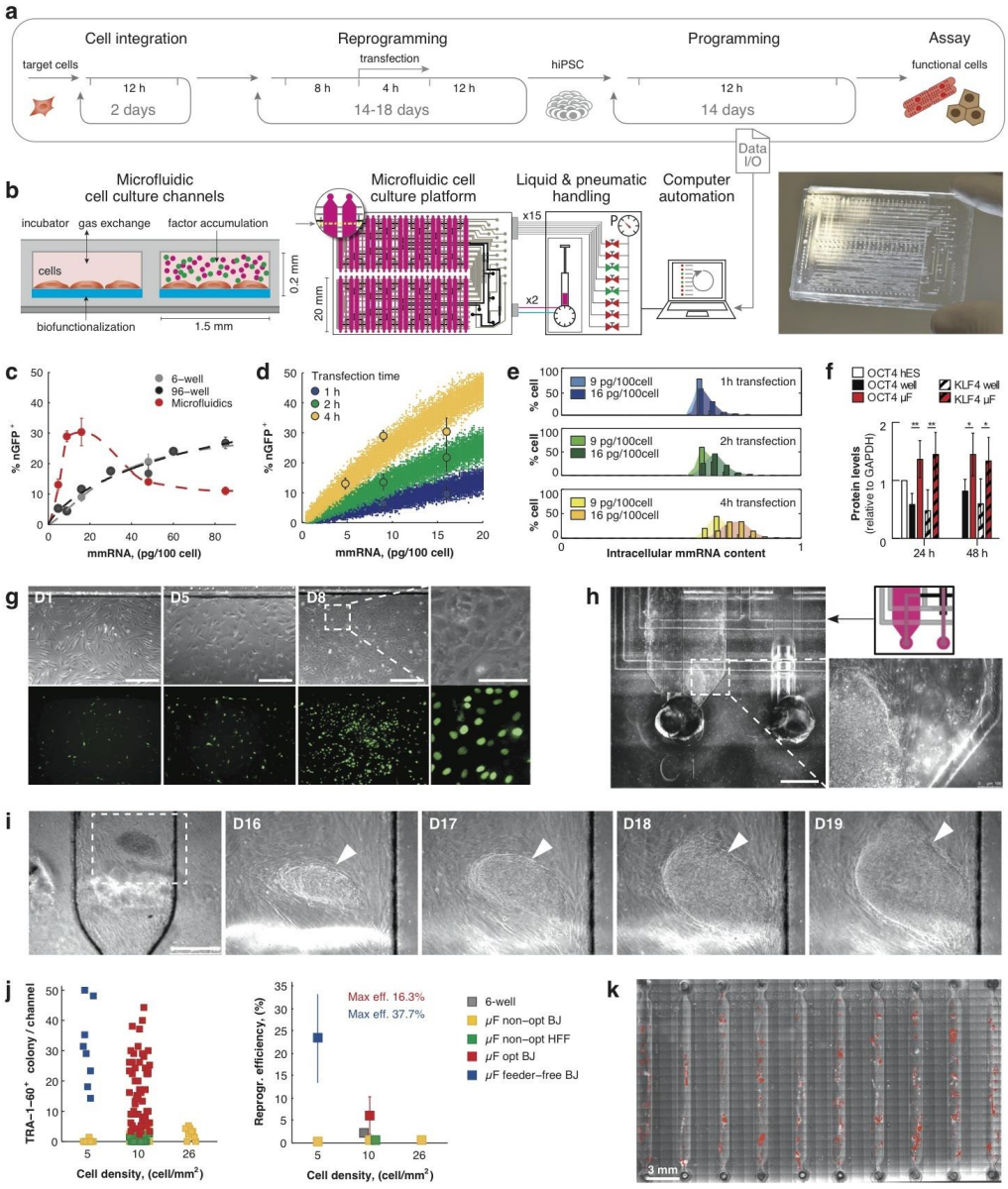

Fig. 2 | Design and validation of microfluidic technology for cell reprogramming. (**a**) Microfluidics reprogramming and differentiation of somatic cells are integrated in a joint workflow. (**b**) Automated microfluidic platform setup, comprising a microfluidic chip, which accommodates 32 parallel microchannels, and a liquid handling (2 ports) and pneumatic control of fluids (15 ports) managed remotely by a computer. (**c**) Efficiency of transfection of nGFP in BJ fibroblasts as a function of mmRNA amount, derived from images taken 24 h after a single transfection by RNAiMAX (RiM). Error bars, mean±s.d. (n>4). (**d**) Experimental (large dots) and mathematical model-derived (small dots) transfection efficiency for different incubation periods (RiM). Error bars, mean±s.d. (n>4). (**e**) *In silico* simulation of mmRNA content distribution in the cell population, as a function of mmRNA amount and transfection duration. (**f**) Western blot analysis of the indicated proteins expressed from exogenous mmRNAs of single microfluidic channels and wells, and appropriate controls, performed 24 h after two daily mmRNA transfections in BJ fibroblasts. Error bar, mean±s.d. (*n*=4). (**g**) Transfection progression in microfluidics during reprogramming, verified by nGFP expression. Scale bar, 500 and 150 µm (macro). (**h**) Representative hiPSC colony generated inside an automated microfluidic chip. (**i**) Expansion of primary hiPSC in a microfluidic channel. Scale bar, 750 µm. (**j**) Reprogramming efficiencies of different cell types under optimal (opt) or non-optimal (non-opt) conditions. Error bar, mean±s.d., (n>8). (**k**) Microfluidic chip with superimposed TRA-1-60^{+} colonies at the end of reprogramming protocol with feeders cells.

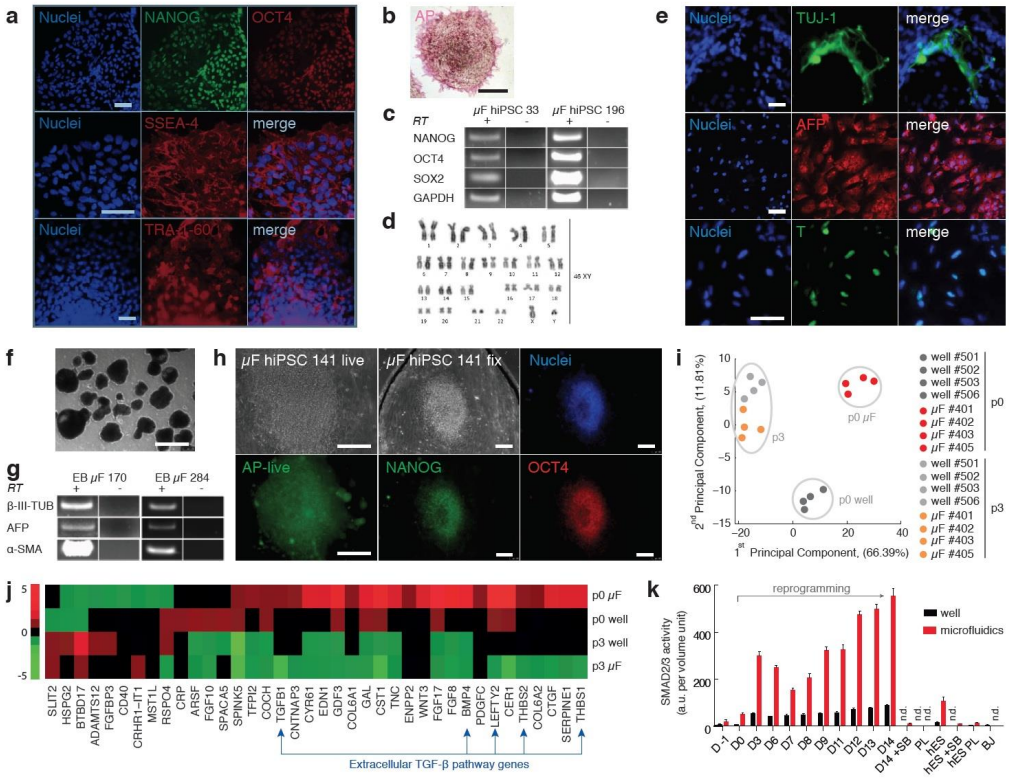

Fig. 3 | Characterization of microfluidic-generated hiPSC. hiPSC were expanded in wells for at least 12 passages and characterized by means of (**a**) immunofluorescence, (**b**) alkaline phosphatase, (**c**) RT-PCR, and (**d**) karyotype. (**e**) Expanded microfluidic hiPSCs are able to generate cells expressing markers from the three germ layers after directed differentiatio. (**f**) Embryoid bodies from microfluidic hiPSC, and (**g**) their characterization by RT-PCR of germ-layers markers. (**h**) *In situ* immunofluorescence characterization of microfluidic hiPSC before and after fixation. (**i**) Principal component analysis of freshly-derived and expanded hiPSC from microfluidics and wells, grouped according to results from hierarchical clustering. (**j**) Microarray-derived expression profiles of genes differentially expressed between the 4 conditions in Fig. 2I, belonging to GO category extracellular space and to TGF-β KEGG pathway. (**k**) TGF-β pathway activation during reprogramming measured as SMAD2/3 activity of a reporter line. Error bar, mean±s.d. (n=3). Scale bars, 25 μm (a,e), 500 μm (f), 200 μm (h).

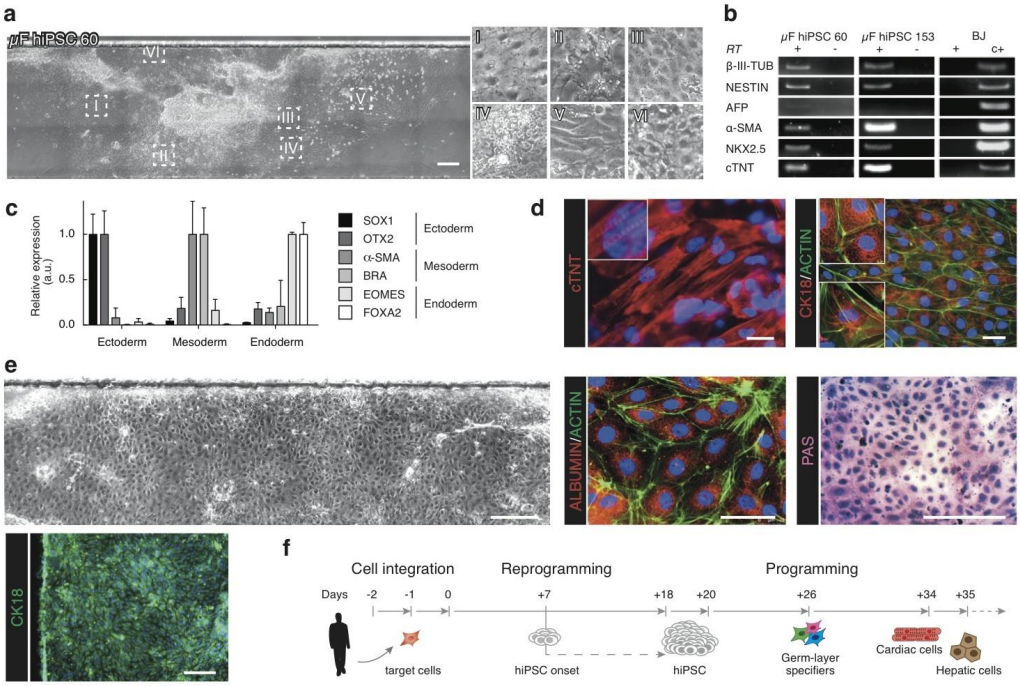

Fig. 4 | Differentiation of freshly obtained hiPSC in microfluidics. (**a**) hiPSC differentiated in aspecific medium comprising cells with different morphological phenotypes (scale bar, 250 μm) and (**a**) expressing markers of the three germ layers, as evidenced by RT-PCR. (**c**) qPCR analysis to detect specific early germ-layer commitment of hiPSC colonies purified and directly seeded in new microfluidic channels for differentiation. Error bars, mean±s.d. (n=10). (**d**) Cardiomyocytes (cTNT) and hepatic-like (CK18 and actin) cells from late-stage specification of hiPSC, extracted and pooled into new channels for differentiation. Scale bars, 50 μm. (**e**) One-step maturation of primary microfluidic hiPSC into hepatic lineage. Each colony differentiated in large areas of mature cells, also presenting functional markers (albumin, PAS, CK18). Scale bars, 250 μm, 50 μm (albumin). (**f**) Schematic summary describing the one-step process of reprogramming and differentiation in microfluidics without intermediate passaging.